“An optimist will tell you the glass is half-full; the pessimist, half-empty; and the engineer will tell you the glass is twice the size it needs to be.”

- Anonymous Author

University of Alberta

Spatial statistics as a means of characterizing mixing and segregation

by

Alena Kukukova

A thesis submitted to the Faculty of Graduate Studies and Research
in partial fulfillment of the requirements for the degree of

Doctor of Philosophy
in
Chemical Engineering

Department of Chemical and Materials Engineering

Spring 2011
Edmonton, Alberta

Examining Committee

Suzanne M. Kresta, Department of Chemical and Materials Engineering

Joelle Aubin, Laboratoire de Génie Chimique, Universite de Toulouse, France

Jos Derksen, Department of Chemical and Materials Engineering

Clayton Deutsch, Department of Civil & Enviromental Engineering

Natalia Semagina, Department of Chemical and Materials Engineering

James Gilchrist, Department of Chemical Engineering, Lehigh University, USA

To Vasek and Matej.

Abstract

Although a number of definitions of mixing have been proposed in the literature, no single definition accurately and clearly describes the full range of problems in the field of industrial mixing. Based on the review of mixing and segregation characterization techniques in chemical engineering, spatial statistics and population studies, a definition of industrial mixing is proposed in this thesis, based on three separate dimensions of segregation. The first dimension is the intensity of segregation which quantifies the uniformity of concentration; the second dimension is the scale of segregation or clustering; and the last dimension is the exposure or the potential to reduce segregation. The first dimension focuses on the instantaneous concentration variance; the second on the instantaneous length scales in the mixing field; and the third on the driving force for change, i.e. the mixing time scale, or the instantaneous rate of reduction in segregation. The definition is introduced using concepts, theory and mathematical equations. This definition provides a theoretical framework for the rigorous analysis of mixing problems, encompassing all industrial mixing processes and allowing a clear evaluation of experimental methods. In this work, the three dimensions of segregation are presented and defined in the context of previous definitions of mixing, and then applied to a range of industrial mixing problems to test their accuracy and robustness. Suitable quantities for direct measurement of the dimensions of segregation are then investigated in detail. The result is a toolkit of ready-to-use methods for the measurement of the intensity (CoV) and the scale of segregation (maximum striation thickness on a transect, point-to-nearest

neighbour distributions and variogram), provided as Matlab codes. The chosen methods are thoroughly investigated by testing their applicability, limitations, sampling strategies and meaningfulness of the results using selected sets of mixing data, resulting in creation of guidelines for the use of each of the provided methods. The developed definition of mixing, together with tools and guidelines for measurement of mixing will help researches to further develop the field of mixing, engineers to solve practical industrial mixing problems, and instructors of chemical engineering courses to introduce mixing concepts more easily.

Acknowledgements

I would like to thank my supervisor Dr. Suzanne Kresta for her support and knowledge, for being an inspiring woman researcher role model and for helping me find creative solutions both for my research and for completing my degree while growing a family.

Many thanks to my co-supervisor Dr. Joelle Aubin, for bringing a fresh perspective to our work and for being another example that "women can have it all".

Thanks to my family who passed "the technical gene" onto me and who lovingly let me into the world to fulfill my potential, wherever that might take me.

To all my colleagues in the Mixing Group, Shad, Oscar, Pete, Solomon, Inci, Imran, Benjamin, Marcio and Patrick, thank you for all the fun we had while both working and not working.

Thanks to all the support staff at the University of Alberta who made my degree as smooth as possible, and particularly the computer support guys Bob Barton and Jack Gibeau, who always had a smile on their faces.

I would like to thank Michal Mostek, Jos Derksen, Hugo Hartmann, Lorenz W. Sigurdson, Graeme M. G. Watson and an anonymous corporate colleague for providing the mixing data which were used in this work.

I would also like to thank the NSERC for financial support.

Calgary, January 2011

Table of Contents

List of Tables

List of Figures

List of Symbols

Roman Characters

a	interfacial area (m^2)
a_{ij}	contact area (-)
A	sample region (-)
A, B, C	species or reagents
AR_{tr}	threshold aspect ratio (-)
b	constant (-)
$\dot{B}_d$	birth rate (s^{-1})
c	constant (-)
C	concentration (mol/L or 1)
$\overline{C}$	mean concentration (mol/L or 1)
$C_i(x)$	concentration at location x (mol/L or 1)
C_{imp}	impeller off-bottom clearance (m)
C_{is}	standardized concentration value at location x (-)
C_{mean}	average concentration (mol/L)
C_{min}	lower limit of the concentration threshold (mol/L or 1)
C_v	volume fraction of unmixed additive (-)
CoV	coefficient of variance (-)
CoV_r	relative reduction in the coefficient of variance (-)
d	probe diameter (m)
D	impeller or pipe diameter (m); dissimilarity index (-)
d_g	micromixer groove depth (μm)
d_p	particle diameter (m)
dx	grid spacing in x direction (m)
dxz	length of the hexagon side in the sampling grid (m)
dz	grid spacing in z direction (m)
D_{BA}	molecular diffusivity (m^2/s)
$\dot{D}_d$	death rate (s^{-1})

D_f	fractal dimension of the cluster (-)
D_{pipe}	pipe diameter (m)
D_r	impeller diameter (m)
E	exposure (mol/s)
$f(x)$	function for distinguishing striations (-)
h	data separation distance (m, pixels); microchannel height (μm)
H	tank height (m); micromixer height (μm)
i, j	measurement location index, drop interval index or number of particles in a cluster (-)
I	intensity of segregation or index of dispersion (-)
i_{max}	maximum cluster mass in the system (-)
I_{disp}	index of dispersion (m)
k	Boltzmann constant (1.38×10^{-23} J/K); number of grid points in one direction (-)
k_{imp}	constant (-)
K	strength of interaction (-); constant (-)
k_La	volumetric mass transfer coefficient (mol/s/m^3)
K_o	number of fluid divisions in a mixer element (-)
L	length (m)
L_D	mean length scale calculated from the correlogram (m, pixels)
L_i	drop size in interval I (m)
L_V	mean length scale calculated from the variogram (m, pixels)
L_1, L_2	crystal width and length (m)
m	number of grid points or nearest distances (-); measurement location number (-)
M	total number of measurement locations (-)
n	normal vector (-); crystal number density (1/m^3/m/m); number of particles in area A; number of mixer elements (-)
N	impeller rotational speed (rps or rpm)
n_d	number of drops (particles) (-)
n_r	impeller rotation frequency (rps)

N_b	number of neighbouring squares (-)
N_B	molar flow rate (mol/s)
$N(h)$	total number of pairs of data separated by distance h (-)
N_i	number of drops in interval i (-)
$N_i(t)$	number of aggregates of mass i at ime t (-)e
N_{js}	just-suspended impeller speed (rps or rpm)
N_{jd}	just drawn down impeller speed (rps or rpm)
N_P	dimensionless power number (-)
N_t	total number of measurement locations (-); number of time steps/impeller revolutions (-)
p	total number of particles in area A (-)
P	proportion of species of interest in the sample region (-)
Re	Reynolds number (-)
Re_d	jet Reynolds number (-)
$R_x(h)$	coefficient of correlation at separation distance h (-)
t	time (s)
T	tank diameter (m)
t_m	constant (-)
$\bar{U}$	velocity vector (m/s)
V	volume of crystallizer (m^3)
w	microchannel width (m)
W	Fuchs stability ratio (-); micromixer width (μm)
w_g, W_g	micromixer groove width (μm)
x, y, z	Cartesian coordinates (m)
x_A	volume fraction of component A at a given point and instant (-)
$\overline{x_A}$	average volume fraction (-)
x_G	mean grid spacing (m)
x_i	nearest distance for ith grid point (m)
$\overline{x_i}$	mean PNN distance (m)
x_R	PNN variance filter threshold (m)

Δx	particle separation threshold (m)
Δz	transect height (m)

Greek Characters

$\gamma_x(h)$	variogram at separation distance h (-)
Γ	incomplete gamma function
ε	turbulence kinetic energy dissipation rate (J/kg/s)
η	kinematic viscosity (m^2/s)
θ	tangential position in tank (°)
θ_{95}	blend time to reach 95% homogeneity (s)
ξ	x coordinate of the point on the $R_x(h)$ curve where the curve crosses 0 (m)
ρ	density (kg/m^3)
ρ_c	continuous phase density (kg/m^3)
σ	standard deviation (-); surface tension (N/m)
σ^2	variance (mol^2/L^2 or 1)
σ_M^2	normalised concentration variance (-)
σ_R^2	filtered PNN variance (m^2)
σ_{R0}^2	filtered PNN variance at the micromixer inlet or at time = 0 (m^2)
ϕ	volume fraction of dispersed phase (-)

Chapter 1: Introduction

History of Mixing

Mixing is almost as old as humankind. Mixing is involved in kneading dough and scientific evidence shows that prehistoric man may have eaten a type of bread 30,000 years ago in Europe (Revedin et al., 2010). As soon as cooking vessels were first created in rock depressions or made of clay (Glasse, 2010), stews and soups could be cooked and mixing was used to speed up the heat transfer. In the beginning, the mixing equipment used was most probably just hands or a stick and a clay pot. As the time passed, mixing was used not only for producing food, which we can see in Figure 1-1, but also for manufacturing purposes, e. g. fabric dyeing as shown in Figure 1-2. A range of materials including wood, metal and ceramics were then used for the construction of mixing equipment.

Figure 1-1. Medieval kitchen.

Venetian Dyer.
From the historically
important manual
of Dyeing (1540):
Plictho de Larte de Tentori.

Figure 1-2. Dyeing .

With the onset of the industrial revolution in the 18th century and the invention of steam engines to power processes, large scale manufacturing of food, textiles and chemicals in factories began, with a need for industrial mixers to mix large quantities of materials. From then on, the development of mixing processes shifted into a higher gear.

When looking around now, mixing is present everywhere – from the kitchen to virtually every manufacturing process. A mixer can be as simple as a spoon or a whisk or more sophisticated as an electronic blender, mixer or an industrial impeller. Mixing vessels can be a cup, pot, barrel, test tube, beaker or industrial tank and are made of a variety of traditional and new materials (glass, plastic or composite materials), depending on the purpose. Mixers can be found in unexpected places as well; e. g. washing machines and pumps are both good mixers. From the history, it can be seen that mixing is a very old unit operation that is still important today and that it occurs in many processes, ranging from household to large industrial operations.

Industrial Mixing Processes and Studies

Industrial mixing includes a wide variety of processes where liquid is the major phase, as well as the cases of solid-solid and powder mixing. Mixing processes can be divided into classes, according to various criteria, for example according to process objectives, mixing equipment or flow regimes (laminar, turbulent or transitional). The criterion that will emerge as the most important in this thesis is the process objective. Based on the process objective, mixing processes belong in one of these three categories:

1. Blending of miscible liquids.
2. Multiphase mixing.
3. Chemical reactions.

Blending of miscible liquids is a common mixing operation. The goal of blending is to achieve uniformity of concentration of the minor species to a specified degree. Blending of low viscosity fluids is usually performed in a turbulent regime and for highly viscous fluids in a laminar regime. For turbulent blending, the homogeneity of concentration is the process objective. In laminar blending, mixing occurs as large striations of the minor phase decrease in time. The objective here is to reach a specified size of striations.

Multiphase mixing can be further divided into liquid-liquid, gas-liquid, solid-liquid and solid-solid mixing. In the case of immiscible liquid-liquid mixing, one of the phases usually forms drops dispersed in the continuous phase (Paul et al., 2004). Production of cosmetic lotions is an example of such a process. Here, oil droplets are dispersed in a water phase. The oil phase has to be broken down by an agitator to drops of a very small size, such that the two phases will not separate.

An example of gas-liquid mixing can be found in waste water treatment. Bacteria need oxygen in order to decompose organic waste material in the water, so the waste waters must be aerated with oxygen bubbles and the dissolved oxygen has to be well distributed to reach all the bacteria.

As the name suggests, solid-liquid mixing involves particles of solid phase being mixed into a liquid phase. When producing most paints, small particles of

solid pigment are suspended in a liquid such as oil or water. The quality and the resulting colour of the paint strongly depend on the size and distribution of the pigment particles throughout the carrier liquid.

Solid-solid powder mixing is important for example in the pharmaceutical industry, where active ingredient has to be homogeneously mixed into a carrier substance, in order to produce tablets with known amount of the active ingredient.

Several objectives can be sought in multiphase mixing. One objective may be to achieve a specified size of drops, bubbles or particles. For other processes, the goal is to disperse the drops, bubbles or particles homogeneously in the liquid. In some cases, the minor phase does not have to be dispersed homogeneously but it is sufficient to stop at a point where the macro-scale segregation is disrupted, e.g. using the impeller speed at which particles with higher density than the fluid are just suspended from the vessel bottom (just suspended speed). In other cases, multiphase mixing is done to maximize the rate of mass transfer. Mass transfer is dependent on the contact area between the two phases and therefore mixing is needed to disperse the bubbles, drops or particles of the minor phase in the fluid to expose as much surface area as possible. In addition to this, mixing is responsible for circulating the fluid and bringing fresh fluid to the interface to keep the concentration gradient at the interface as high as possible, thus facilitating the mass transfer.

The effect of mixing on chemical reactions is most apparent for reactions where the mixing rate and the reaction rate are similar or when the mixing rate is slower than the reaction rate (Paul et al., 2004). Mixing is critical for the so-called ‘mixing-sensitive reactions’ where undesired byproduct forms from the reactants or by decomposition of the desired product if given the opportunity and time. In the pharmaceutical industry, if the mixing is not fast enough the drugs may contain impurities, which can be dangerous for patients. In addition to the speed of the mixing process, mixing has to reach a small enough scale to allow for the molecular contact of reactants in order for the reaction to happen. For heterogeneous reactions, the drops, bubbles or particles of one phase have to be dispersed in the continuous phase in order to maximize the surface contact area to

enable reaction and maximize the reaction yield. Mixing also serves here to bring fresh reactants to the particle surface and remove the product to keep the surface available for further reaction, thus ensuring a concentration gradient between the minor and major phases to promote the reaction.

There are many different categories of mixing processes, as explained above. Each of them deals with different physical phenomena, different objectives and applications, different materials and their interactions, different flow regimes and moreover; there is also a variety of mixing equipment used for their application. All this variety makes the study of mixing a substantial task to undertake. However, in order to manufacture products with a desired quality, with high yields and minimal energy or material losses, comprehensive understanding of mixing is critical.

Because the physical phenomena in industrial mixing vary considerably, knowledge about mixing was initially gained through the design of specific processes and the troubleshooting of existing installations. Over the years, many experimental and numerical studies of mixing processes have been made (Paul, 2004), and today, there is an extensive body of research on various mixing processes. Specific applications are well researched and general observations have been summarized into correlations and design rules, e. g. Zwietering's solids suspension correlation (Zwietering, 1958) or Grenville's blend time correlation (Grenville, 1992).

In addition to the study of specific mixing processes, there have been many attempts to define mixing as a state. One of the major steps in understanding mixing is the realization that mixing is not only the physical *process* of mixing but also the *state* of the system. In a mixing process, the system's components usually move from a segregated to a more homogeneous state of mixing. In order to characterize the state of mixing, exact quantitative measures are needed for engineering applications. The first attempts at characterizing the state of mixing were done in the 1950's by Danckwerts (Danckwerts, 1958). His idealized approach defines perfect mixing as a state when everything is instantaneously mixed on a molecular scale and perfect

segregation as the condition when components never mix. These concepts are useful but are not sufficient to provide a good definition for real-life problems, all of which exist between these two limits. Later, researchers characterized mixing using different quantities. A literature review of these methods can be found distributed through the introductions of all of the following chapters.

Despite all of these attempts, the field of industrial mixing still lacks a single rigorous definition of mixing which embraces all of the important applications and process objectives. This lack of formal definition became vivid, when the editors had to introduce the concept of mixing in the introductory chapter of the Handbook of Industrial Mixing (Paul et al., 2004), which is the most comprehensive collection of mixing knowledge up-to-date. A second example is the fact that even though mixing is present in most industrial processes and that it is often a central operation for ensuring desired product quality, it is a subject that is almost completely missing in the basic chemical engineering curriculum. The place of mixing in engineering courses and the basic concepts that could be introduced are discussed in the following section. A rigorous definition of mixing would not only provide a natural introduction to mixing but would also form the framework for the theoretical development of the field, and for the well grounded evaluation of experimental methods.

Mixing in Undergraduate Engineering Curriculum

Mixing is a central operation in most industrial processes; however, mixing concepts are almost completely missing in the basic undergraduate chemical engineering curriculum. Following is a list of courses where mixing is relevant and suggestions where introducing mixing concepts might be both beneficial and transparent.

In the introduction to materials course, mixing influences the development of material properties during processing. For example, carbon nanotubes are added in a polymer matrix to create a nanocomposite material with electrically conducting properties, which can be used for antistatic or electromagnetic shielding applications. The electric properties of the resulting material strongly

depend on how well the carbon nanotubes are dispersed throughout the polymer which is achieved by mixing (Lin et al., 2006).

In introductory fluid mechanics, the concepts of flow in pipes, T-junctions, jets and pumps would be enriched and complemented by also discussing their role as mixing equipment and including simple and reliable blend time correlations for this equipment. Occasionally, unit operations labs address one of these topics (Sharp et al., 2008).

In transport phenomena courses, mixing plays a significant role in heat and mass transfer. Heat and mass transfer are increased with convective flow driven by mixing; mixing also serves to increase the contact surface area where the heat or mass transfer takes place, particularly in multiphase flow. This is normally discussed implicitly as the area for mass transfer. Adding the mixing step, where the area is generated, would make the concept more concrete and closer to engineering design.

A whole new chapter about mixing could be included in unit operations courses. Once the definition of mixing is complete, the concept of mixing as a process and as a state should be explained here, together with the ways to measure mixedness. This could be followed by a description of different mixing applications (blending, multiphase mixing, reactions) and equipment (pipes, stirred tanks…), the design guidelines, as well as the impact of mixing on surface area generation and phase equilibria.

In many reactor design courses, most of the course is devoted to cases where mixing is considered to be either perfect (continuous stirred tank reactor) or perfectly segregated (plug flow reactor) in order to make the calculations simpler. Mixing effects are also considered but the calculations are based on the measurement of the residence time distributions which can produce identical results for a wide variety of mixing scenarios. A new definition of mixing might be helpful in development of this field to include real mixing effects on the process results.

Thesis Objective and Scientific Approach

The objective of this thesis is to introduce a rigorous definition of mixing, which is based on theory and is quantifiable by equations, and to identify the methods that can be used to measure mixing in industrial applications according to this definition.

In the initial stages of the thesis, an extensive review of mixing characterization and measurement methods was made. A review of the quantities used for the measurement of mixing in chemical engineering applications revealed that a wide spectrum of approaches (e. g. Danckwerts, 1958; Gates et al, 1975; Ottino, 1989; Bałdyga and Bourne, 1999; Paul et al, 2004) exist, and also that no single definition or quantity is applicable to the whole range of industrial mixing problems. A detailed review of quantities used to measure mixing in chemical engineering can be found in the introductions of Chapters 2 - 4.

The apparent lack of a well grounded definition of mixing in chemical engineering lead the focus to other fields of research where mixing and segregation has been also been studied. Literature reviews of segregation in the fields of spatial statistics (Diggle, 2003; Cressie, 1993), geostatistics (Deutsch, 2002), plant ecology (Perry, 1979; Mead 1974), zoology (McGarvey, 2005) and population segregation studies (Morrill, 1991; Wong, 2004) provided insight on additional measures and measurement strategies. The residential segregation researchers Massey and Denton (1988) provide the most rigorous definition of segregation based on five independent dimensions of segregation of human populations.

Using the analogy between mixing and segregation of human populations and mixing and segregation in industrial processes, Massey and Denton's (1988) definition was then applied to mixing problems in chemical engineering as the next step in this thesis. It was found that only three of Massey and Denton's (1988) five dimensions of segregation are relevant to industrial mixing. Based on this investigation, a rigorous definition of mixing was developed:

Mixing can be quantified as a control of segregation. Segregation has three independent dimensions. The first is the intensity of segregation, which quantifies

the uniformity of concentration. It is usually expressed in terms of the concentration variance. The second is the scale of segregation or clustering, which quantifies the distribution of length scales in the mixing field or the spatial dispersion of a population (particles, drops or bubbles). The third dimension is exposure, which quantifies the rate of reduction of segregation. Exposure is dependent on the strength of interaction of the populations, their opportunity to interact and the distance from minimum segregation.

Through this definition the state of mixing of any system at any instant in time can be fully characterized by three dimensions of segregation. This is illustrated in the bottom part of Figure 1-3. Using the proposed definition of mixing and segregation, any mixing field can be exactly placed in a three dimensional system of mixing coordinates, composed of the intensity of segregation, the scale of segregation and exposure. Looking at the eight simplified mixing fields shown inside of the cube below, it can be seen that the size of the black drops is smaller for the pictures on the left side, which translates to a smaller scale of segregation. Comparing the top pictures with the bottom pictures, the scale of segregation is the same but the concentration difference between the drops and the surrounding fluid gets smaller from top to bottom. The concentration variance therefore drops from top to bottom, which is quantified by a decrease in the intensity of segregation. A change in the third dimension of segregation, exposure, is shown when moving from the front face of the cube to the back face. Comparing the picture pairs on the front and back face of the cube, both the intensity of segregation and the drop size (or the scale of segregation) stay the same, however, the interface between the black and white phases has increased significantly. This increase in interfacial area gives the two phases much larger opportunity to interact, which increases the exposure.

In order to quantify the dimensions of segregation for different mixing applications, the previously reviewed measures of mixing coming from chemical engineering and other disciplines were considered and the appropriate ones for each dimension of segregation were selected and thoroughly investigated. The whole process of selecting methods to characterize different mixing problems

within the proposed framework of the three dimensions of segregation is illustrated in Figure 1-3. The main focus was then put on the final objective of the thesis, which was the creation of a toolkit of ready-to-use methods for the measurement of segregation with guidelines for their use. This was done by creating Matlab programs of selected methods and by testing their applicability, advantages, disadvantages, limitations, sampling strategies and meaningfulness of the results using selected sets of mixing data.

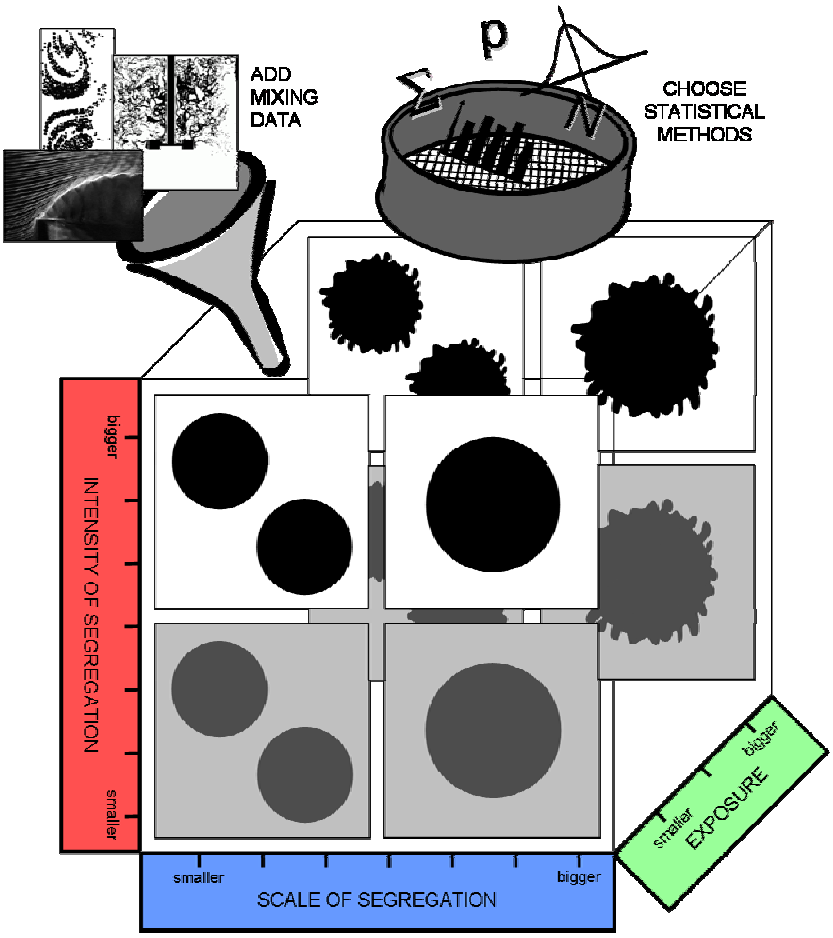

Figure 1-3. Thesis visual abstract.

Thesis Structure

The thesis is based on three extensive papers on the dimensions of segregation. The first defines the three dimensions of segregation, the second investigates the intensity of segregation, and the third the scale of segregation.

Chapter 2 explains the problems with current definitions of mixing in detail. The initial definition of mixing based on the three separate dimensions of segregation is described here. The first dimension focuses on the instantaneous concentration variance; the second on the instantaneous length scales in the mixing field; and the third on the driving force for change, i.e. the mixing time scale, or the instantaneous rate of reduction in segregation. With these three dimensions in hand, it is possible to speak more clearly about what is meant by the control of segregation in industrial mixing processes. In this paper, the three dimensions of segregation are presented and defined in the context of previous definitions of mixing, and then applied to a range of industrial mixing problems to test their accuracy and robustness.

Chapter 3 explores the effect of the sampling scale and sampling method on two distinct measures of mixedness: the coefficient of variance *CoV* (intensity of segregation) and the maximum striation thickness (scale of segregation). Three methods of sampling: quadrats, probes and transects, were used. Two data sets from CFD simulations were used as test cases. The first test case is the dispersion and dissolution of floating particles in a turbulent stirred tank and the second test case is the laminar mixing of mass-less tracer particles in a staggered herringbone micromixer. A large number of probes (>100) are needed to accurately track the *CoV* of the mixing field as it evolves, and the scale of measurement at each probe should be matched to the smallest mixing scale of interest. The final value of the *CoV* is shown to vary by up to a factor of 5 as the probe size changes. The most useful data was obtained from the measurement which changed the most in the later stages of mixing: intensity of segregation, or *CoV*, for the turbulent case and scale of segregation, or maximum striation thickness on a transect, for the laminar case.

Chapter 4 investigates the use of four methods to extract length scales from mixing data: the maximum striation thickness, point to nearest neighbour distributions (PNN) the correlogram and the variogram. Four test data sets were analysed: blending in a micromixer; particle dispersion in a stirred tank; dispersion of a smoke plume; and a pulse tracer test in a reactor. The maximum

striation thickness captures the largest length scale. The PNN method quantifies differences between clustered, random and regular spatial distributions. The correlogram calculation cannot be consistently used for all types of mixing data and has therefore been rejected. The variogram reveals both large scale segregation and periodicity. Sub-sampling is needed to isolate smaller structures. The variogram, PNN, and transect methods all successfully extracted mixing length scales from large 2D data sets.

Chapter 5 contains overall conclusions drawn from this work and recommendations for future work.

References

Bałdyga, J. and Bourne, J. R., 1999, *Turbulent mixing and chemical reactions*, Wiley, New York, USA.

Cressie, N. A. C., 1993, *Statistics for spatial data*, in *Wiley series in probability and mathematical statistics*, John Wiley & Sons, Inc., New York, USA.

Danckwerts, P. V., 1958, *The Effect of Incomplete Mixing on Homogeneous Reactions*, Chem. Eng. Sci., **8**, 93-102.

Deutsch, C. V., 2002, *Geostatistical reservoir modeling*, in *Applied geostatistics series*, Oxford university press, New York, USA.

Diggle, P. J., 2003, *Statistical analysis of spatial point patterns*, 2nd ed., Oxford University Press, New York, USA.

Gates, L. E.; Fenic, J. G. and Henley, T. L, 1975, *How to Select the Optimum Turbine Agitator,* Chem. Engg., December 8, 110-114.

Glasse, H., 9 Nov. 2010, *Cooking* in *Encyclopedia of World Biography*, Detroit: Gale, 1998. *Gale World History In Context*. Web.

Grenville, R. K., 1992, *Blending of viscous Newtonian and pseudo-plastic fluids*, Ph. D. Thesis, Cranfield Institute of Technology, Cranfield, England.

Lin, B.; Sundararaj, U. and Pötschke, P., 2006, *Melt Mixing of Polycarbonate with Multi-Walled Carbon Nanotubes in Miniature Mixers*, Macromol. Mat. Eng., **291**, 227-238.

Massey, D.S. and Denton, N.A., 1988, *The Dimensions of Residential Segregation,* Soc. Forces, **67**, 281-315.

McGarvey, R; Byth, K.; Dixon, C. D.; Day, R.W. and Feenstra, J. E., 2005, *Field Trials and Simulations of Point-Nearest-Neighbor Distance Methods for Estimating Abalone Density,* J. Shellfish Res., **24**, 393-399.

Mead, R., 1974, *Test for Spatial Pattern at Several Scales Using Data from a Grid of Contiguous Quadrats*, Biometrics, **30**, 295-307.

Morrill, R. L., 1991, *On the measure of geographic segregation*, Geo. Res. Forum, **11**, 25-36.

Ottino, J.M., 1989, *The Kinematics of Mixing: Stretching, Chaos, and Transport*, Cambridge Texts in Applied Mathematics, Cambridge University Press, Cambridge, New York, USA.

Paul, E.L.; Atiemo-Obeng, V.A. and Kresta, S.M. (Editors), 2004, *Handbook of Industrial Mixing: Science and Practice*, John Wiley & Sons, Inc., New Jersey, USA.

Perry, J. N.; Mead, R., 1979, *Power of the Index of Dispersion Test to Detect Spatial Pattern*, Biometrics, **35**, 613-622.

Revedin, A.; Aranguren, B.; Becattini, R.; Longo, L.; Marconi, E.; Lippi, M. M.; Skakun, N.; Sinitsyn, A.; Spiridonova, E. and Svoboda, J. A., 2010, *Thirty thousand-year-old evidence of plant food processing*, PNAS, **107**, 18815-18819.

Sharp, D.; Zhang, M.; Xu, Z.; Ryan, J.; Wanke, S. and Afacan, A., 2008, *Mixing Hot and Cold Water Streams at a T-Junction*, Chem. Eng. Edu., **42**.

Wong, D. W. S., 2004, *Comparing traditional and spatial segregation measures: A spatial scale perspective*, Urb. Geo., **25**, 66-82.

Zwietering, T. N., 1958, *Suspension of solid particles in liquid by agitators*, Chem. Eng. Sci., **8**, 244-253.

Chapter 2: A Rigorous Definition of Mixing and Segregation: Three Dimensions of a Key Process Variable*

Early Definitions of Mixing

The study of mixing dates back many years before the first journal publications, and the idea of "well mixed" is easily discarded as intuitively obvious. A search of the early literature provides a range of qualitative concepts and limiting cases. Several of these papers marked the beginning of three major areas of investigation: mixing in reaction engineering, solids mixing, and polymer processing. Starting from the late 1950's, Danckwerts (1952, 1958) and Zwietering (1959) discussed the difference between complete segregation and perfect mixing in the context of reactor design, particularly for binary mixtures of liquids. Danckwerts (1952) defined the intensity of segregation:

$$I = \frac{\sum_{m=1}^{M}\left(\overline{x_A} - x_{Am}\right)^2}{M\left(\overline{x_A}(1-\overline{x_A})\right)} = \frac{\overline{\left(\overline{x_A} - x_A\right)^2}}{\overline{x_A}(1-\overline{x_A})} \qquad (2\text{-}1)$$

where x_A is the fraction of the component A at a point in space and an instant in time, $\overline{x_A}$ is its average fraction in a binary mixture and M is the number of measurement locations. In this context, a point is defined in the continuum sense: large enough to contain a meaningful number of molecules, but small enough to have uniform concentration. The molecules in a homogeneous mixture are uniformly distributed down to the molecular scale and I is equal to 0; in a completely segregated mixture, as defined at a fixed scale of investigation, I is equal to 1. When the mean concentrations of component A and B are equal, $\overline{x_A} = 0.5$, the denominator is the biggest and the intensity of segregation the smallest. The limit of perfectly mixed allows instantaneous contact of two reagents, A and B, on a molecular scale throughout the reactor. The limit of

* A version of this chapter has been published in Chem. Eng. Res. Des., 87 (2009), p. 633-647.

completely segregated is best illustrated as drops of A and drops of B, both suspended in an inert C, with no possibility for dissolution or diffusion of A or B in C. These two limiting definitions are useful, but fail to describe any realistic industrial mixing problem. Danckwerts (1952) also discussed the scale of segregation in some detail. He recognized the difficulty of defining striations when the concentration varies continuously due to diffusion, and discusses in some detail the use of the autocorrelation of concentration, which he calls the coefficient of correlation, or the correlogram. Several early papers on solids mixing (Lacey, 1954, 1976a,b; Harnby, 1967; Hersey, 1970) also discuss the intensity and scale of segregation, using the normalized coefficient of variance and addressing the problem of selecting the best sample size (Lacey, 1954, Harnby, 1967), and later considering the scale of segregation, particularly with respect to the auto and cross correlation functions (Lacey, 1976a, b). At that time, it was extraordinarily labor intensive to collect the data densities needed to calculate scales of segregation, and the authors concluded that this measure was not accessible for the solution of realistic problems. Mohr et al. (1957) attempted to relate the rate of reduction in striation thickness to the shear rate in laminar flow systems, with applications to polymer processing, thus marking the beginning of a third parallel path in the history of industrial mixing.

During the 1970's, Chemineer published the Chemscale (Gates et al, 1975) as a qualitative description of the intensity of mixing in a tank and this concept was widely used for process design for many years. From the 1960's to the 1980's, Bourne, Villermaux and others (Baldyga and Bourne, 1999) developed more refined ideas about macromixing, mesomixing, and micromixing, but again the definitions are somewhat indirect: clear to the expert, but difficult to explain to a novice. Concurrently, Corrsin (1957, 1964), Toor (1969), and Brodkey (Lee and Brodkey, 1964, McKelvey et al., 1975) all investigated the impact of turbulence on mixing through measurements of concentration fluctuations at a point, sometimes calling this the segregation, with the idea that as the variance in concentration drops to zero, the fluid approaches perfect homogeneity. In the early 1990's, chaos theory examined laminar chaotic mixing with a fresh

analytical perspective (Ottino, 1989), and computational fluid dynamics promised numerical solutions to many complex problems (Paul et al, 2004, Chapter 5). In spite of this increasing body of work, the field of industrial mixing lacks a single definition of mixing that allows one to proceed directly from

1. a rigorous conceptual definition to
2. experiments which directly measure "mixing," and
3. equations and theory which quantify the definition.

Figure 2-1 shows a selection of important mixing problems encountered in industry. In all of these problems, there is global progress from a segregated state toward a more homogeneous state, but the physical phenomena vary widely. Figure 2-1a is the concentration field in a turbulent jet, measured using PLIF (Planar Laser Induced Fluorescence). The dispersion of minor species by turbulent eddies is evident, as is the range of length scales. This concentration field underlies the problem of byproduct formation in a feed plume, known as the mesomixing limit. The critical mixing objective is to achieve dilution of the feed plume before the undesired reaction has time to proceed. Figure 2-1b shows mixing in a pipeline at a high laminar Reynolds number. The feed jet is efficiently dispersed using an SMV static mixer. The mixer elements are yellow. Figure 2-1c shows the concentration field in a cross section of an SMX static mixer in laminar flow. Again, the initial objective is to achieve homogeneity in the fluid, but there can also be tight process specifications on the smallest allowable striation. Striations larger or smaller than the specified size can lead to unacceptable final products, particularly where optical clarity or color are key properties. Figure 2-1d is a composite material (Corian™ counter top) where several minor phases must be evenly but randomly dispersed in the final product. This is an example of a mixing specification that requires attention to the spatial organization of the minor phase. Figure 2-1e shows the initial stages of liquid drawdown in a liquid-liquid mixing application. For this application, the optimal geometry and the rotational speed required to draw down the liquid are needed. The final process specification may involve the rotational speed and time required to achieve some final drop size. This application may also require the addition of surfactants or stabilizers,

kill solution to stop a reaction, phase inversion, and/or mass transfer in a mixer settler or liquid-liquid extraction application. Figure 2-1f shows the entrainment of gas bubbles from the surface of a stirred tank. In gas-liquid mixing, the objective is most often gas-liquid mass transfer, but the problem can be substantially complicated by loss of power due to flooding of the impeller and changing conditions in boiling or coalescing systems. In many of these applications, several mixing objectives occur simultaneously in a single vessel or application. These objectives can be grouped into three categories:

- blending of miscible liquids, with possible complications due to high viscosity or non-Newtonian behavior
- multiphase mixing with at least one of several objectives: “just contacted”, completely distributed throughout the vessel, size reduction, or mass transfer,
- reaction: either homogeneous or heterogeneous

A closer examination of these applications, and a number of others, reveals three variables which are directly related to mixing: a reduction in the segregation of concentration; a reduction in the scale of segregation; and/or a mixing time scale that must be accomplished or predicted.

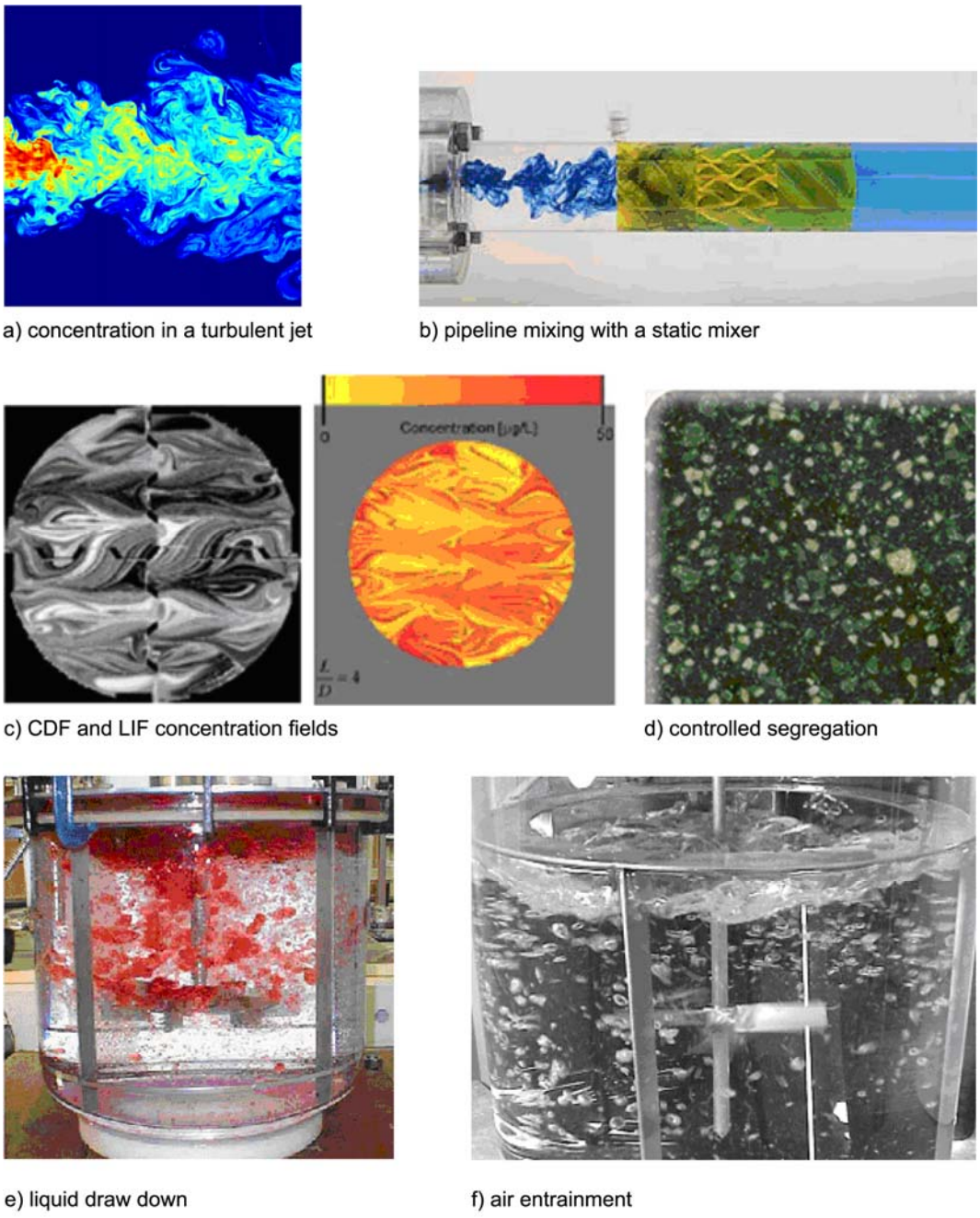

Figure 2-1. Illustrations of the range of mixing objectives encountered in industrial applications.*

* Image credits for Figure 2-1 are as follows: a) Paul et al., 2004, cover image b) and c) Sultzer ChemTech: http://www.sulzerchemtech.com, Jul 15, 2008 d) DuPont Corian Products: http://www2.dupont.com, Sep 29, 2008 e) Paul et al., 2004, Figure 4.24b f) Bhattacharya et al., 2007, Figure 4c

In Danckwerts' (1958) perfectly mixed limit, all three variables approach zero, and in the simplest mixing problems, the measurement of one variable (e.g. homogeneity of concentration) is often used to infer information about the others. In a second class of problems, for example liquid-liquid dispersions, the concentration remains infinitely segregated but a specific scale of segregation (e.g. drop size) must be achieved. For more difficult mixing problems, there may be a limiting time scale or mixing rate needed to reach homogeneity of concentration over a sub-volume of the vessel (e.g. the mesomixing and reaction problem, or the heterogeneous reaction problem with simultaneous mass transfer). In this case the intensity of segregation, the scale of segregation, and the local mixing time are all important, but the relationship between these variables is not as straightforward as our intuition suggests.

In this paper, a definition of mixing is proposed which provides a bridge between our current understanding of industrial mixing and more theoretical models of mixing (Fox, 2003; Paul et al., 2004 (Ch3)) to give a framework for further research, development, and design. The proposed definition is based on a literature review of theories of segregation in a number of other disciplines: spatial statistics, population ecology, segregation of human populations, geostatistics, and image analysis. The definition is introduced with a thought experiment which illustrates the three key concepts: intensity of segregation, scale of segregation, and exposure.

Figure 2-2 shows twelve checkerboard patterns which are organized from left to right by the size of the pattern, and from top to bottom by the variation in concentration. The mean concentration is the same for all 12 checkerboards: black squares have $C_i = 1$, white squares have $C_i = 0$, gray squares have $C_i = 0.5$ and the mean concentration $C_{mean} = 0.25$. The intensity of segregation for each checkerboard is calculated as the CoV:

$$CoV = \sqrt{\frac{1}{N_t}\sum_{i=1}^{N_t}\left(\frac{C_i - C_{mean}}{C_{mean}}\right)^2} \qquad (2\text{-}2)$$

The CoV is identical in each row, with the middle two rows showing a change in pattern with no change in the number of black, gray and white squares. The scales of segregation start with the largest possible scales on the left, and reducing to the smallest possible scales on the right of each row. As the patterns become more complex, the number of scales present in a single checkerboard increases. The exposure is calculated from

$$E \cong \sum_{i=1}^{N_t} \sum_{j=1}^{N_b} \frac{1}{2} K a_{ij} \left(C_i - C_j \right) \qquad (2\text{-}3)$$

where N_t = 256 = total number of squares in the checkerboard, N_b = 2,3, or 4 = number of neighbouring squares, K = 1 is the strength of interaction, a_{ij} = 1 is the contact area per side, and (C_i - C_j) is the concentration difference between two consecutive neighbors. This is analogous to a simplified calculation of the rate of mass transfer.

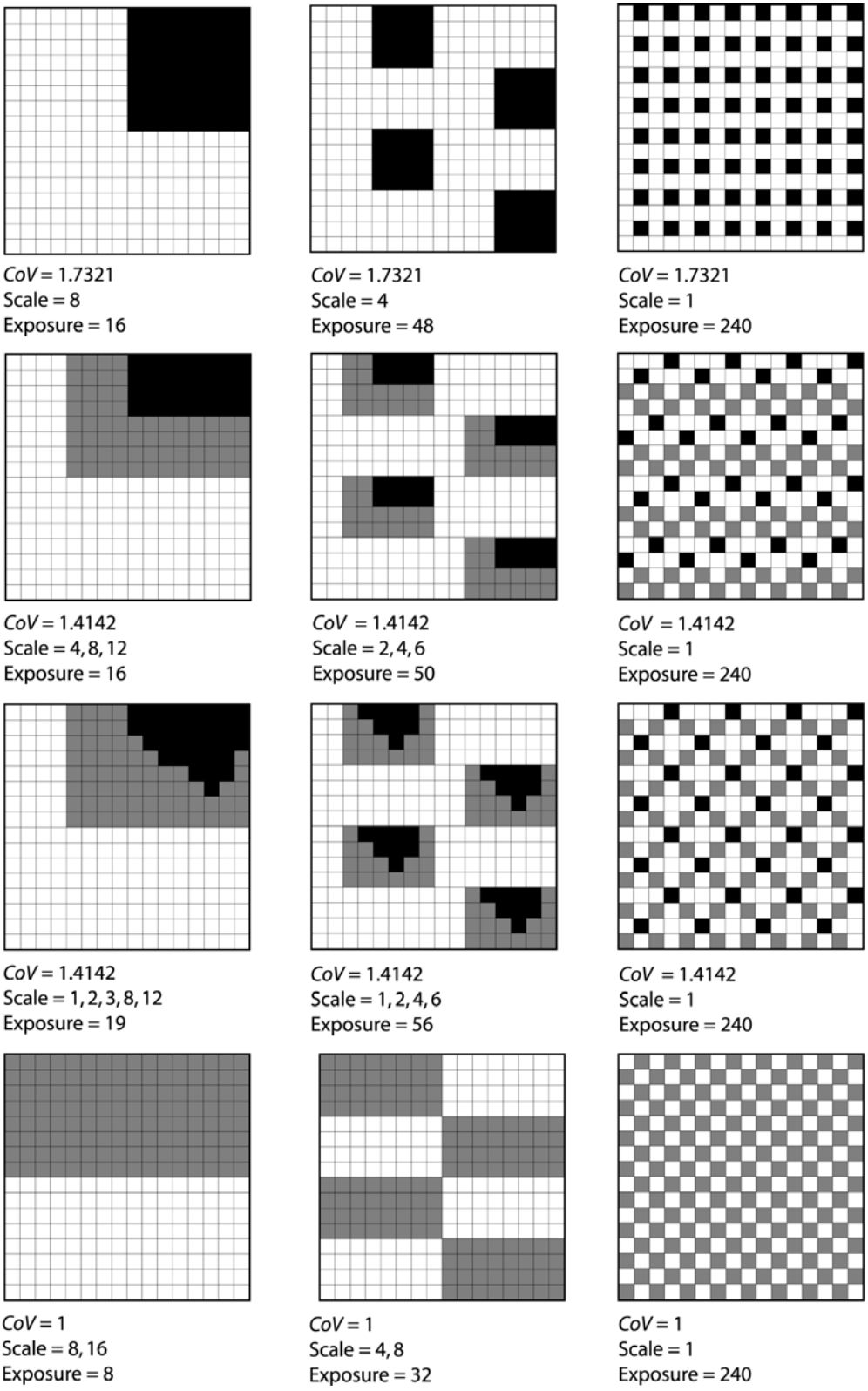

Figure 2-2. Three dimensions of mixing and segregation: intensity of segregation (*CoV*), scale of segregation (striation thickness) and exposure (rate of change in segregation).

A non-expert observer would undoubtedly say that the mixing improves from left to right in Figure 2-2. The intensity of segregation (*CoV)*; however, remains constant. It is the scale of segregation which decreases from left to right. The intensity of segregation quantifies how widely the concentration varies, but contains no information about the arrangement of black and white squares. A second look at the equation for the coefficient of variance makes this point clear. From this we conclude that the intensity of segregation is not enough to completely define mixing. The scale of segregation also plays an important role.

It is also possible to normalize the *CoV* to remove effects of initial concentration by dividing by the initial *CoV*. In the checkerboard case, the initial *CoV* is 1.73, giving CoV/CoV_o=1.0 for the first row equal, indicating complete segregation. For the second and third rows, CoV/CoV_o=0.709, and for the last row, CoV/CoV_o=0.578.

The exposure dimension is related to both the concentration variance and the scales of segregation, but in quite a complicated way. Before discussing the exposure results in Figure 2-2, consider the illustration of exposure in Figure 2-3. In this figure, the exposure increases from left to right. In (a) both the contact area and the concentration difference are at a minimum, while in (f), both the area and concentration difference are at a maximum. The intermediate pairs (b and c) and (d and e) must have at least a doubling of the total interfacial area to overcome the drop in concentration difference from 1.0 to 0.5. Because the interface has been distorted and folded, the exposure will increase slightly from (b) to (c) and from (d) to (e). Figure 2-3 differs from what we would see in an experiment, where the contact area increases rapidly under the influence of turbulent mixing at the same time as the concentration difference continuously drops due to convective mass transfer. The counteracting local effects of scale and intensity make the exposure dimension behave in ways that can be quite complex.

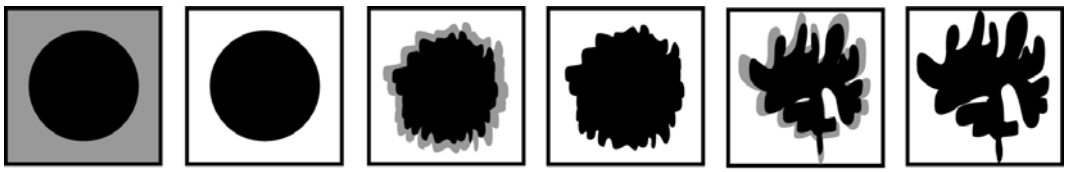

(a) (b) (c) (d) (e) (f)

Figure 2-3. Example of increasing exposure showing the effects of concentration difference and area of contact between the two populations. The first case has less exposure than the second, because the concentration difference is smaller in the first case. Each pair, moving from left to right, has an increasing area of contact.

In the first row of Figure 2-2, the exposure increases from 16 to 48 to 240 as the scale of segregation drops. Comparing the top and bottom rows suggests that the exposure decreases when the *CoV* decreases, but as the scale of segregation gets smaller, the effect of concentration variance becomes less important. A closer look shows that at intermediate values of *CoV* with slightly more complicated patterns and a range of length scales, the relationship between *CoV* and exposure is unpredictable due to the coupling between interfacial area and concentration difference. Decreasing the scale of segregation rapidly increases the exposure for all values of *CoV*. These results are collected in Figure 2-4 where the exposure dimension is plotted against the intensity and minimum scale of segregation. This figure clearly illustrates the need for a third dimension: in Figure 2-4a the relationship between *CoV* and exposure alone is random; in Figure 2-4b the exposure decreases rapidly as the minimum scale increases, but there is a wide range of results for exposure at small scales. This simple thought experiment clearly shows that the exposure dimension is not a simple linear combination of intensity and scale of segregation. The scales of segregation are distributed over a range of values, and are correlated to the interfacial contact area in a complex and non-linear way. In the calculation of exposure, the interfacial area is further coupled with local concentration differences. The exposure dimension combines these effects to describe a third dimension of mixing and segregation, the rate of change of segregation.

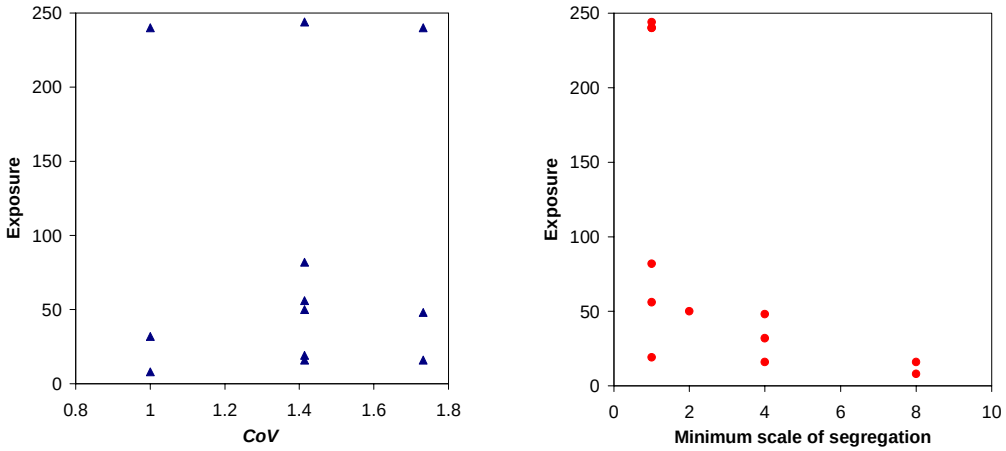

Figure 2-4. Relationship between exposure and a) intensity of segregation and b) minimum scale of segregation for the checkerboard patterns in Figure 2-2.

In summary, the *CoV* (intensity of segregation) tells us nothing about the scale of mixing because the definition contains no information about the characteristic length scales or the arrangement of the fluid volumes in the mixing field. This requires a second dimension, the scale of segregation. Exposure is proposed as a third variable, which is a non-linear function of both the intensity and scale of segregation. All three variables play an important role in industrial mixing problems, which are becoming more and more focused on the *control of segregation*, often at intermediate length scales. This is a more complex problem than the classical perfectly mixed limit.

Segregation Studies in Other Disciplines

A literature search reveals that segregation has been studied in a number of fields, and a broad spectrum of useful knowledge has developed in parallel with industrial mixing. The mathematical foundation is defined primarily by the field of spatial statistics. The fields of geostatistics and image analysis describe segregation in data sets that are fixed in time, but may require three dimensional reconstruction from limited data sets (e.g. geological core samples). Both population ecology and forest management grapple with the interaction of populations, and with extracting meaningful information from limited data. The population ecologists focus on quadrat samples, originally a 1m × 1m square area,

and the foresters use transect sampling (typically a 2m wide line sample) extensively. The tendency of populations to cluster, and the opportunities for species to interact with their environment and with other species are both central questions in these fields. This has led to some very useful ways to reconstruct the scale of segregation from limited data sets. Finally, the study of segregation in human populations considers both the instantaneous distribution of populations, and their potential for integration. All of these fields have well developed theory and formalisms, including partial definitions of segregation (Diggle, 2003), but the work by Massey and Denton (1988) is the most complete and quantitative analysis of the dimensions of segregation, integrating all of the key ideas in one overarching definition.

Massey and Denton (1988) reviewed the literature in population segregation and identified 20 different proposed measures of segregation. They applied these measures to 180 independent data sets and used PCA (principal components analysis) to determine which measures contain the most information, which measures are highly correlated with each other, and which measures contain a negligible amount of information. PCA, or PLS (partial least squares) is a regression technique applied to large multivariate data sets to determine which input variables describe the principle dimensions of variance in the results (Kresta et al., 1991). Variables grouped together in a single dimension are collinear and contain similar information (e.g. tray temperatures in a distillation column). Variables appearing in separate dimensions are orthogonal and contain information which pushes the result in a different direction. Massey and Denton's analysis revealed that the data sets contain independent information about 5 distinct dimensions of segregation. The remaining 15 measures did not provide any additional information. The PCA analysis is very significant because it provides a quantitative measure of which variables contribute significantly to the variance in the data. The fact that 5 dimensions are required reflects the complexity of the underlying data sets; the fact that only 5 of the 20 proposed measures of segregation provided independent information gives us some confidence that the 5 proposed dimensions enable a complete description of

segregation. We have retained the meaning of Massey and Denton's 5 proposed dimensions, but reworded them to obtain rigorous definitions that can be applied to a wide range of problems:

1. ***Evenness*** is the uniformity of concentration of the minor species. Evenness is defined relative to the volume of investigation and the scale of resolution of the measurement.
2. ***Clustering*** is the degree of spatial continuity or adjacency of members of a population, and is highly correlated to the spatial proximity of members of the population. Clustering is inversely correlated to the degree of spatial dispersion of the species.
3. ***Exposure*** determines the rate of reduction in segregation. It depends on the deviation from the minimum state of segregation, the physical contact between populations, and the strength of interaction between members of the populations (either attractive or repulsive). Exposure may be thought of as the driving force for change.
4. ***Density*** is the population density expressed as (number or mass) per (volume or area). The population density includes all species, not just the minor species, so it is distinct from evenness and clustering.
5. ***Centralization*** is the tendency of a population to concentrate spatially around some central or specified point.

Each of these measures applies at a single instant in time. The five dimensions of segregation are now discussed in more detail and evaluated for their usefulness and applicability to the field of industrial mixing.

Evenness is the first and simplest definition of "good mixing" - perfect homogeneity of the concentration field. The intensity of segregation measures the deviation from homogeneity at an instant in time. The cleanest measure of evenness in the mixing literature is the ***CoV*** (coefficient of variation) which is the standard deviation over the mean. The spatial statistics literature provides two other measures: ***I***, the index of dispersion, which is the variance of the population relative to the variance of a completely random distribution; and ***D***, the dissimilarity index, which is the fraction of the minor population that would have to move to eliminate segregation and achieve perfect homogeneity. The index of dispersion is interesting, because in a perfectly random Poisson distribution, the variance is equal to the mean (***I*** = variance/mean) and ***I*** = 1 if the distribution is

perfectly random. An index of dispersion, $\boldsymbol{I} < 1$, indicates a more regular or homogeneous distribution, and $\boldsymbol{I} > 1$ when there is significant clustering in the population (Diggle, 2003). This provides a more physically meaningful interpretation of the intensity of segregation, should the user be willing to address the issue of dimensional scaling. In multiphase mixing, evenness is achieved when the second phase is homogeneously distributed over the volume of the vessel. This does not require that the bubbles, drops, or particles be monodisperse or small, only that the volume fraction of the minor phase be the same everywhere. The interaction of the scale of segregation with the scale of measurement remains important: as the size of the dispersed particles increases, the size of the averaging volume must also increase in order to retain a meaningful volume averaged concentration. As in the checkerboard example, a large intensity of segregation contains no information about where the non-homogeneity appears in the vessel, or how large the areas of segregation are. In this case, the intensity of segregation only reveals that the concentration is not uniform.

Clustering appears in the mixing literature as the instantaneous scales of segregation. The study of clustering is well developed in chaotic mixing (Szalai et al., 2004); in population ecology where the clustering of populations is a key indicator of behavior, food sources, and mating (McGarvey et al., 2005; Mugglestone and Renshaw, 2001; Keeling et al., 1997); in geostatistics, where the location of ore bodies from limited data is the main objective (Cressie, 1993), and in image analysis (Mattfeldt, 2005, Anson and Gruzleski, 1999). Measures of clustering include the striation thickness distribution, the stretching distribution, and a family of nearest neighbor methods from spatial statistics. Partial sampling of the scales of segregation in a population can be done using either a transect (line scan) across the volume of interest, or using nearest neighbor analysis over a regular sampling grid. In the past, it was very difficult to obtain enough data to accurately capture all of the scales of segregation in a process, but with increasing resolution in both computational and experimental data, it is now frequently possible to obtain a whole plane of data at quite high resolution, so these methods deserve renewed consideration. In multiphase flow, clustering can characterize

bubble swarms, stratified flow, slugging, and other meso-scale phenomena. Direct measures of clustering may provide the means to quantify these different flow regimes. Drop size, particle size, and bubble size distributions are also measures of the scale of segregation, and where the objective is dispersion of a minor phase to a specific scale of segregation, this dimension defines the process.

Exposure *is* a way of seeing mixing that is implicit in most multi-mechanism models of mixing, but is usually not explicitly addressed. It quantifies the physical contact between two (or more) populations, the strength of interaction between members of the populations (either attractive or repulsive), and the instantaneous departure from the state of maximum mixedness. Together, these terms determine the rate of change of segregation. As an illustrative first example, exposure can be related to Fick's first law for mass transfer:

$$Exposure = N_B = \int_a D_{BA} \nabla C_B \cdot n \, da = \int_V D_{BA} \nabla^2 C_B \, dV \tag{2-4}$$

Where the rate of mass transfer (N_B in moles/s) equals the molecular diffusivity (D_{BA} in m^2/s) times the interfacial area (a in m^2) and the concentration gradient (c_B in $mol/m^3/m$). While the mixing literature is quite distinct from the large literature on mass transfer, the creation of surface area, a, is certainly a key role of mixing equipment. Exposure measures postulated by Wong and others for racial segregation studies also use concentration differences and areas of contact between populations, combined with distance weights and estimated interaction functions between humans (Wong, 2002, 2005). Their interaction function is directly analogous to the molecular diffusivity. In the design of process equipment the objective is mass transfer. Detailed local measurements of area and concentration are usually not possible. The engineering solution is to lump everything into a single empirical mass transfer coefficient, $k_L a$, which depends on the equipment used, and use a single average concentration driving force. Returning to an understanding based on the underlying physics, however, often leads to improved understanding and better designs. Exposure can also be related

to the rate of reaction, drop breakup and coalescence kernels in population balance equations, and the Corrsin model of scalar dispersion by turbulence.

Density is the total population density, or the mass density. It is distinct from the concentration, or fraction, of the minor species. Both total density and concentration may vary locally, as is the case for high density housing in low income areas vs. low density housing in higher income suburbs. In population studies, there may be a correlation between the concentration of a minority group and the total population density, but this is not necessarily the case. The situation is quite different in industrial mixing. In liquid mixing problems, the total population density per volume (eg molecules/ml or kg/m^3) is constant and the density dimension is not useful as a measure of segregation. In multiphase mixing problems, the mass density may vary substantially over the vessel due to spatial variations in the concentration of the dispersed species. Local concentration measurements, however, will exactly track density changes, so the density dimension of segregation does not provide any new and useful information for a definition of segregation in industrial mixing.

Centralization is the tendency of a population to concentrate spatially at some central point. It can be expressed in physical terms as the centroid or the moment of mass. In population studies this has relevance for the location of populations relative to the city center. In terms of process objectives, this dimension of segregation could be calculated for demixing problems in, for example, centrifuges, cyclones, and rotary kilns, but again, it does not add information about the mixing problem beyond the scale and intensity of segregation.

In summary, the first two dimensions of segregation, evenness and clustering, are directly analogous to the intensity and the scale of segregation. Exposure can be related to the rate of mass transfer, reaction, drop breakup, and a number of other phenomena where the mixing field interacts with some other property to achieve a process objective over some elapsed time. Density and centralization are not useful for a definition of segregation in industrial mixing.

Definiton of Segregation in Industrial Mixing

Building on the reviews of mixing and segregation literature, the following definition of industrial mixing is proposed:

Industrial mixing is the control of segregation in unit operations. The instantaneous segregation of a minor species has three dimensions, the intensity of segregation, the scale of segregation, and the rate of reduction in segregation. The intensity of segregation is the uniformity of concentration of the minor species. Intensity of segregation is defined relative to a fixed volume of investigation and scale of measurement. The scale of segregation is the degree of spatial proximity, or clustering, of members of a population, and is inversely correlated with the degree of spatial dispersion of the minor species. The rate of reduction in segregation is determined by the exposure, or potential for reduction in segregation. The exposure is determined by three factors: the deviation from the minimum state of segregation, the physical contact between populations, and the strength of interaction between members of the populations (either attractive or repulsive).

In summary, three variables are needed to characterize the state of segregation:

Intensity of segregation = variance in concentration

Scale of segregation = distribution of length scales

Exposure = rate of change of segregation
= (strength of interaction) × (distance from minimum segregation) ×
× (opportunity to interact)

Before evaluating the definition more closely, the reader may ask why the definitions are useful and important. In any field of study, definitions provide a foundation for the development of questions, theory, and design. In engineering, it is often said that defining the right problem is halfway to the solution. A good definition of mixing forces us to clarify the way we define the field. It will allow us to classify problems more easily, to describe problems more clearly, and to explain mixing problems unambiguously to non-experts. Clear definition naturally leads to fruitful mathematical modeling and more focussed and powerful experimental investigations because it identifies the key variables for a particular unit operation and their place in the problem definition. In short, a strong definition of mixing and segregation will provide clarity, focus and insight for teaching, research, and engineering applications.

Tests of the Adequacy of the Definition

The definition is tested against the three following criteria:

1. A good conceptual definition will clarify what is mixing, and what is not mixing. It will allow problems to be clearly described and classified, with specifications and explanations which are unambiguous.
2. A physically grounded definition identifies the key variables and their place in the problem definition, providing a structure for the design of experiments.
3. A strong theoretically based definition can be expressed as an equation.

The definition of segregation in industrial mixing is now tested conceptually through application to the body of industrial mixing problems, illustrated by application to three test cases, and placed in the context of existing mathematical models of mixing. At each stage, the definition is evaluated for its usefulness, rigor, and completeness using the criteria identified above.

Conceptual

Table 2-1 provides a classification of all of the classical industrial mixing problems in terms of the intensity, scale, and exposure dimensions. Each problem is first identified as either a rate problem, or a state of mixing problem. The dominant dimension of mixing is then highlighted, and all of the important dimensions are marked with an X. Multiphase mixing problems have been grouped together, rather than separating them into gas-liquid, liquid-liquid, solid-liquid, and solid-solid classes. The scale of segregation dimension has been subdivided into the familiar macro- meso- and micromixing subclasses. The physical meaning of these subclasses emerges from exploring the definition of mixing. Macromixing is the volume filling stage of mixing, which takes place at the scale of the vessel. Mesomixing is the scale reduction stage, which in turbulent mixing occurs over the inertial convective scales of turbulence and in laminar mixing occurs over the full range of length scales. Micromixing occurs at the smallest scales of mixing, where molecular diffusivity plays a controlling role in the rate of reduction of segregation. For the applications where the exposure plays a role, Table 2-2 sets out the process objective, the two populations which

interact, and the exposure terms for strength of interaction, minimum segregation, and contact between populations.

Table 2-1. Range of industrial mixing applications with dominant dimension(s) of segregation.

Mixing operation	Process specification		Intensity of segregation ($CoV \rightarrow 0$)	Scale of segregation			Exposure
	State	Timescale		Macro-	Meso-	Micro-	
Blending of miscible liquids							
Turbulent		Blend time	**X**			X	X
Laminar		Blend time	X		**X**	X	X
Non-Newtonian	Caverns fill volume			**X**			
Multiphase mixing							
Size reduction	Specified size	Equilibrium time			**X→**	**X**	X
Just contacted	N_{js}, N_{jd}			**X**			
Homogeneous	N for uniform suspension		**X**		X		
Mass transfer		Dissolution time	X			X	**X**
Mixing sensitive reactions							
Single phase	Minimum by-product or maximum yield	Feed time	X		X→	X	**X**
Multiphase	Minimum by-product or maximum yield	Mass transfer limited	X		X→	X	**X**

* Highlighted values indicated the dominant variable.

Table 2-2. Exposure definitions for mixing applications involving a timescale or rate.

Mixing operation	Process objective	Population 1	Population 2	Strength of interaction given by	Minimum segregation occurs at	Contact of populations is given by
Turbulent blending	$CoV \rightarrow 0$	Minor species	Eddies of major species	Turbulent diffusivity	$CoV = 0$	Time in high ε zone
Laminar blending	Scale $\rightarrow 0$	Minor species	Shear field of major species	Stretching distribution	Scale = 0	Surface area of lamellae
Liquid-liquid dispersion (size reduction)	Specified drop size	Drops of dispersed phase	Eddies of continuous phase	Interfacial tension and attractive forces	Equilibrium drop size	Time in high ε zone
Solids dissolution (mass transfer)	Large exposure $\rightarrow$ MTF	Particles	Eddies of continuous phase	MTF coefficient, k_L	Saturation or complete dissolution	Interfacial surface area, a
Homogeneous reactions	Minimum by-product	Limiting reactant B (feed)	Excess reactant A (bulk)	Competing reaction rates	$CoV = 0$ or scale = 0 or complete consumption of B	Time in high ε zone or surface area of lamellae
Heterogeneous reactions (mass transfer limited)	Minimum by-product	Dispersed species B	Continuous species A	Mass transfer coefficient	Saturation or complete consumption of B	Interfacial surface area, a

Taking the major applications in turn, turbulent blend time is dominated by a reduction in *CoV*. The blend time is defined as the point where the *CoV* drops below a fixed threshold, usually 5% from the perfectly mixed state. The injected minor species is dispersed throughout the vessel through interaction with turbulent eddies. While the mean flow plays a role in the volume filling, or macro mixing stage, it is the inertial convective eddies which reduce the scale of segregation below the required limit. This explains why the Corrsin scaling approach gives a better result for the blend time correlation than a fixed number of tank turnover times.

For laminar blending, the process specification often involves a minimum scale of segregation. Chaotic mixing analysis has repeatedly shown that the stretching distribution function for a particular mixer geometry determines the rate of reduction in scale of segregation (Zalc et al., 2002; Alvarez et al., 1998). Laminar blending is an interesting process specification because the scale of mixing is the process objective, but the exposure determines the length of pipe, or the mixing time, required to achieve that objective. In contrast, cavern formation in yield stress fluids is strictly a macro-scale mixing problem, where the mixer must be designed to eliminate dead volumes in the mixer. No time scales or concentration scales come into play, so the exposure dimension and the intensity of segregation are not interesting.

Multiphase mixing provides the largest challenges to a general definition of mixing, because the mixing objectives are so varied. The first objective of multiphase mixing occurs at the largest scale of mixing. The just contacted objective (just suspended solids, just drawn down buoyant liquids and solids, the point of air entrainment from the head space, and the flooding point of a gassed impeller) identify a macro-scale segregation. The design criterion is the point at which the macro-scale segregation is disrupted, but this is far from the point of complete homogeneity of the second phase. The second objective is the complete dispersion. In this state of mixing, the *CoV* (measured on a meso-scale significantly larger than a single bubble, drop, or particle) drops to zero and the volume averaged concentration is uniform throughout the vessel. The third

objective of multiphase mixing considers size reduction, particularly of liquid drops in emulsions and suspensions, but sometimes also of solids (e.g. milling machines), and possibly of gases in foams. In the drop break-up application, the exposure dimension appears in the breakage and coalescence kernels of population balances, giving the instantaneous rate of change of the drop size distribution as it moves toward the final equilibrium drop size. The strength of interaction between the drops and the turbulent eddies is associated with the turbulent energy dissipation rate, the opportunity for contact between drops and eddies is given by the number of drops in each size, and the distance from equilibrium is associated with the distance from the equilibrium drop size, usually given by some kind of exponential decay function where the probability of a change in drop size gets smaller as the drops approach the final equilibrium size. The process objective is the scale of segregation, but the design specification is the strength of interaction (dissipation, or power per mass) required to achieve a fixed scale of segregation (drop size). The fourth objective identified for multiphase mixing is the mass transfer requirement. In this step, the dissolution time (for solids) or the rate of mass transfer (for liquids and gases) is the key mixing specification, and the exposure is the dominant dimension. When the solids are completely dissolved, the scale of segregation and the intensity of segregation both drop to zero. The rate of mass transfer and the dissolution time are determined by the mass transfer coefficient (the strength of interaction), the interfacial area (contact between phases), and the concentration difference (distance from minimum segregation).

The final class of industrial mixing problems involves mixing sensitive reactions. This is the most varied and complex class of mixing problems, as these reactions typically encompass multiple mixing objectives, often simultaneously. The single phase homogeneous reaction problem is considered first. In this problem, the objective is to minimize by-product formation by ensuring that the reagents are well mixed at a rate that is much faster than the rate of undesired reaction. When meso-scales of segregation are present, more by-product is formed. Increasing exposure quickly and eliminating meso-scales ensures the

success of the mixing operation. The equations for the exposure dimension for homogeneous reactions are discussed in more detail in the next section. Heterogeneous reactions are a second class of mixing sensitive reactions, with most of the more difficult problems limited by mass transfer or contact between the two phases. Once the reaction is mass transfer limited, the exposure dimension reduces to the same terms as discussed earlier under multiphase mass transfer, with the added possibility of having zero concentration in the continuous phase if the reaction goes to completion as soon as the dispersed species B is able to contact with the bulk species A.

Heat transfer in mixing vessels is not consistent with this definition of mixing problem, because no minor species is present. All of the core problems identified in Chapters 9-15 of the Handbook of Industrial Mixing (2004) are encompassed by the new definition, thus satisfying criterion 1. The definition provides a clearer focus for identifying the key design criteria, and also allows us to consider secondary design criteria and primary variables in the problem definition.

Physical and Experimental

Three quantitative examples have been chosen to illustrate the dimensions of segregation. The first two focus on blending problems, the first for turbulent dispersion of dissolving particles in a stirred tank, where the intensity of segregation dominates, the second is the maximum striation thickness in a laminar micromixer, and the third is the break up and dissolution of dissolving drops in a stirred tank, where the exposure dimension is of greatest interest. These three examples illustrate the different approaches to analysis of mixing problems that can be taken when different dimensions of segregation dominate. They also illustrate how the three dimensions interact in practical applications.

Intensity of Segregation

Figure 2-5 shows the reduction in intensity of segregation for turbulent dissolution of particles in a tank (Hartmann et al., 2006). The last four images illustrate the reduction in scale of segregation (mesomixing), while the first two

clearly illustrate the volume filling stage (macromixing). Time steps beyond sixty rotations of the impeller complete the micromixing and dissolution stage. The *CoV* analysis is reported more extensively in Kukukova et al. (2008). Considering the scale of segregation in parallel with the intensity of segregation reveals the sensitivity of *CoV* to the scale of measurement. Note that the reduction in *CoV* is very rapid for macromixing, but slower for mesomixing. Attempts to track the scale of segregation for this problem were less successful because turbulent dispersion rapidly smears out striation boundaries.

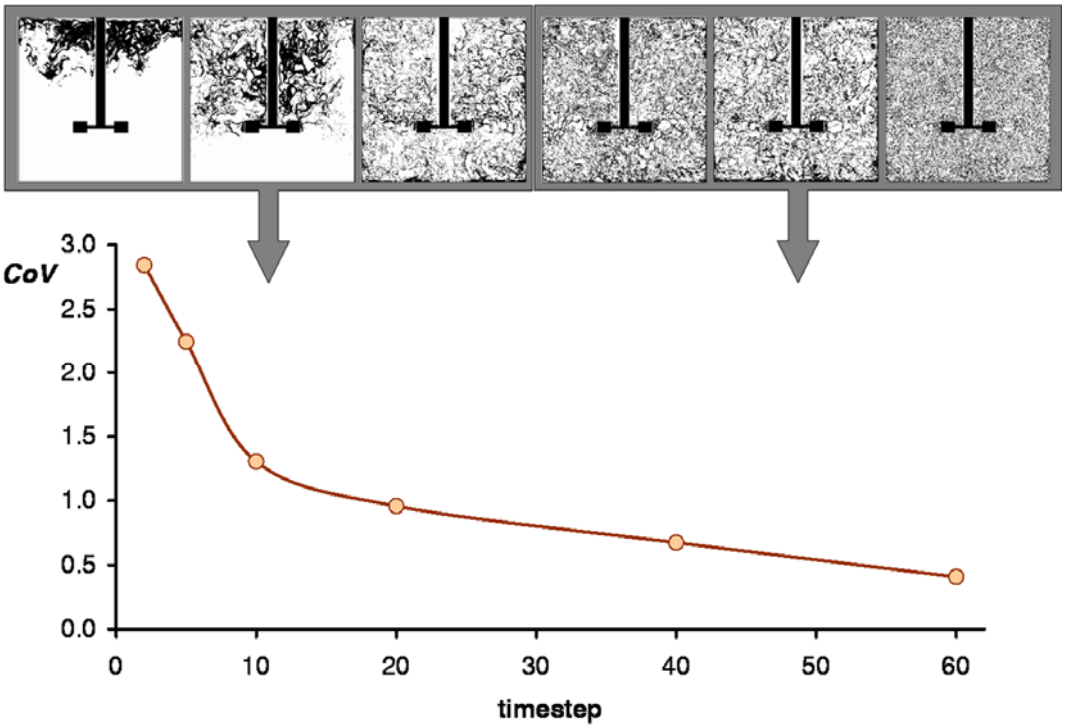

Figure 2-5. Turbulent dissolution in a stirred tank: two-stage process showing the volume filling, or macromixing stage, and the scale reduction, or mesomixing stage.

Scale of Segregation

Figure 2-6 illustrates the importance of the scale of segregation in laminar mixing. For this work (Aubin et al., 2005), the *CoV* was not able to accurately track the differences in performance for three different micromixers, but a transect of the striation thicknesses shows the smooth reduction in maximum striation thickness (*s*) and accurately characterizes the different mixers. In this case, the

volume filling and scale reduction stages occur simultaneously, so the mesoscale dominates. Because the mixing is laminar, the striations remain coherent and accurate measurement of the *CoV* requires measurement resolution at the scale of individual striations. As the smallest scales of segregation shrink, this becomes impractical.

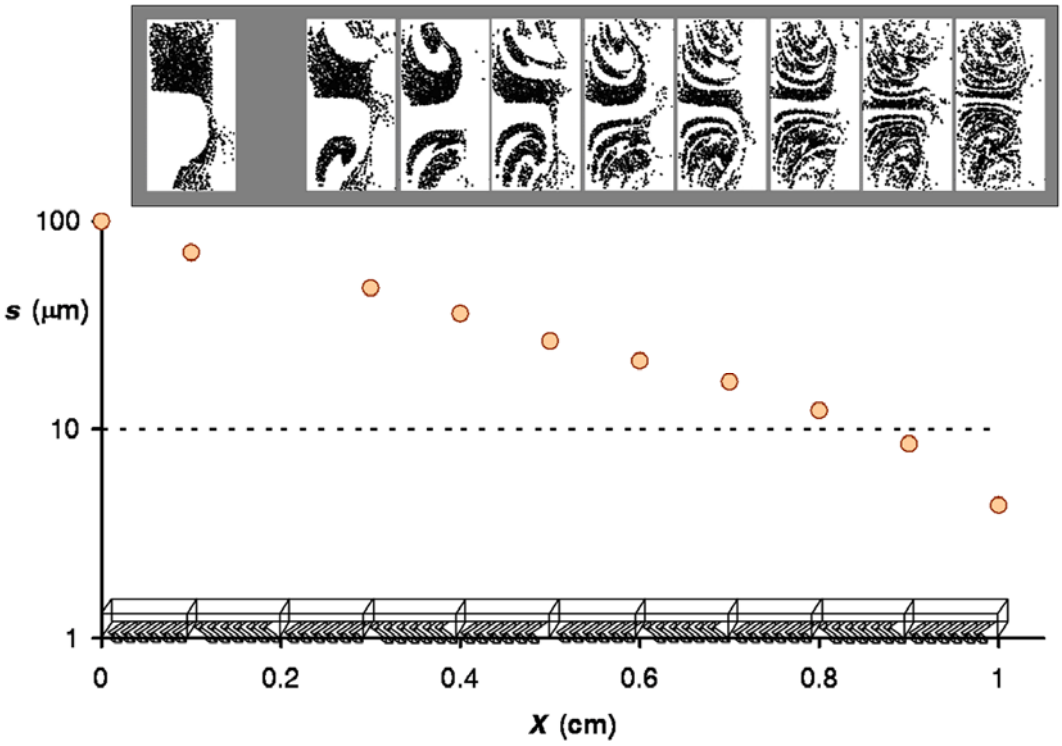

Figure 2-6. Maximum striation thickness (s) on a transect for a laminar micromixer.

Exposure

Figure 2-7a illustrates the interaction of the three dimensions of segregation in a mixing and dissolution problem. In this example, an additive is injected close to the impeller. The amount injected is equal to the solubility limit of the additive. On each pass through the impeller, the drop size is reduced, initially very rapidly, but then much more slowly as the equilibrium drop size is approached. As the drops travel through the bulk of the tank, they dissolve and the bulk concentration in the tank increases. Figure 2-7b shows snapshots of the volume of fluid as time progresses. The steps (1→2, 3→4, 5→6, and 7→8) show drop break-up at the impeller. The steps (2→3, 4→5, 6→7, 8→9 and 9→10) show dissolution in the

bulk. The values for time, drop size, *CoV*, and exposure are given in the table below, and then plotted in Figure 2-7c. The values for drop size and dissolution rate used for this illustrative example are based on the work by Ibemere and Kresta (2007).

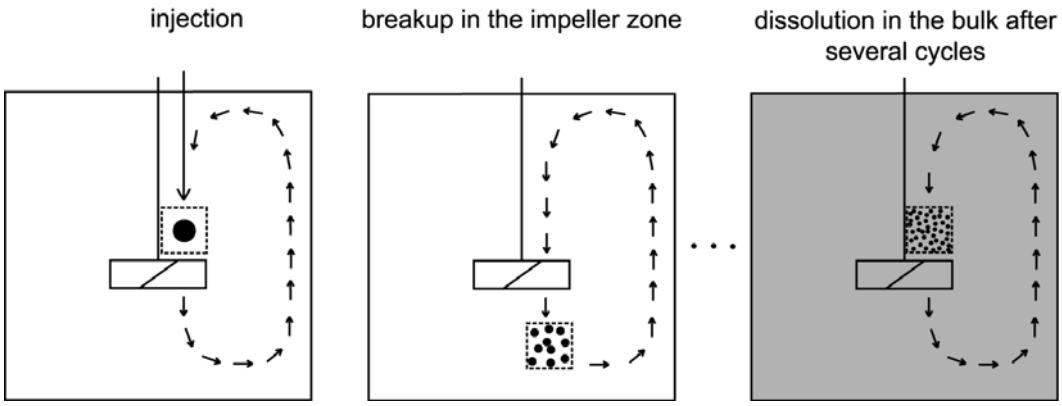

Figure 2-7a. Progress of an injected additive as drops break up and dissolve over time. Drop break-up is restricted to the impeller zone, and dissolution is restricted to the bulk.

In this example, the intensity, scale, and rate of change of segregation all drop to zero over time. The scale drops in a stepwise way, the *CoV* drops off smoothly, and the exposure shows a sawtooth behavior as the concentration difference drops, but the interfacial area increases. On the first pass through the impeller, the exposure more than doubles from its initial value and stays quite high over most of the dissolution time. As the drops approach their equilibrium size, the functions for both scale and exposure become smoother. This complicated interaction between drop size reduction and concentration difference may explain the wide variation in the drop size exponent reported in liquid-liquid mass transfer correlations for stirred tanks (Ibemere, 2005).

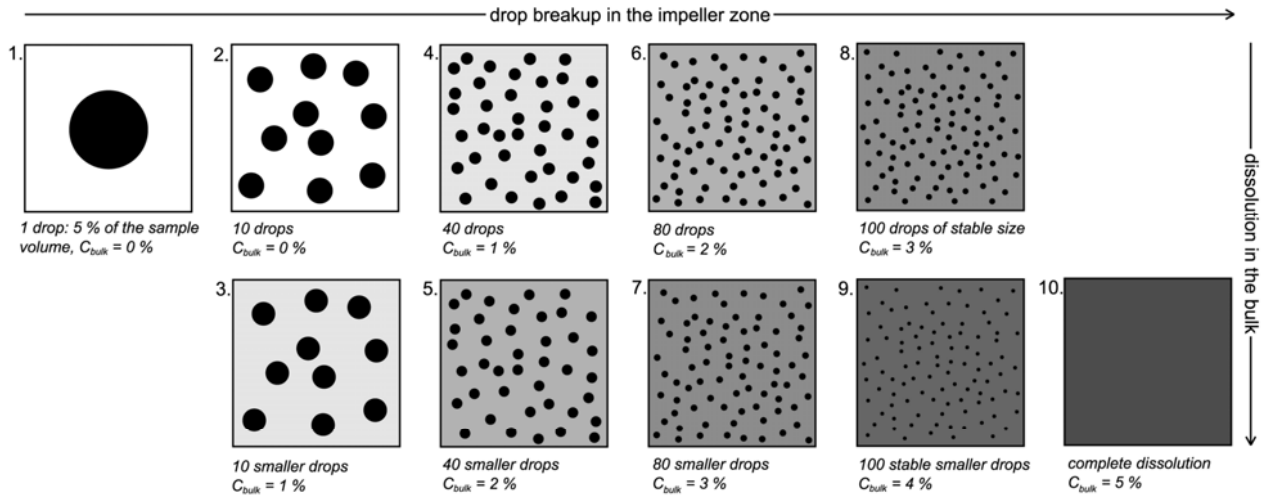

time (s)	0	0.09 5.38	5.47 10.77	10.85 16.15	16.24 24.54	∞
drop size/scale of segregation (μm)	457	212 197	124 113	89 78	73 58	0
CoV (-)	4.36	4.36 0.68	0.68 0.24	0.24 0.09	0.09 0.02	0
exposure x 10^7 (kg/s)	3.28	7.07 4.87	7.74 4.79	6.03 3.07	3.31 1.04	0

Figure 2-7b. Snapshots of the sample volume over the dissolution process. Dissolution steps are from the top row to the bottom row, and the corresponding values of time, drop size, *CoV*, and exposure are given in the table.

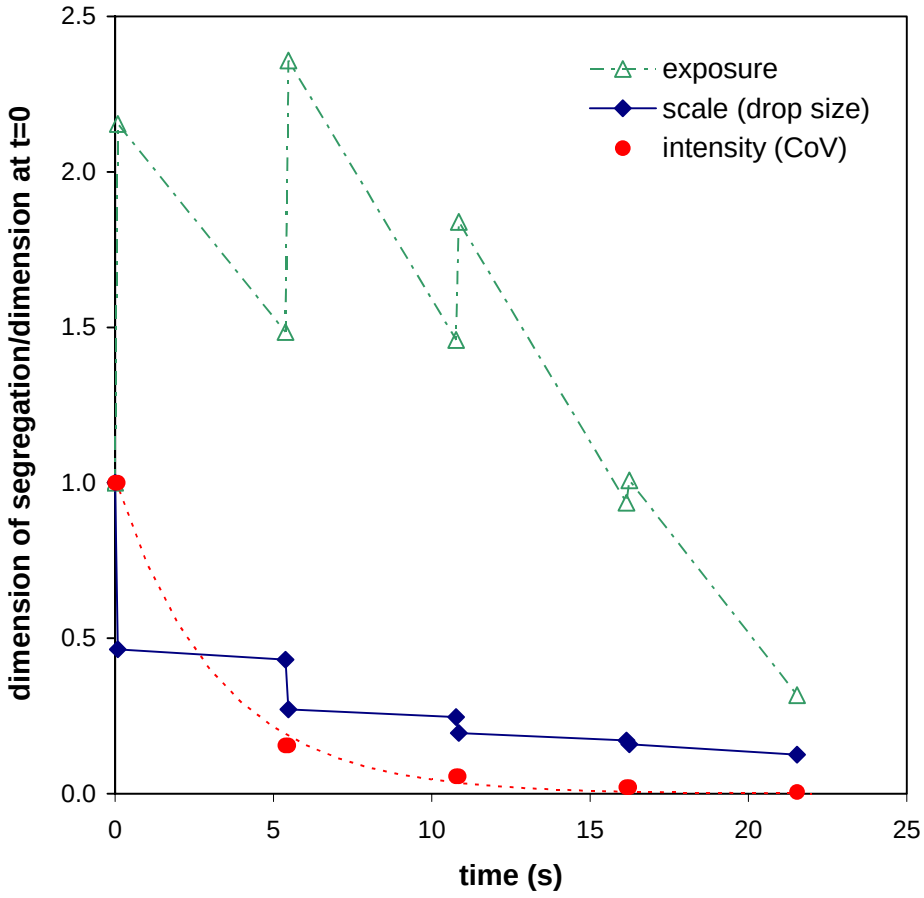

Figure 2-7c. Comparison of the scale, intensity, and rate of change of segregation as they change over time, all normalized with the initial values in step 1.

Mathematical

Criterion 3 requires that the three dimensions of mixing have direct translations to physically meaningful equations which describe industrial mixing problems. The full range of equations that have been proposed to describe the dimensions of segregation across all mixing applications is enormous, with new attempts appearing in the literature on a regular basis. The reader is referred to individual review papers and texts presented earlier in the paper for the full mathematical details of specific applications. In this section, the objective is to illustrate how the core concepts of the dimensions of segregation consistently appear in the most successful model equations.

Taking the three dimensions in turn, the intensity of segregation is described by Equation 2-2 for the CoV. Many other variations of a coefficient of variation have been proposed in the literature. All of the equations contain the same essential features, with the key differences being the variable used to normalize the variance, and whether the variance or the standard deviation is reported. Kukukova et al. (2008) have discussed the impact of sampling on the value of CoV, and considered the impact of the classical MAUP (modifiable areal unit problem) on measurements of the variance in mixing applications. Both of these principles, developed for other applications of segregation, provided new insights for the measurement of mixing.

The scale of segregation is a rich problem with more work needed on mathematical descriptions of the scale of segregation, particularly now that experimental techniques and computational power are able to capture the full complexity of coupled multiscale mechanisms. Early researchers (e.g. Danckwerts, 1952 and Lacey, 1976b) recognized methods that can only recently be fully exploited as experimental data moves to high resolution full field instruments. As these new instruments come into play, the field of spatial statistics provides a rich new selection of measures and methods that can extract useful information in a mathematically sound way (see the review under Clustering in section 4 for references). Diffusion and turbulence lead to systems where the

concentration varies continuously and the edges of striations are diffuse rather than sharp. In many of these problems, it will be the time scale related to the reduction in segregation, rather than the scale of segregation, which is the defining variable. Equations exist to describe both the diffusing case (Danckwerts, 1952, Cressie, 1993). The timescale, or exposure dimension, is discussed below.

The reader may also legitimately ask what is to be done with the full spectrum of scales of segregation often observed in realistic problems. First, the physics often offers an elegant simplification, returning self-similarity in drop size distributions (Mishra et al., 1998), striation thickness distributions and stretching distributions (Alvarez et al. 1998; Hobbs and Muzzio, 1998), aggregate and crystal size distributions (Marchisio et al 2003 a, b) and many others. This means that given an initial distribution and the correct scaling parameters over time (e.g. decay of the mean drop size), the distributions all collapse onto a single line. This enormously simplifies the modelling and computational demands, since the complete distribution can be tracked using a small number of variables (e.g. Marchisio et al., 2003 a, b). The scale of segregation is increasingly used as a specification for consumer products, cosmetics, crystals, polymer composites, and some pharmaceuticals, so the industrial need for solutions will undoubtedly drive further research in this area.

Finally, the rate of change of segregation, or the exposure dimension, appears in many existing models of mixing processes. Typical mixing variables are related to the exposure dimension in Table 2-2. Taking three illustrative examples from mass transfer, population balances, and the reaction-diffusion equation, the model equations are shown to follow the form of the exposure definition:

1. **Mass transfer**: in this case, the exposure is related to the flow of component A in moles/s through the standard diffusion equation:

$$Exposure = \int_A D_{AB} \nabla c_A \cdot n \quad dA \tag{2-5}$$

The diffusivity D_{AB} is the strength of interaction, or the willingness of the two populations to interact; the minimum segregation is complete homogeneity and

the concentration gradient ∇c_A gives the distance from minimum segregation; and the interfacial area, A provides the opportunity for molecules to interact. Note that A is not always the surface of a sharp striation, but can also be the surface of a computational cell or control volume of interest where the concentration varies continuously throughout the system.

2. **Population balances**: the literature on population balance modeling is extensive, and has applications over a wide range of processes. The general form of the population balance for a flow system is (Paul et al, 2004):

$$\frac{\partial n_d}{\partial t} + \nabla.(\bar{U} n_d) - \dot{B}_d + \dot{D}_d = 0 \qquad (2\text{-}6)$$

where n_d is the number of drops or particles being balanced, so the first two terms are the accumulation and convection terms, and $\dot{B}_d$ and $\dot{D}_d$ are the birth and death rates, respectively. The exposure dimension is found in the birth and death terms of the population balance. To illustrate this, three examples of the birth or death terms in drop breakup, aggregation kinetics, and crystallization are examined in more detail.

a) **Drop breakup** (*Ibemere, 2007*):

$$Death\ term = -\sum_{j=1}^{i-1} \frac{1}{2} \frac{-2.4738(1-\phi)}{b^{8/11}} \left(\frac{\varepsilon}{L_j^2} \right)^{1/3} \begin{Bmatrix} \left[\Gamma(8/11, t_m) - \Gamma(8/11, b)\right] + \\ +2b^{3/11}\left[\Gamma(5/11, t_m) - \Gamma(8/11, b)\right] + \\ +b^{6/11}\left[\Gamma(2/11, t_m) - \Gamma(2/11, b)\right] \end{Bmatrix} \Delta L_j \times N(L_i, t) \qquad (2\text{-}7)$$

The death term of this drop breakup model represents the death by drop breakage. By close examination of the expression, all three components of exposure can be observed. The term in front of the curly brackets combines the physical properties of drops, the dispersion characteristics and the hydrodynamic conditions to find the strength of interaction; the term inside the brackets and including ΔL_j represents the distance from the equilibrium drop size with the gamma function showing how the drops are increasingly likely to break when they are much larger than the equilibrium drop size; and the number of drops of size *i,* present at time *t*

($N(L_i,t)$) determines the opportunity for drops to interact with the flow and break up.

b) **Aggregation kinetics** (*Lattuada, 2004*):

$$Birth\ term = \frac{1}{2}\sum_{j=1}^{i-1}\frac{8kT}{3\eta W}\frac{\left(i^{1/D_f}+j^{1/D_f}\right)\left(i^{-1/D_f}+j^{-1/D_f}\right)}{4}N_{i-j}(t)N_j(t) \tag{2-8}$$

In this example of aggregation kinetics, the birth by aggregation also has a form of exposure. The first fraction term again represents the strength of interaction by including the fluid physical properties, temperature and hydrodynamic and Van der Waals interactions in the system. The second fraction term contains the fractal dimension D_f, together with the sizes of interacting clusters (i and j are the numbers of particles in the cluster) which defines the distance from aggregate equilibrium size. The last term describe the number of clusters of particular sizes in the system ($N_{i-j}(t)N_j(t)$) and quantifies the opportunity clusters have to interact with each other.

c) **Crystallization** (*Sato, 2008*):

$$Death\ term = k_{imp}\frac{\rho_S n_r^3 D_r^5}{V}L_1^2 L_2 \times \frac{1}{2}\left(\tanh\left(k\left(\frac{L_2}{L_1}-AR_{tr}\right)\right)+1\right)\times n(L_1,L_2) \tag{2-9}$$

This death term represents the death by breakage of crystals with width $L_1$and length L_2. All exposure components can be again found in this expression. The strength of crystal interaction is given by the hydrodynamic conditions in the system described by the impeller diameter and rotational frequency, properties of the mixture like crystal dimensions, crystallizer volume V and crystal density, all included in the first term before the multiplier. The middle term describes the distance from equilibrium crystal size: AR_{tr} is the threshold aspect ratio and crystals are only prone to breakage when their aspect ratio exceeds this value; the *tanh* function again adds the increasing probability for breakage as the crystal size

moves further away from the equilibrium point. The last term, the number of crystals, again quantifies their opportunity to meet and interact.

3. Reaction Kinetics

When studying the mixing time scale for reactions, two types of exposure can be identified. When all reactants are present in sufficient quantities and the only concern is to get them into molecular contact in order for the reaction to proceed, the reaction is mass-transfer limited and the exposure expression that dominates this problem is the mass transfer exposure defined in 1. If, on the other hand, reactant A is limiting e. g. for a reaction

$$A + B \xrightarrow{k} Products\ ,\ c_A \to 0 \qquad (2\text{-}10)$$

the reaction rate is integrated over the volume of the reactor to obtain the expression for exposure, which in this example is also the rate of consumption of species A, where B is present in large excess:

$$Exposure = \int_V k \cdot c_A \cdot c_B dV \qquad (2\text{-}11)$$

Here, the strength of interaction is represented by the rate constant k, the concentration of reactant A, c_A, is the distance from the equilibrium state with the reaction no longer proceeding after the reactant A has been depleted, and the concentration of reactant B, c_B, is the opportunity for reactants to interact if A is present. The field of mixing sensitive reactions is a complex one, with no consideration given here to the question of continuous systems with the added complication of backmixing in time. From a mathematical perspective, this is treated as a fourth dimension in the data, but the practical application of this fourth dimension can be very challenging.

The reaction rate equation, break up and coalescence kernels in population balance equations for crystals, aggregates, and drops, Corrsin's model for the dispersion of scalar in a turbulent mixing field, and as illustrated in this paper, the mass transfer equation, all follow the form suggested by the definition of exposure. Additional examples are available in a number of detailed models

where direct computation of the interaction between the scale and intensity of segregation with reaction and/or mass transfer have been carried out through high resolution computations (see Fox, 2003; Kresta et al., 2004; Alvarez et al, 1998, and many others). More work is warranted here, particularly using experimental data where the key scales of segregation can be measured. The concept of exposure provides a clearer path to model development and validation, and may help to identify the problems where detailed modeling of many scales with coupled mechanisms will prove most productive.

Conclusions

A definition of industrial mixing is proposed based on three dimensions of segregation: intensity of segregation (concentration scale), scale of segregation (length scale), and exposure (rate of change of segregation). A series of checkerboard patterns are used to illustrate the three dimensions. These variables are well established in the fields of spatial statistics, population ecology, and population segregation both conceptually and mathematically, and provide an expanded theoretical and experimental toolkit for the analysis of mixing problems.

The proposed definition satisfies three criteria for a good definition: conceptual, physical and mathematical; and provides a direct path from the definition to equations and measurements. Three examples are used to illustrate how the definition can improve our understanding of mixing problems. The first two examples clarify the distinction between macro- meso- and micromixing, and highlight the utility of considering the scale of segregation instead of intensity of segregation for laminar mixing problems. The exposure dimension is introduced through an example of drop break up and dissolution, showing both the distinct behavior of exposure, and its dependence on the scale and intensity of segregation. The exposure dimension is essential for mixing problems that are dominated by a mixing time scale, such as mixing sensitive reactions and mass transfer.

Given a strong definition, the physical phenomena and process objectives can be framed in ways that match both the complexity of the problem and our intuitive understanding. This provides clarity, focus, and insight for teaching, research, and engineering applications. While this definition may subsequently prove to be incomplete or require clarification, it is our hope that it is general enough to encompass the full range and complexity of industrial mixing problems, but specific enough to be clear.

References

Alvarez, M. M.; Muzzio, F. J.; Cerbelli, S.; Adrover, A. and Giona, M., 1998, *Self-Similar Spatiotemporal Structure of Intermaterial Boundaries in Chaotic Flows*, Phys. Rev. Let., **81**, 3395.

Anson, J.P. and Gruzleski, J.E., 1999, *The Quantitative Discrimination between Shrinkage and Gas Microporosity in Cast Aluminum Alloys Using Spatial Data Analysis,* Materials Char., **43**, 319-335.

Aubin, J.; Fletcher, D.F. and Xuereb, C., 2005, *Design of micromixers using CFD modelling,* Chem. Eng. Sci*.,* **60,** 2503-2516.

Baldyga, J. and Bourne, J.R., 1999, Turbulent Mixing and Chemical Reactions, Wiley.

Bhattacharya, S.; Hebert, D. and Kresta, S. M., 2007, *Air Entrainment in Baffled Stirred Tanks*, Chem. Eng. Res. Des., **85**, 654-664.

Corrsin, S., 1957, *Simple theory of an idealized turbulent mixer*, AIChE J*.,* **3**, 329-330.

Corrsin, S., 1964, *The Isotropic Turbulent Mixer .2. Arbitrary Schmidt Number*, AIChE J., **10**, 870-877.

Cressie, N., 1993, *Statistics for Spatial Data*, Wiley, New York.

Danckwerts, P. V., 1952, *The Definition and Measurement of Some Characteristics of Mixtures*, Appl. Sci. Res. A, **3**, 279-296.

Danckwerts, P.V., 1958, *The effect of incomplete mixing on homogeneous reactions*, Chem. Eng. Sci., **8**, 93-102.

Diggle, P.J., 2003, *Statistical Analysis of Spatial Point Patterns***,** Hodder Arnold, London.

Fox, R.O., 2003, *Computational Models for Turbulent Reacting Flows,* Cambridge University Press, New York.

Gates, L. E.; Fenic, J. G. and Henley, T. L, 1975, *How to Select the Optimum Turbine Agitator,* Chem. Engg., December 8, 110-114.

Harnby, N, 1967, *A comparison of the performance of industrial solids mixers using segregating materials,* Powder Technol., **1**, 94-102.

Hartmann, H; Derksen, J. J. and Van den Akker, H. E. A., 2006, *Numerical simulation of a dissolution process in a stirred tank reactor,* Chem. Eng. Sci., **61**, 3025-3032.

Hersey, J. A., 1970, *Sampling and assessment of powder mixtures for cosmetics and pharmaceuticals,* J. Soc. Cosmetic Chem., **21**, 259-269.

Hobbs, D. M. and Muzzio, F. J., 1998, *Reynolds number effects on laminar mixing in the Kenics static mixer*, Chem. Eng. J., **70**, 93-104.

Ibemere, S. and Kresta, S. M., 2007, *Modeling the Mixing and Dissolution Kinetics of Partially Miscible Liquids,* Chem. Eng. Res. Des., **85**, 710-720.

Ibemere, S., 2005, *Dissolution Kinetics of Liquid-Liquid Dispersions using Local Rates of Turbulent Dissipation*, MSc. Thesis, University of Alberta, Canada.

Keeling, M.J.; Mezic, I; Hendry, R.J.; McGlade, J. and Rand, D.A., *Characteristic length scales of spatial models in ecology via fluctuation analysis,* Phil. Trans. R. Soc. London B, **352**, 1589-1601.

Kresta, J. V.; MacGregor, J. F. and Marlin, T. E., 1991, *Multivariate statistical monitoring of process operating performance,* Can. J. Chem. Eng., **69**, 35-47.

Kresta, S.M; Anthieren, G.L. and Parsiegla, K., 2004, *Mixing Effects in Silver Halide Precipitation: Linking Theory with Practice using a Multi-Mechanism Model,* Chem. Eng. Res. Des., **82,** 1117-1126.

Kukukova, A.; Shah, S. I. A.; Aubin, J. and Kresta, S. M., *Quantifying Mixing: The Exposure Dimension,* 6th International Symposium on Mixing in Industrial Processes, Niagara Falls, August 17-21, 2008.

Kukukova, A.; Noel, B.; Kresta, S. M. and Aubin, J., 2008, *Impact of Sampling Method and Scale on the Measurement of Mixing and the Coefficient of Variance,* AIChE J., **54**, 3068-3083.

Lacey, P. M. C., 1954, *Developments in the theory of particle mixing I,* J. Appl. Chem., **4**, 257-268.

Lacey, P. M. C. and Mirza, F. S. M. A., 1976, *A study of the structure of imperfect mixtures of particles. Part I Experimental Technique,* Powder Technol., **14**, 17-24.

Lacey, P. M. C. and Mirza, F. S. M. A., 1976, *A study of the structure of imperfect mixtures of particles. Part II Correlational Analysis,* Powder Technol., **14**, 25-33.

Lattuada, M.; Wu, H.; Sandkuhler, P.; Sefcik, J. and Morbidelli, M., 2004, *Modelling of aggregation kinetics of colloidal systems and its validation by light scattering measurements,* Chem. Eng. Sci., **59**, 1783-1798.

Lee, J. and Brodkey, R. S., 1964, *Turbulent Motion and Mixing in a Pipe*, AIChE J., **10**, 187-193.

Marchisio D. L.; Vigil, R. D. and Fox, R. O., 2003, *Quadrature method of moments for aggregation-breakage processes*, J. Coll. Int. Sci., **258**, 322-334.

Marchisio D. L.; Pikturna, J. T. and Fox R. O., 2003, *Quadrature method of moments for population-balance equations*, AIChE J., **49**, 1266-1276.

Massey, D.S. and Denton, N.A., 1988, *The Dimensions of Residential Segregation,* Social Forces, **67**, 281-315.

Mattfeldt, T., 2005, *Explorative statistical analysis of planar point processes in microscopy,* J. Microscopy, **22**, 131-139.

McGarvey, R; Byth, K.; Dixon, C. D.; Day, R.W. and Feenstra, J. E., 2005, *Field Trials and Simulations of Point-Nearest-Neighbor Distance Methods for Estimating Abalone Density,* J. Shellfish Res., **24**, 393-399.

McKelvey, K.N.; Yieh, H. N.; Zakanycz, S. and Brodkey, R. S., 1975, *Turbulent motion, mixing and kinetics in a chemical reactor configuration*, AIChE J., **21**, 1165-1176.

Mishra, V.; Kresta, S. M. and Masliyah, J. H., 1998*, Self-Preservation of the Drop Size Distribution Function, and Variation in the Stability Ratio for Rapid Coalescence of a Polydisperse Emulsion in a Simple Shear Field*, J. Colloid and Interface Sci., **197**, 57-67.

Mohr, W.D.; Saxton, R.E. and Jepson, C.H., 1957, *Mixing in Laminar Flow Systems,* Ind. Eng. Chem., **49**, 1855-1856.

Mugglestone, M.A. and Renshaw, E., 2001, *Spectral tests of randomness for spatial point patterns,* Env. and Ecol. Stat., **8**, 237-251.

Ottino, J.M., 1989, *The Kinematics of Mixing: Stretching, Chaos, and Transport*, Cambridge University Press, New York.

Paul, E.L.; Atiemo-Obeng, V.A. and Kresta, S.M. (Editors), 2004, *Handbook of Industrial Mixing: Science and Practice*, John Wiley & Sons, Inc., New Jersey, USA.

Sato, K.; Nagai, H.; Hasegawa, K.; Tomori, K.; Kramer, H. J. M. and Jansens, P. J., 2008, *Two-dimensional population balance model with breakage of high aspect ratio crystals for batch crystallization*. Chem. Eng. Sci., **63**, 3271-3278.

Szalai, E.; Alvarez, M. and Muzzio, F. J., *Laminar Mixing: A Dynamical Systems Perspective*, Chapter 3 in Paul et al., 2004.

Toor, H.L., 1969, *Turbulent mixing of two species with and without chemical reaction,* I&E C. Res., **8**, 655-659.

Wong, D. W., 2002, *Modeling local segregation: a spatial interaction approach,* Geog. Env. Modelling, **6**, 81-97.

Wong, D. W., 2005, *Formulating a general spatial segregation measure,* The Professional Geographer, **57,** 285-294.

Zalc, J. M., Szalai, E. S., Muzzio, F. J. and Jaffer, S., 2002, *Characterization of flow and mixing in an SMX static mixer,* AIChE J., **48**, 427-436.

Zweitering, T.H., 1959, *The degree of mixing in continuous flow systems,* Chem. Eng. Sci., **11,** 1-12.

Chapter 3: Impact of Sampling Method and Scale on the Measurement of Mixing and the Coefficient of Variance*

Introduction

Many measures of mixing have been proposed in the literature, including mixing entropy (Ogawa, 2007), various dimensions of chaotic flows (Ottino, 1989; Szalai et. al., 2004), Bourne reaction models (Baldyga and Bourne, 1999), and population balance modeling (Ramkrishna, 2001; Fox, 2003). In this paper, it is not our intent to review all of these methods in detail, but rather to focus on the accurate determination of two measures of mixing: the *CoV*, which is used directly for the design of static mixers, and indirectly for determination of the blend time in stirred tanks, and the maximum striation thickness on a transect, which is of significant interest as a contrasting measure, particularly for laminar mixing (Aubin et. al., 2005).

Dankwerts (Danckwerts, 1958) defined two extreme states of mixedness: complete and instantaneous mixing on the molecular scale, where each molecule experiences the same environment at all times, and complete segregation. Dankwerts gives a description of complete segregation, "The incoming fluid is broken up into discrete fragments or streaks which are small compared to the tank and uniformly dispersed in it, but in which molecules entering together remain together indefinitely…" This might be physically realized as drops of one component, A, and a second component, B, both suspended in an inert medium in which they are both completely insoluble and where no coalescence can occur. In the completely segregated case, the size of the drops does not matter, but in many real flows and practical applications the size of the segregated regions is critically important, and molecules are neither completely segregated nor perfectly mixed. Moreover, real times greater than zero and smaller than infinity are of interest.

*A version of this chapter has been published in AIChE Journal, 54 (2008), p. 3068-3083.

Dankwerts' initial ideas eventually evolved into the definition of various mixing scales which are now widely used in the mixing literature. Macromixing is identified with the scale of the equipment, e.g. the tank diameter, and with the blend time. Mesomixing occurs at intermediate scales and is identified primarily with reaction effects due to mixing limitations in the feed plume. Micromixing is identified with the smallest scales of motion and concentration segregation, where molecular viscosity and diffusivity dominate. These definitions have proven difficult to explain to non-experts, which suggests that their current formulation is somewhat less than crystal clear. This difficulty is partly due to the differences between mixing in turbulent flows and mixing in laminar flows. In this paper, the two regimes are compared side by side to highlight the differences and similarities in their behavior.

Turbulent mixing is a complex multiscale process ranging from macromixing on the scale of the vessel, usually characterized as the blend time, to micromixing on the scale of the smallest eddies, often characterized using the Kolmogorov time scale, or the engulfment rate (Baldyga and Bourne, 1999). Turbulence is three dimensional, random, and time varying, and is normally characterized using the local mean and rms (standard deviation) of the velocity and concentration. A statistical approach is therefore a natural fit to the characterization of turbulent mixing, and point-based statistics collected over time have been applied to turbulent mixing for many decades.

Laminar mixing is ultimately limited by molecular diffusion. For efficient mixing, the fluids must be manipulated to increase the interfacial area and decrease the thickness of fluid lamellae in order to promote diffusional mixing. Laminar mixing measurements need to be able to resolve the fine structures of the fluid lamellae. Some spatial statistics and similarity analyses have been applied to this problem, but characterization methods that are both practical and powerful are still a subject of active research (Arratia and Gollub, 2005).

The field of spatial statistics (Diggle, 2003) includes applications ranging from population ecology to the study of human populations, disease, and racial

segregation, to forestry and geostatistics. All of these applications have one thing in common: the underlying data has a complex pattern, and the local concentration of each species is of interest for understanding the problem. Spatial statistics provides a set of knowledge not previously applied to mixing problems in the field of chemical engineering. Two principles are of particular interest. First, mixing is a multidimensional problem which cannot be completely characterized with a single variable, or dimension. Second, the goal of statistical analysis is to extract the maximum information from the minimum amount of data. The penalty to be paid for this efficient use of data is that the sampling method becomes very important.

From a review of the wide ranging literature on spatial statistics, three dimensions of segregation emerge as important to the study of mixing in chemical processes: the scale of segregation, the intensity of segregation, and the exposure (Kresta and Aubin, 2006). The scale of segregation is most easily defined for this paper as the striation thickness distribution. The intensity of segregation is directly related to the *CoV*. The exposure dimension is related to the ease and rate of reduction in segregation but is not of interest for this paper. A simple thought experiment is used to illustrate the importance of distinguishing between the intensity and scale of segregation. Taking a square that measures 16 mm × 16 mm, consider two mixing fields: in the first, there are four squares which measure 8 mm × 8 mm each, two of them black and two of them white; in the second, there are 256 squares each measuring 1 mm × 1mm, again, half black and half white. Both fields are arranged in a checkerboard pattern. We might quickly conclude that the mixing is better in the second case because the scale of segregation has been reduced by a factor of 8, but calculation of the *CoV* will return exactly the same result for both mixing fields. The intensity of segregation is independent of how the squares are arranged. Further exploration of this example shows that the scale of averaging used to calculate the *CoV* can also dramatically affect the result (Kresta and Aubin, 2006).

In this work, two test cases were used to evaluate two measures of "well-mixed": the *CoV*, which characterizes the intensity of segregation, and the

maximum striation thickness, which characterizes the scale of segregation. The objectives of the investigation are:

1. to explore the data density and sampling protocols needed to get accurate measures of CoV for two ideal data sets,
2. to explore the data density needed to get an accurate measure of striation thickness for the same data sets,
3. to compare the CoV and the maximum striation thickness for laminar mixing at a very small scale and turbulent mixing at a relatively large scale to better understand the strengths and weaknesses of each approach.

Before detailing the test cases and the sampling experiments which were performed, the definitions and background theory for the coefficient of variance and for the three sampling strategies of interest are reviewed.

Definition of the Coefficient of Variance

Two quantities are widely used in the mixing literature to evaluate the intensity of segregation: the blend time for batch stirred tanks and the decay of the coefficient of variance (CoV_{r}) in continuous static mixers. Both measures are evaluated from concentration measurements at several locations.

The batch blend time is based on the decay of the *normalized* concentration variance:

$$\sigma_M^2(t) = \frac{1}{M}\sum_{m=1}^{M}\left(\frac{C_m - C_{m,0}}{\overline{C} - C_{m,0}} - 1\right)^2 \qquad (3\text{-}1)$$

where $C_{m,0}$ is the initial concentration at probe m, C_m is the concentration at time t, $\overline{C}$ is the average concentration for a homogeneous mixture and M is the number of measurement locations. When the initial concentration is zero at all measurement locations, Equation 3-1 reduces to:

$$\log\left(\sigma_M^2\right) = \log\left[\frac{\sum_{m=1}^{M}\left(C_m - \bar{C}\right)^2}{M\bar{C}^2}\right] \tag{3-2}$$

The blend time is defined as the time when $\sigma_M^2 = 0.0025$ and $\log\sigma_M^2 = -2.6$, which is a 95% approach to the perfectly mixed state (Brown et. al., 2004).

The second measure of intensity of segregation is known as the *CoV*, or the coefficient of variance. This criterion is usually applied to static mixers, particularly for laminar blending applications. The *CoV* is the ratio of the standard deviation of the concentration measurements to the mean concentration (Etchells and Meyer, 2004), and it is exactly equal to the square root of the blend time variance decay criterion:

$$CoV = \frac{\sigma}{\bar{C}} = \frac{\sqrt{\frac{1}{M}\sum_{m=1}^{M}\left(C_m - \bar{C}\right)^2}}{\bar{C}} = \sigma_M \tag{3-3}$$

In this case, a well mixed threshold corresponding to 95% of the perfectly mixed state can also be set such that $\sigma_M^2 = 0.0025$.

Laminar static mixer data for a well designed mixer typically follows an exponential decay of the *CoV* following the relations (Etchells and Meyer, 2004):

$$CoV_0 = \left(\frac{1 - C_v}{C_v}\right)^{0.5} \tag{3-4}$$

$$CoV = CoV_0 K^{L/D} \tag{3-5}$$

$$CoV_r = \frac{CoV}{CoV_0} = K^{L/D} \tag{3-6}$$

where C_v is the volume fraction of unmixed additive. CoV_0 is 1.0 for 50% additive and increases to 3 for 10% additive. Using CoV_r collapses the data for static mixers onto a single line for a range of inlet concentrations.

Both definitions of *CoV* require the use of multiple concentration samples, but minimal guidance is available as to the required number of samples, or

regarding limitations on the size of the probe. To resolve some of these questions, we begin by reviewing what is known about sampling requirements for spatial statistics.

Sampling Methods used for Spatial Statistics

In order to calculate the intensity of segregation, a concentration data set must be extracted from a three dimensional mixing field. Two types of concentration data are available from experiments and/or numerical simulations. The first is the concentration of a second chemical species, the second is the concentration of tracer particles which have been released into the mixing field. Where a full three dimensional data set is not available, a representative plane must be selected, and where a full plane of data is not available, a representative transect or traverse or a set of sampling points may be selected. As the available data becomes sparser, the sampling method and statistical analysis become more important. The choice of the sampling strategy will be constrained by the amount of data available, but it must also be well matched to the problem statement and definition.

Figure 3-1 illustrates three classes of sampling strategies used in spatial statistics: quadrats, probes and transects. The term quadrat was originally defined as a 1 m × 1 m sample area for ecological studies (Clements, 1905). Today, the term quadrat refers to any two dimensional sample area. Its size and shape is arbitrary, and is not necessarily uniform (e.g. census data). Quadrat sampling covers a full plane of data: in statistical terms it is an *area filling* sampling method. Point probes are mathematically zero dimensional, in the sense that they are centered at a point in space and occupy no volume. Practically, however, they must have a finite sampling area or measurement volume in order to sample a physically and statistically meaningful number of molecules, or tracer particles (Danckwerts, 1958). Transects are one dimensional and traverse the measurement volume along a single line. Again, the line is mathematically of zero thickness, but a finite thickness is required to sample a statistically and physically meaningful number of real particles or molecules. The purpose of the transect sample differs from the quadrat and probe samples. While the mean and variance

along the transect can be calculated to give a measure of the intensity of segregation, the transect is primarily used to profile concentration (Hessel et. al., 2003) and to determine a striation thickness distribution, thus giving information about the scales of segregation. Quadrats, probes, and transects can all be used to sample either a plane or a volume of data.

(a) (b) (c)

Figure 3-1. Illustration of sampling strategies: (a) rectangular quadrats (b) point probes (c) transect of thickness Δz.

In quadrat analysis, the plane of interest is divided into a number of areas (quadrats), often of the same size and shape. The number of quadrats, and thus their size, depends on the desired level of spatial resolution. Ideally, the concentration in a quadrat is uniform and the quadrat size is matched to the smallest scale of the concentration striations. However this is not always possible, either because the smallest scales are unknown, or because it is not possible to measure concentration with such a high resolution. When the quadrat is larger than the local scale of segregation, the mean quadrat concentration depends on the size and shape of the quadrat. This dilemma, most simply illustrated by the checkerboard thought experiment, causes a number of difficulties for analysis, and is known as the modifiable areal unit problem (MAUP) in population studies. It is discussed in some detail in the literature (Reardon and Sullivan, 2004; Wong, 2004; Mead, 1974; McGarvey et. al., 2005). Once the size and shape of the quadrats has been defined, the mean concentration in each quadrat is calculated from the raw data. The CoV is then evaluated using Equation 3-3, where M is now the number of quadrats.

When using probes to get concentration data, a set of probe locations is selected. As with the quadrat selection, some attention to the sampling strategy is warranted. If the underlying data has a regular pattern, the probe locations must

either be randomized, or there must be enough probes to accurately sample the entire mixing field. When the data set is complete and the mixing field is either irregular or can be densely sampled, a regular sampling grid is both useful and efficient. If the number of probes available is very limited, however; as is the case for typical blend time measurements, then the probe placement must be based on sound physical reasoning and an understanding of the process. At least one of the probes must be located in the last-mixed region if accurate blend times are to be obtained (Brown et. al., 2004).

Once the probe locations are selected, the probe size must be identified. Ideally, the probe size should match the smallest scales of mixing that are to be measured, however; practical limitations mean that the scale of resolution of the measurement method is usually limited by the actual size of the probe. If a physical probe is used, the concentration is averaged over the measurement volume and is assumed to be uniform within the measurement volume. If a CFD simulation is used with scalar transport, the concentration is averaged over the cell volume. If CFD with particle tracking is used, the resolution of particle motion is limited by the step size in the particle paths, and the resolution of striations at any instant in time is limited by the number of particles in the simulation. When particle concentration is calculated from discrete particle data, the particle concentration is based on the number of particles in the probe. The probe size should be small enough to get local data, but also large enough to contain a statistically significant number of particles. As a result, the smallest scale of resolution of the concentration probes is limited by the number of particles in the simulation. To avoid counting tracking particles twice, the probe areas should not overlap, so the maximum probe size is limited by the number of points in the sampling grid.

To get the most valuable information about mixing, a transect should pass through the worst mixed part of the mixing field, and as much as possible should be oriented to be perpendicular to the striations of greatest interest. A transect has two variable dimensions: the height of the transect, Δz, and the striation thickness

threshold. In forestry studies, the width of a foresters' arms, or a $\Delta z = 2$ m is used to sample a forest. A particle is included in the transect if its z-coordinate equals the z-coordinate of the transect $\pm \Delta z/2$. Aubin et al.(2005) selected a transect height, Δz, equal to the mean particle spacing in the mixing field. The height of the transect, Δz, allows for the capture of a single particle, and transect sampling then assumes that all particles in the 2D transect are associated with the equivalent 1D line through the mixing field. The striation thicknesses on the transect are determined using the function f, which has the following properties:

$$\Delta x(\text{neighbours}) \leq \Delta x: \quad f(x) = 1$$

$$\Delta x(\text{neighbours}) > \Delta x: \quad f(x) = 0 \qquad (3\text{-}7)$$

Striation thicknesses on the transect are calculated directly from the function $f(x)$: when two consecutive particles in the transect are within Δx of each other, they are both in the same striation. If Δx is too large, the striations will be unrealistically large; if it is too small, no striations will be detected. In a real striation, the particles will be closer together than the mean particle spacing, so we expect the Δx value to be smaller than the Δz value. If concentration data are used to determine striation thickness distributions on a transect, a concentration threshold must be defined to replace Δx, the threshold distance between tracking particles. No full field concentration data is available to test this thresholding requirement in the current work, but some initial thresholding work in the time domain is reported by Hilderman and Wilson (1999) and Hilderman et al. (1999). Note that transects through time at a single point in space are statistically and mathematically equivalent to transects through space at a single instant in time (Diggle, 2003).

Experimental

The CoV obtained from both probe and quadrat sampling methods and the maximum striation thickness measured on a transect are all affected by the size and shape of the sample. Probe sampling can be affected by the location, number, and size of the probes, while quadrat sampling requires attention to the modifiable

areal unit problem, MAUP. Transects require the user to define the threshold value for particle separation, and the thickness of the transect. These requirements are well documented in other fields of study, as discussed earlier in the paper.

The two objectives of the sampling experiment are to compare quadrat and probe sampling methods in the context of blend time calculations for two test cases, and to compare measurements of the scale and intensity of segregation. Quadrat and probe sampling are compared on the basis of number of probes or quadrats, size of probes or quadrats, and the resulting *CoV*. Transect sampling is explored for different transect heights and separation thresholds to determine the effect of spatial resolution on the maximum striation thickness. The results are compared globally to better understand what each measure reveals about mixing.

Test Cases

Two test cases were used to study the effect of sampling on measurements of mixing. The first test case is the dispersion and dissolution of floating particles in a turbulent stirred tank, shown in Figure 3-2 and Figure 3-3. The second test case is the laminar mixing of mass-less tracer particles in a staggered herringbone micromixer, shown in Figure 3-4. These test cases represent two extremes of scale (tank diameter $T = 0.2335$ m and the micromixer width w = 200 μm); two extremes of mixing and dispersion (multiphase turbulent mixing and dissolution in the first case; single phase laminar blending in the second); and widely varying data densities (7×10^6 particles versus 2 480 particles). In both cases, planes of data are extracted from three dimensional CFD simulations of mixing. These simulations provide exceptionally complete data sets for the evaluation of statistical sampling and data analysis methods.

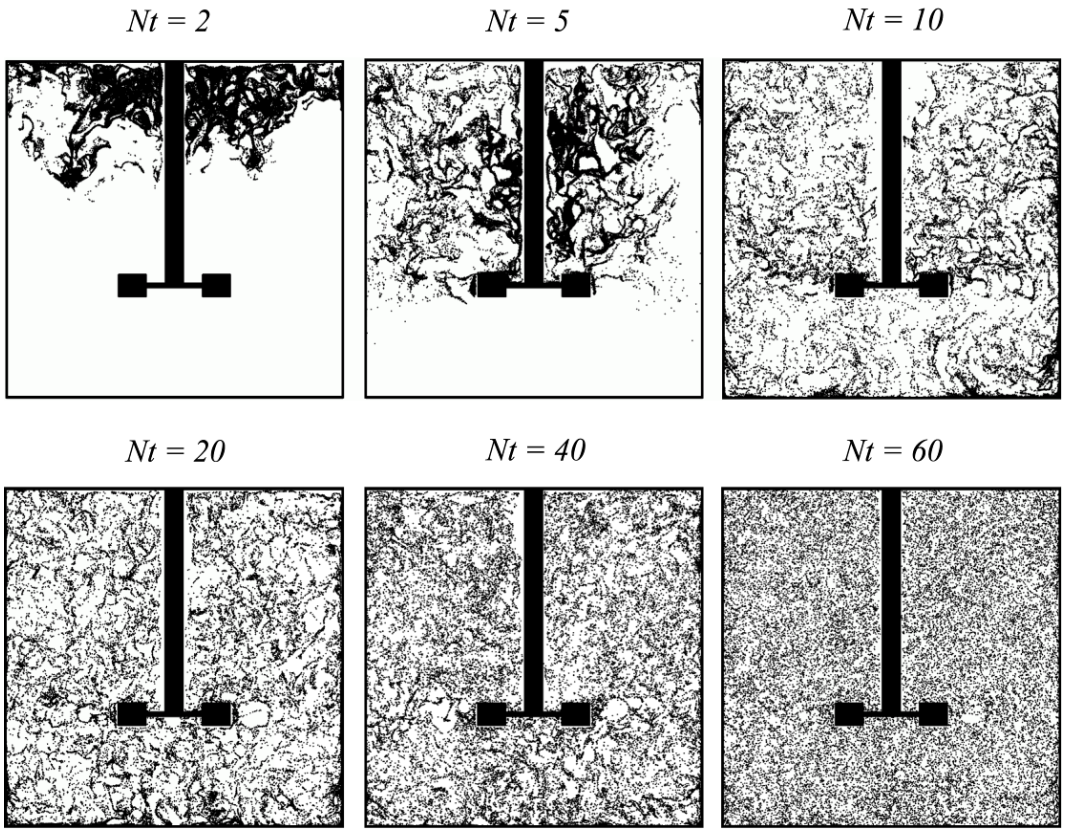

Figure 3-2. Particle distribution in the mid-baffle plane of the turbulent stirred tank, T = 0.2335 m, $D = T/3$, $C = T/3$, N = 990 rpm; Nt = number of impeller revolutions.

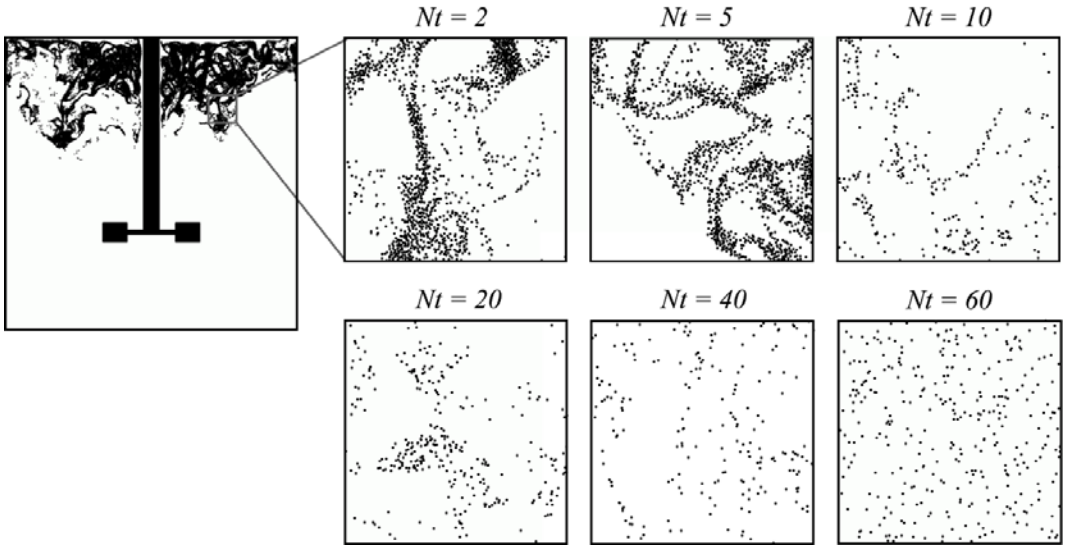

Figure 3-3. Magnified view of the particle distribution in a window $T/10 \times T/10$ big centered at $r = T/4$ and z (axial coordinate) = $0.75T$.

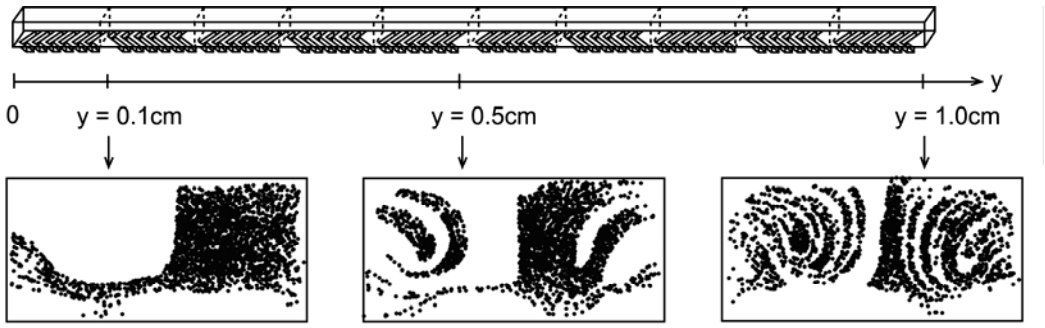

Figure 3-4. Geometry of the rectangular micromixer. Channel height (h = 77 μm) and channel width (w = 200 μm). Three groove depths are tested (d_g = 0.*23h*, 0.*30h*, and 0.35*h*). The three cross sectional sampling planes at three locations along the laminar micromixer illustrate the particle distribution for a groove depth of 0.23*h*.

The first test case is the dispersion and dissolution of floating particles suspended in a tank stirred by a Rushton turbine. The cylindrical, flat bottomed tank has a diameter $T = 0.2335$ and is fitted with four standard baffles of width *0.1T* and a six-bladed Rushton turbine impeller of diameter $D = T/3$. The impeller is mounted at height of $C_{imp} = T/3$ above the vessel bottom and rotates at a speed of $N = 990$ rpm (fully turbulent). It was filled with water ($\rho_l = 1000$ kg/m^3) to a height of $H = T$. At the beginning of the simulation, 7×10^6 mono-disperse spherical particles with diameter $d_p = 0.3$ mm and density $\rho_p = 2150$ kg/m^3 were released in the upper part of the tank. The particle distribution and dissolution simulation was performed using a transient large eddy simulation with the Eulerian-Lagrangian particle tracking approach. More details about the simulation can be found in the paper by Hartmann et al. (Hartmann et. Al, 2006). Figure 3-2 and Figure 3-3 show the data set extracted from the simulation for analysis: particle positions in a vertical cross-section mid-way between two baffles at six different times during the simulation. In this case, the particles dissolve and move randomly in and out of the sampling plane and as a result the number of particles in the slice varies between 28 000 and 56 000. Figure 3-3 illustrates the spatial resolution of the simulation: in this case a mean particle separation of 1 mm, or roughly 0.5% of the tank diameter.

The second test case is laminar mixing in a staggered herringbone micromixer, as shown in Figure 3-4. The mixer is a rectangular channel with a width of w = 200 μm, height h = 77 μm and length L = 0.01 m, with grooves of depth $d_g = 0.23h$, $0.30h$ and $0.35h$ and width W_g = 50 μm. A total of 2480 uniformly distributed mass-less particles were placed on the right hand side of the solved flow field at the mixer inlet and were followed using the Lagrangian particle tracking method. The details of the simulation procedure are described by Aubin et al. (2005). The objective of the simulation is to compare the mixing efficiency for three different groove depths. Vertical planes along the micromixer were sampled at intervals of 100 μm in order to compare the designs.

Sampling Experiments

The first sampling method considered is probes. Figure 3-5 shows the regular hexagonal grid (Aubin et. al., 2005) used to set the probe locations in both the tank and the micromixer. For the stirred tank case, grids containing 36, 142, 274, 536, 1093 and 2209 probe points were tested. The points located in the shaft and impeller areas were omitted. The probe area A_k was set equal to the area of a circle that would contain a fixed number of particles, k, in a perfectly homogeneous distribution:

$$A_k = k\frac{A}{p} \tag{3-8}$$

where A is the area of the slice minus the area of the impeller and shaft and p is the total number of particles in the slice. Three aspects of the probe sampling were studied here; namely the effect of the probe location, size, and number. To investigate the effect of probe location, six sets of 3 probes were selected as shown in Figure 3-6. The probe locations are summarized in Table 3-1. To analyze the effect of the probe size on the resulting CoV, the 536-probe grid was used with probe sizes of k = 3, 10, 30 and 180 particles. The effect of the number of probes was studied by calculating the CoV for all grids with a constant 10-particle-probe size (k = 10). For the micromixer case, only the effects of probe

number (using hexagonal grids of 30, 60, 105, 198 and 640 points) and probe size (k = 3, 5, 10, 20, 50) on the *CoV* were evaluated.

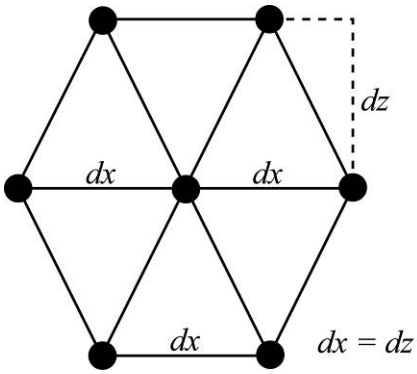

Figure 3-5. Hexagonal grid used for setting probe locations in the stirred tank and the micromixer. In the tank $dx = dz$ and in the laminar micromixer $dx \approx dz$.

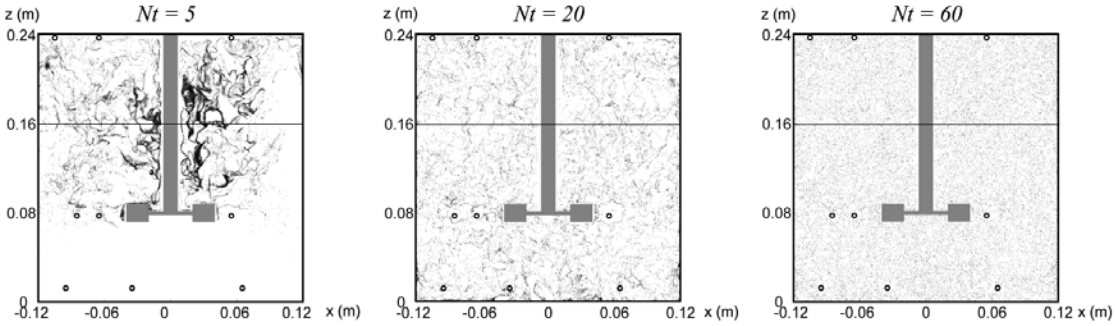

Figure 3-6. Location and size of probes and transects at three time steps (Nt = 5, d = 3.59 mm; Nt = 20, d = 4.55 mm; Nt = 60, d = 4.89 mm, where d is the probe diameter). The transect height is $z = 2T/3$.

The effects of the quadrat sampling parameters on *CoV* were studied using the herringbone micromixer test case. At each cross-sectional plane along the micromixer, the data was divided into 10, 24, 40 and 640 equal rectangular quadrats and the *CoV* was calculated. Here, the quadrat size is inversely proportional to the number of quadrats (since quadrats cover the whole region of study). To compare the probe and quadrat analyses, the *CoV* was calculated from the grid containing 640 circular probes (with a maximum probe size of 2.92 particles per probe) and compared with the *CoV* calculated from 640 rectangular quadrats.

Table 3-1. Positions of probes used to study the effect of probe location. All probes lie in the vertical mid-baffle plane, $\theta = 0°$.

***x*/m**	**z/m**	**used in sets**
-0.1050	0.2375	up, left
-0.0650	0.2375	up, middle
0.0550	0.2375	up, right
-0.0850	0.0775	center, left
-0.0650	0.0775	center, middle
0.0550	0.0775	center, right
-0.0950	0.0125	down, left
-0.0350	0.0125	down, middle
0.0650	0.0125	down, right

Transect sampling was used to determine the maximum striation thickness in both the stirred tank and the micromixer test cases. The maximum striation thickness on a transect in the stirred tank was calculated using Equation 3-3. The transect was located at two thirds of the tank height, as shown in Figure 3-6. For the base case, the resolution in the axial direction, Δz, was set equal to the mean particle spacing for a perfectly homogeneous distribution of 39 330 particles:

$$\Delta z \cong \sqrt{\frac{A}{p}} \cong 1 \text{ mm} \qquad (3\text{-}9)$$

where A is the area of the tank cross section after substracting the impeller and shaft areas and p is the average number of particles in the data plane. The effect of transect thickness, Δz, on the maximum striation thickness was examined by varying $\Delta z = \Delta x = 0.5$ mm, 1 mm and 2 mm.

Different resolutions in the x-direction, Δx, were used to isolate the effect of Δx on the striation thickness. The transect thickness was fixed at $\Delta z = 1$ mm for Δx resolutions of 2 mm, 1 mm, 0.75 mm and 0.5 mm. A finer resolution would require more tracer particles, with the number of particles required increasing as $1/\Delta x^2$. For the staggered herringbone micromixer, the striation thickness

calculation was performed using a single resolution of $\Delta z = \Delta y = 5$ μm, which is equal to the mean particle spacing given in Equation 3-9.

Results and Discussion

The case of the turbulent stirred tank with dissolving solid particles is discussed first, followed by the herringbone micromixer case. Both cases are used to explore the effect of probe location, number and size on the *CoV*. The maximum striation thickness on a transect is also calculated as the mixing evolves, using varying transect resolutions. In the laminar mixing case, probe and quadrat sampling strategies are compared and contrasted with the evolution of the maximum striation thickness on a transect. The results shed additional light on the information contained in the two different measures of mixing.

Turbulent Mixing: CoV Results

The selection of the number and location of the probes is a partially unresolved issue for the *CoV* calculation, and thus for the measurement of blend time, or the decay of intensity of segregation. In order to obtain full spatial resolution of the three dimensional mixing field, a very large number of probes would be required. When a limited number of probes are available, at least one probe must be located in the worst-mixed part of the vessel if the *CoV* is to detect the final stages of mixing (Brown et. al., 2004). Figure 3-7 illustrates the impact of the probe location for the six different sets of three probes shown in Figure 3-6 and a seventh set of three randomly selected probe locations. These results are compared with the true *CoV* determined using 4292 probes evenly spaced throughout the mixing field. For each set of three probes, the evolution of the *CoV* is different, and none of the sets of three probes tracks the true *CoV*. When three probes are used, as recommended in the blend time protocol given by Brown et al. (2004), the evolution of the *CoV* strongly depends on the location of the probes.

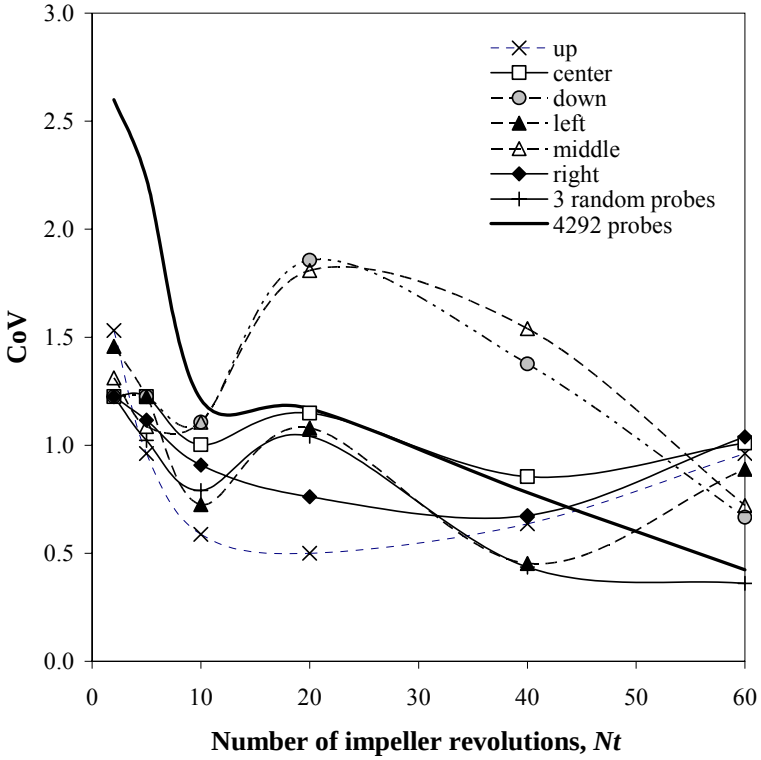

Figure 3-7. *CoV* for the seven different sets of three 10-particle probes shown in Figure 3-6. The dark solid line for a large number of probes provides a reference to the true evolution of the *CoV* in the tank.

Three probes are clearly not enough to correctly sample a complex mixing field. The next question to address is, "How many probes are needed, given an ideal data set?" As the number of probes increases, the *CoV* calculated from a full plane of data will approach the true *CoV* in the tank. In most experimental applications, the use of a large number of probes is impractical, and could change the flow field enough to endanger the accuracy of the measurement. The optimum balance between the number of probes and the accuracy of the *CoV* measurement is illustrated in Figure 3-8. For a small number of probes, the measured evolution of *CoV* is unreliable, but as the number of probes increases to 274 and beyond, the curves converge onto one curve which is representative of the whole population, as highlighted in Figure 3-8(b).

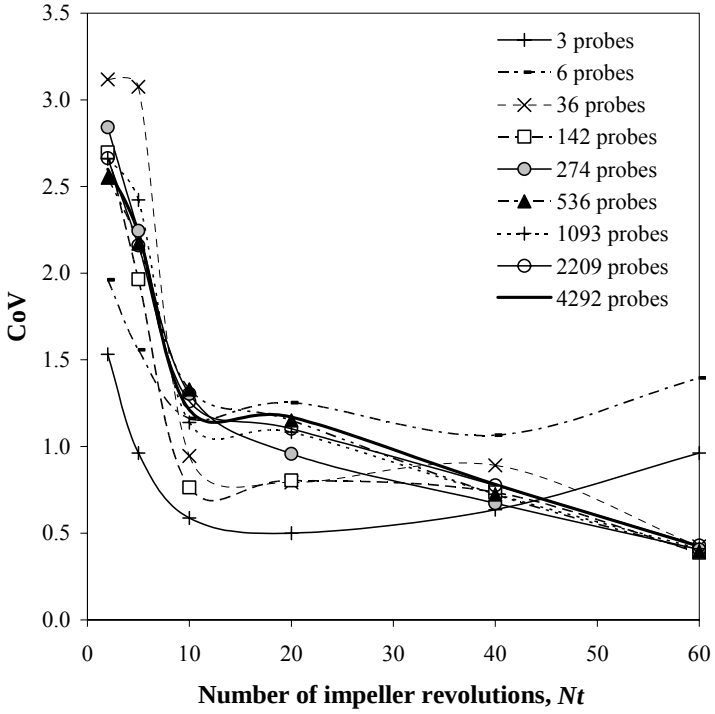

(a)

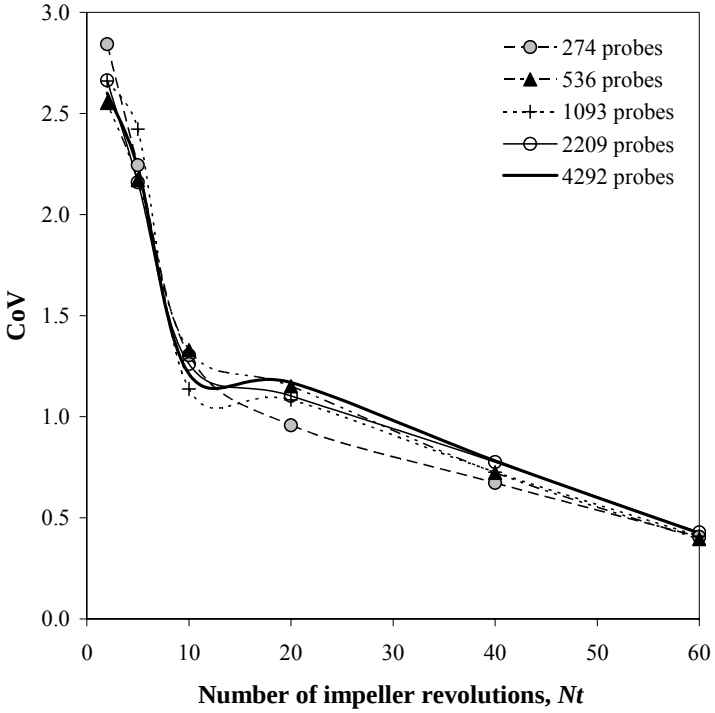

(b)

Figure 3-8. Influence of the number of probes on *CoV*. A 10-particle probe size was used for each time-step, causing the probe size to vary slightly as the number of particles in the plane varied over time. Figure 3-8(a) shows all of the data, while Figure 3-8(b) focuses on the data which is independent of the number of probes.

Returning to Figure 3-8(a), note that for $Nt \geq 40$, the curves for 36 probes or more converge. From this, one might conclude that for long times, or for a small threshold on the final *CoV*, even the curve for three probes may approach the true value. This is an important finding because if only a very small number of probes are available, then setting a "well mixed" criterion to a very small *CoV* value will ensure that the required degree of mixing is achieved. Referring back to the blend time protocol (Brown et. al., 2004), we find a very small equivalent *CoV* threshold of 0.0025. This conservative limit ensures that measured blend times are consistent between experimenters and provides an accurate measure of "complete mixedness" which scales up reliably. This is in agreement with both industrial experience, and a number of blend time papers in the open literature (Grenville and Nienow, 2004; Kresta et. al., 2006; Nienow, 1997).

Although the data in this test case is for particle dispersion, rather than blend time, it is interesting to compare the blend time ($N\theta_{95} = 5.20 / N_P^{1/3} \times (T/D)^2 = 27$ (eq. 0-10) in Grenville and Nienow, 2004) with these *CoV* curves. Note the rapid decay of *CoV* up to $Nt = 10$ – clearly the volume filling stage in Figure 3-2 – followed by the slower decay in *CoV* during the scale reduction phase. This suggests that the blend time, or the macromixing time, is primarily related to the inital dispersion of the tracer throughout the volume of the vessel, with a conservative design factor added in to compensate for the small number of probes. We might then redefine "macromixing" as the volume filling stage of mixing, "mesomixing" as the scale reduction stage, which in turbulent mixing is closely related to the inertial convective range of eddies, and "micromixing" as the stage of mixing when the scale of segregation is reduced to the point where molecular mechanisms such as viscous dissipation and molecular diffusivity become dominant.

While the number of probes determines the total area sampled, the spatial resolution of the *CoV* measurement is determined by the probe size. In selecting the size of the probe for a fixed data set, two competing requirements must be satisfied. On one hand, it is important to have enough particles in the probe to

give a statistically meaningful result. If the probe contains only one or two particles on average, the data will be highly variable. On the other hand, if the probe is too big, it will contain many particles, but the spatial resolution of the measurement will be poor and many details of the mixing field will be lost. The goal should be to capture the required scales of mixing using the minimum number of tracking particles, while at the same time maintaining the statistical significance of the measurement.

Setting the mean number of particles in the probe volume to 10, under perfectly homogeneous conditions, means that a deviation from the mean of one particle will cause a 10% deviation in probe concentration. Using a 3-particle probe means that the probe size is smaller and the concentration data has high spatial resolution, but the importance of 1 particle is high, impacting the probe concentration by 33%. This will increase the measured variance significantly. One particle in a 100-particle probe only impacts the probe concentration by 1% but at the expense of the low spatial resolution of the probe.

Figure 3-9 shows the effect of the number of particles in the probe on the calculated CoV. As the number of particles increases, the probe size increases and the calculated CoV gets smaller. Spatial resolution is lost because the local concentration differences (striations or clusters) are averaged over the increasingly large probe volume. To get local data, the probe needs to be smaller than the smallest scale of interest, but large enough to contain a statistically meaningful number of particles. A 10-particle probe size was chosen for all subsequent calculations for the stirred tank test case.

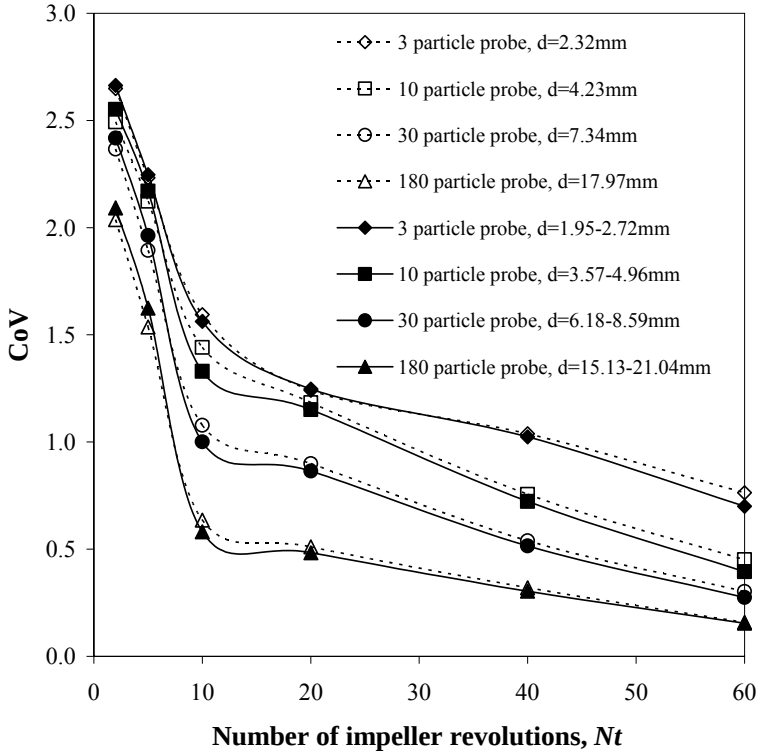

Figure 3-9. Influence of the probe size on *CoV*. The open symbols correspond to a fixed probe diameter for all timesteps, based on the average number of particles in the plane. The filled symbols correspond to a probe diameter which was allowed to vary with time, depending on the number of particles in the plane at that timestep. The number of probes was (M = 536) for all calculations.

Because the particles in this simulation were tracked in three dimensions, and were allowed to dissolve over time, the number of particles in the data plane varied slightly. Two methods were used for setting the probe diameter. The first approach was to calculate the probe diameter from the average number of particles in the plane over all timesteps. The result was a fixed probe diameter for all timesteps for each k-particle probe. The second method used calculated the probe diameter at each timestep for each k-particle probe. This results in a probe diameter that varies slightly over time. A comparison of the two approaches given in Figure 3-9 shows that there is no significant effect on the *CoV* curves.

In future studies, the probe size should first be set equal to the smallest scale of interest. The number of tracer particles required in the simulation can then be set to

$$p = \frac{4k}{\pi}\frac{A}{d^2} \tag{3-11}$$

which ensures that there will be k-particles in each probe when the mixing is perfectly homogeneous. This gives a clear physical meaning to the probe size, and ensures that the number of particles in the simulation is large enough to achieve the desired spatial resolution.

The *CoV* calculations for the stirred tank clearly show the limitations of using 3 probes for the measurement of *CoV*, particularly during the early stages of mixing when the mixing patterns are complex. The sensitivity of *CoV* to the diameter of the probe, or to the number of particles in the probe, emphasizes that *CoV* measures intensity of segregation, not scale of segregation; and that the probe size must be defined based on both the mixing field of interest and the spatial resolution required by the problem. To provide some direct insight into the scale of segregation, the measurement of striation thickness along a transect is considered next.

Turbulent Mixing: Transect Results

Figures 3-10(a)-(f) presents the function *f(x)* used to calculate the maximum striation thickness on a transect using different spatial resolutions in the *x*- and *z*-directions. All plots were created for the time step corresponding to 60 impeller revolutions because at this time the particle distribution is the closest to a homogeneous distribution. The bar widths correspond to the striation thicknesses along the transect. The plots also include a picture of the particle distribution in each transect. Note that the transect widths are not to scale because in reality, they are so small that nothing would be visible from the correct scale.

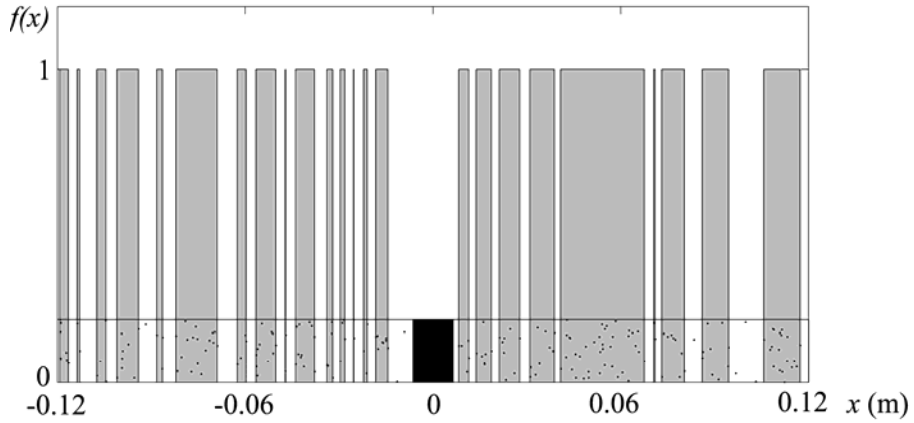
f(x)
1
0
-0.12
-0.06
0
0.06
0.12
x (m)

(a)

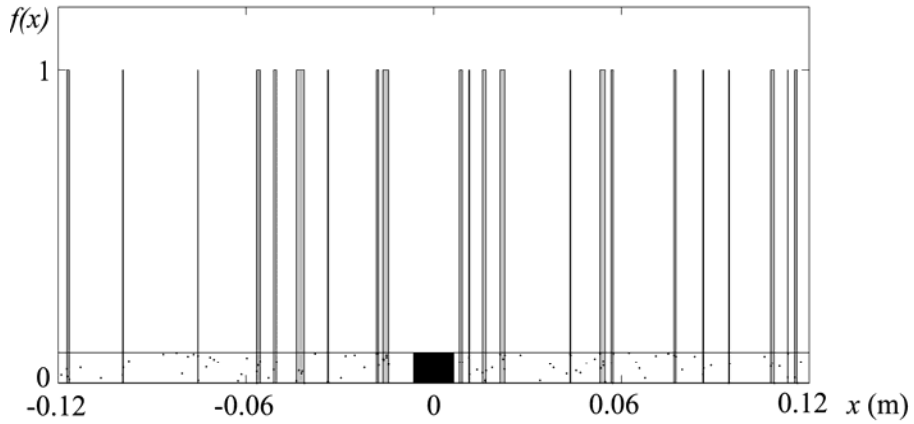
f(x)
1
0
-0.12
-0.06
0
0.06
0.12
x (m)

(b)

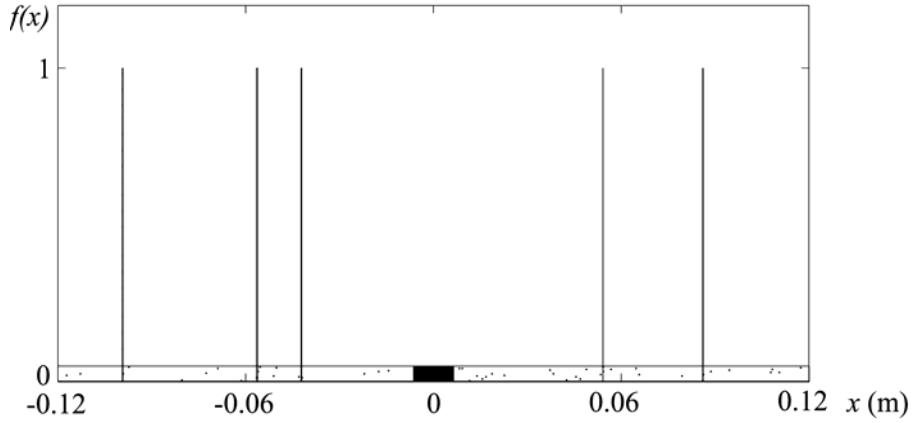
f(x)
1
0
-0.12
-0.06
0
0.06
0.12
x (m)

(c)

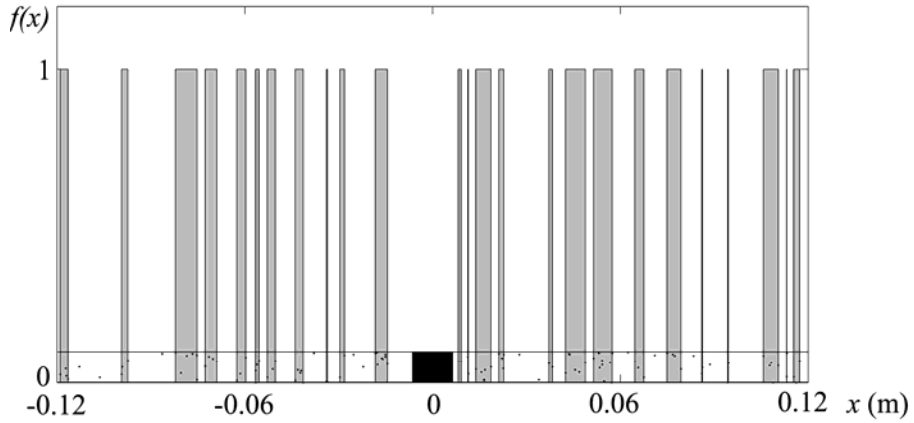

(d)

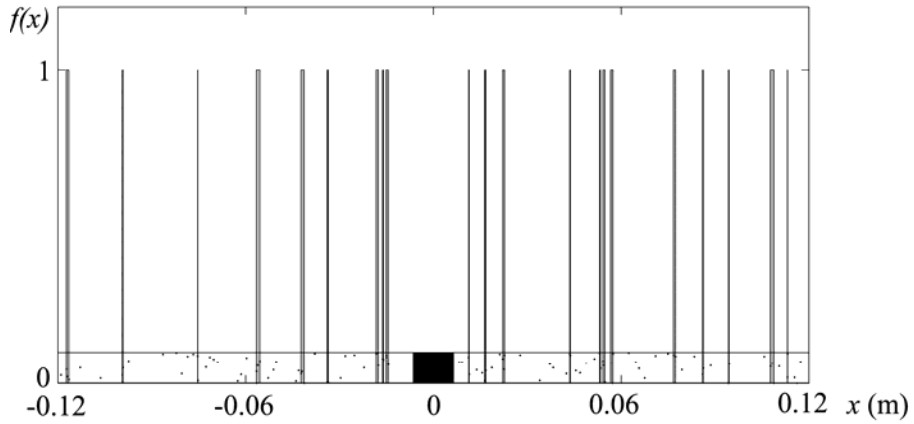

(e)

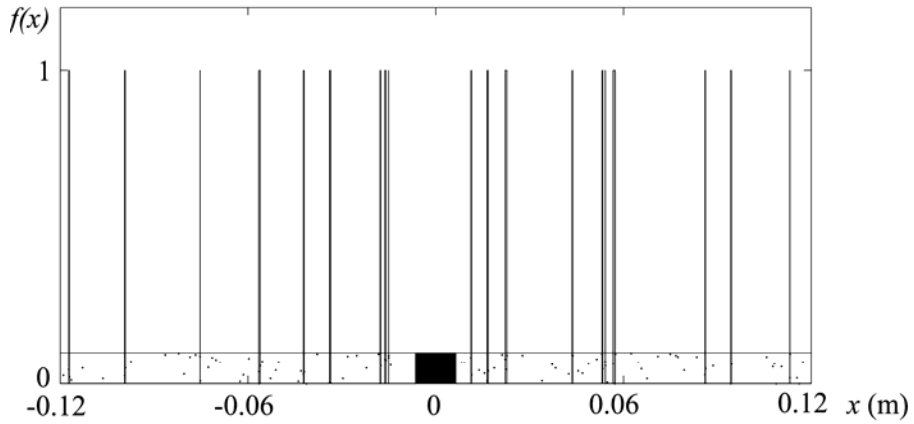

(f)

Figure 3-10. Striation thickness in the tank at a resolution of (a) $\Delta x = \Delta z = 2$ mm (b) $\Delta x = \Delta z = 1$ mm and (c) $\Delta x = \Delta z = 0.5$ mm (d) $\Delta x = 2$ mm, $\Delta z = 1$ mm (e) $\Delta x = 0.75$ mm, $\Delta z = 1$ mm (f) $\Delta x = 0.5$ mm, $\Delta z = 1$ mm. The function *f(x)* is plotted for the transect at $z = 2T/3$ at $Nt = 60$. To compare the striation function *f(x)* with the real particle distribution in the vessel, the particle positions in the transect are shown at the bottom. The height of the transect is not to scale. The black area at the centre of the transect is a part of the shaft.

The striation thicknesses determined with resolutions of $\Delta x = \Delta z = 2$ mm, shown in Figure 3-10(a), indicate that there are very big striations inside the vessel, but visually, the distribution of particles at this time step is very good, as shown in Figure 3-3. The 2 mm resolution is therefore too coarse. A resolution of $\Delta x = \Delta z = 0.5$ mm detects only five very thin striations, as shown in Figure 3-10(c), but since on average a transect that is only half as thick as the mean particle spacing will detect particles only half of the time, this is also a non-physical result. The resolution of $\Delta x = \Delta z = 1$ mm, shown in Figure 3-10(b), has an exact physical meaning. It corresponds to the mean interparticle distance in the case of a homogeneous distribution, and results in a number of striations with small thicknesses. This Δz is used for further calculations.

The effect of Δx is illustrated by comparing Figure 3-10 (b, d-f). It can be seen that as the resolution in the x-direction increases, the striation thicknesses decrease. Weighing the physical meaning of a striation, the Δx resolution should be smaller than the mean particle spacing to indicate that two particles are closer together than expected. Comparing the results for $\Delta x = 1$ mm, 0.75 mm, and 0.5 mm (b, e and f) shows very little change in the f profiles. The maximum striation thicknesses give a closer view of the differences between these Δx's.

Figure 3-11 presents the evolution of the maximum striation thickness. The curves with coarser resolution, in either the z- or x- directions, return higher values of maximum striation thicknesses. With the resolution of $\Delta x = \Delta z = 2$ mm, the maximum striation thickness on the transect decreases at the beginning but starts to increase rapidly as the particles get spread out more evenly. This is non-physical and indicates that the resolution is too coarse. When Δz is reduced to 1 mm, the mean particle spacing, the maximum striation thickness follows a more physical evolution, but for $\Delta z = \Delta x = 0.5$ mm, the striations essentially disappear after $Nt = 10$. A similar evolution is observed when a constant $\Delta z = 1$ mm is used and the x resolution is varied from $\Delta x = 2$ mm to 1 mm, 0.75 mm and 0.5 mm. For Δx less than the mean particle spacing, no significant reduction in the scale of segregation is detected after 10 or 20 impeller

revolutions. From a visual examination of the particle distributions in Figure 3-6 and Figure 3-3, it is clear that this is not true, but the particle density is quite sparse at the smaller scales of segregation. Comparing the striation thickness curves with the *CoV* results in Figure 3-8 reveals that the *CoV* is more sensitive to the later stages of turbulent mixing than the decay of maximum striation thickness on a single transect. The post-processing computational requirement for the accurate calculation of *CoV* is, however; much higher.

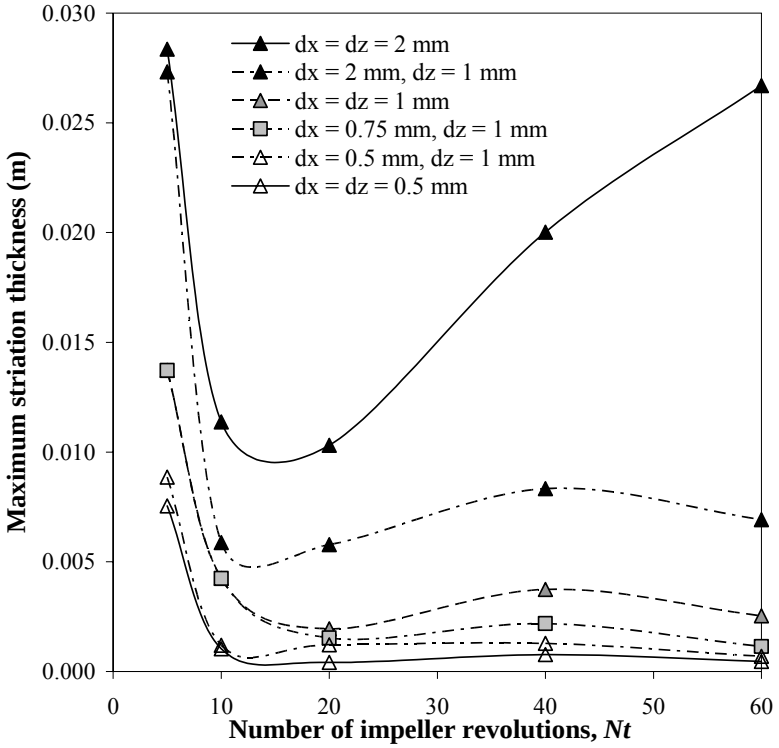

Figure 3-11. Maximum striation thickness on the transect located at $z = 2/3H$ for varying transect and striation resolutions (a) $\Delta x = \Delta z = 0.5$ mm, 1 mm and 2 mm (b) comparison of the previous plot with curves resulting from a fixed transect width $\Delta z = 1$ mm. The mean interparticle distance in the tank is 1 mm.

The transect results are most meaningful when the thickness, Δz, is set equal to the mean particle spacing, and the interparticle spacing threshold is set to be equal to or less than the mean particle spacing. The finest spatial resolution of a transect can be no finer than the mean particle spacing in the flow. The maximum striation thickness within these constraints is not sensitive to the interparticle spacing threshold, and the *CoV* provides more information about the scale

reduction stage of mixing than the direct measure of maximum striation thickness on a single transect.

Laminar Mixing: Transect Results

Figure 3-12 shows the evolution of the maximum striation thickness along the length of the micromixer. The striation thickness calculation in the micromixer was performed using a single resolution of $\Delta z = \Delta x = 5$ μm which is twice the mean particle spacing. The width of the largest striation decreases exponentially as the fluid passes along the mixer. This is characteristic of chaotic flows. This is in contrast with the turbulent case, where the decay in both *CoV* and maximum striation thickness is initially quite sharp, and then levels off. In the laminar micromixer, volume filling and scale reduction happen simultaneously and the decay in the maximum striation thickness is a much smoother curve.

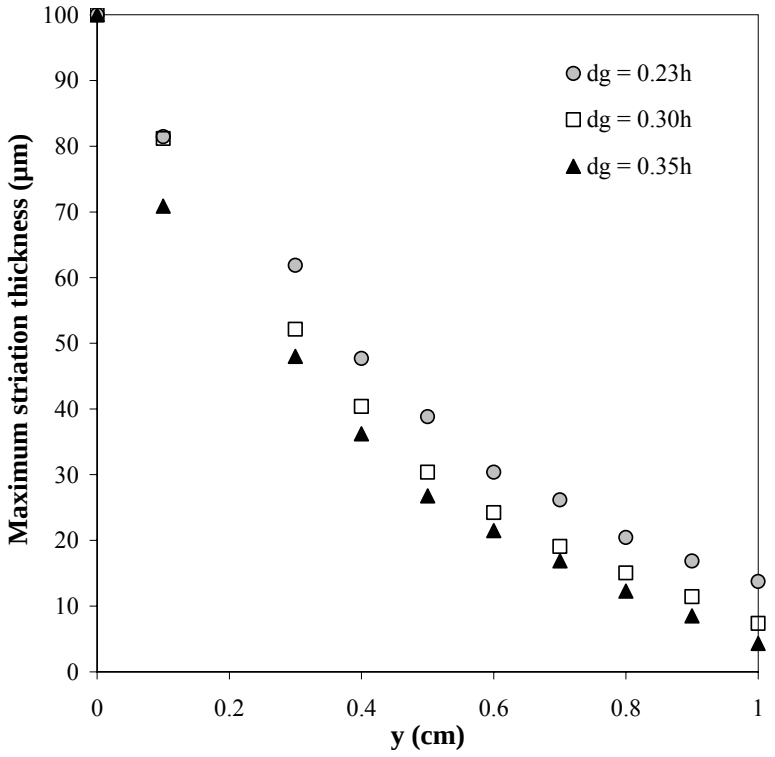

Figure 3-12. Maximum striation thickness decay in the micromixer on a transect of thickness $\Delta z = \Delta x = 5$ μm for a microchannel of 77 μm × 200 μm with 2 480 particle tracks, and an interparticle distance of approximately 2.5 μm.

As the groove depth, d_g, of the mixer increases, the maximum striation thickness at any position along the mixer decreases. This is in agreement with the qualitative visualizations of the spatial distribution of flow followers made by Aubin[7]. The ability of the different mixer designs to reduce striation thickness and improve mixing performance in the laminar micromixer can be clearly distinguished by tracking the decay of the maximum striation thickness, even at this coarse resolution of twice the mean particle spacing. This result is quite different from the turbulent case.

Laminar Mixing: CoV Results

The intensity of segregation in the laminar micromixer was determined at different positions using both the quadrat and probe sampling strategies. The spatial positions of the flow followers on 100 equally spaced cross-sections along the mixer were available for each geometry.

Figure 3-13 shows the influence of the number of 10-particle probes on the *CoV* for the laminar herringbone micromixer. When less than 105 probes are used, the *CoV* curves are noisy. The curves for 105 and more probes tend to converge after 0.6 cm. Although there is an overall decrease in *CoV* along the mixer, fluctuations of the *CoV* are clearly visible. These fluctuations are periodic and correspond to the periodicity of the staggered herringbone geometry. The magnitude of these fluctuations decreases along the mixer length.

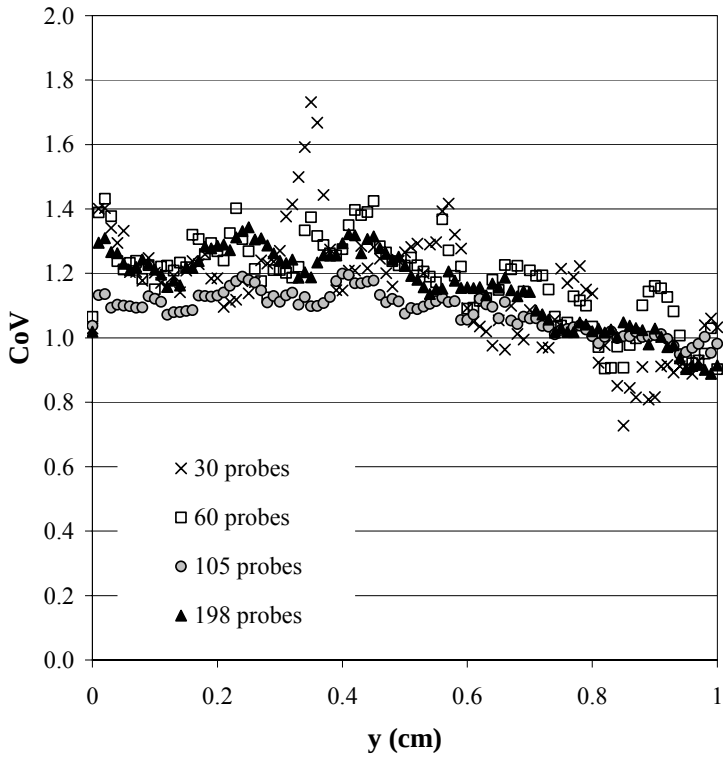

Figure 3-13. Influence of the number of probes on *CoV* in the micromixer for a constant 10-particle probe size (d = 8.89 μm), $d_g = 0.23h$.

The effect of the probe size on the *CoV* is shown in Figure 3-14. In this figure, the number of probes is constant and equal to 105. As for the turbulent stirred tank case, the smaller probe size and thus the finer scale of resolution results in a higher *CoV*. For small probe sizes, the *CoV* curves are noisy and are clearly affected by the relative importance of the local concentration fluctuations, as well as statistical error. As the probe size increases, the noise is damped and the curves become smoother. It should be pointed out that a reduction in noise and the consequent smoothing of the *CoV* with increasing probe size was not observed in the previous turbulent flow example because the *CoV* was determined at only six distinct time steps separated by relatively large time intervals.

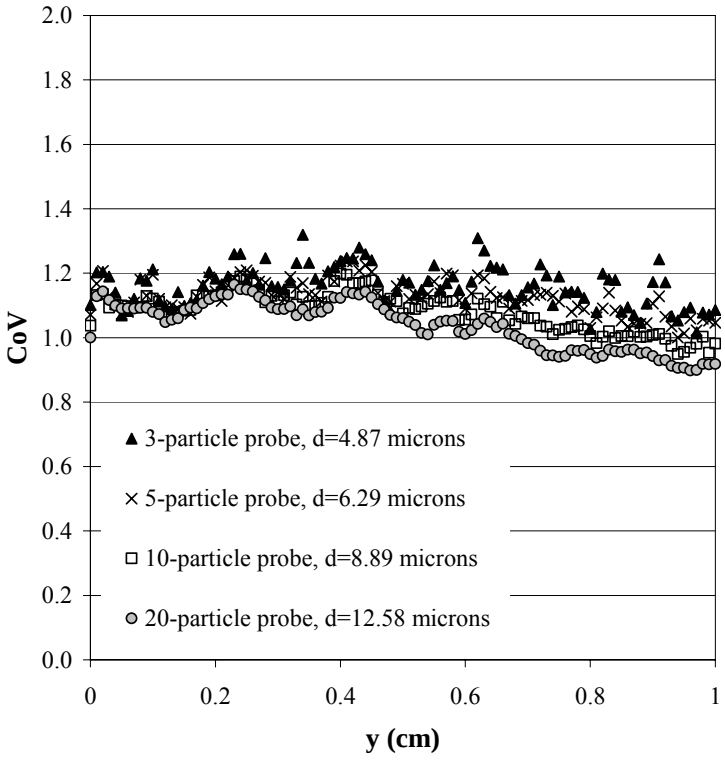

Figure 3-14. Influence of the number of particles in the probe on *CoV* for a constant number of 105 probes in the micromixer, $d_g = 0.23h$.

The combined effect of the probe size and number is shown in Figure 3-15. For each probe size, the number of probes was maximized such that almost all of the area in the data plane was sampled. Only the small areas between the non-overlapping circles remained unsampled. As the probe size increases, the *CoV* decreases because the concentration fluctuations are averaged over increasingly larger probe areas. In the previous section on turbulent mixing, it was recommended that the probe size be set to the smallest scale of interest and to have at least 10 particles per probe. Considering the maximum striation thickness in the micromixer geometry at the end of the mixer (Figure 3-12), the probe size for this case would need to be of the order of 5 μm. With the current simulations, which used 2480 flow followers, this probe size would contain less than 3 particles. In order to obtain higher spatial resolution and reduced statistical error, the number of flow followers used in this simulation would have to be increased.

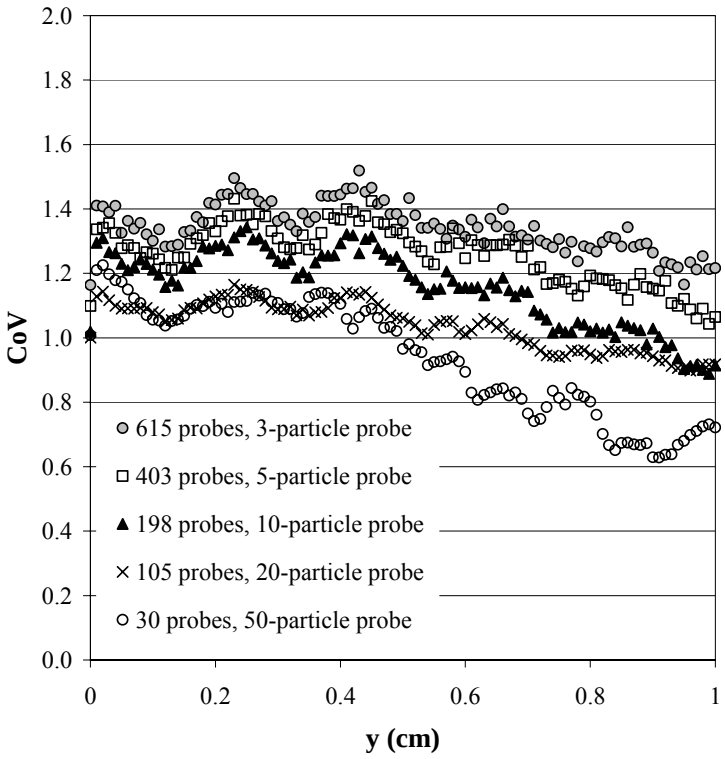

Figure 3-15. Effect of the probe size on CoV when the maximum number of probes is used so that the whole population in the micromixer cross-section is sampled; $d_g = 0.23h$.

Because it is not possible to sample the entire data plane with circular probes, the point probe method and the quadrat sampling method are compared in Figure 3-16. The spatial resolution was fixed to be the smallest possible for the given data set, i.e. 640 probes or quadrats. The mean number of particles expected in one circular probe area is 2.92 and 3.88 particles can be expected in one quadrat. As was mentioned earlier, probes or quadrats with a concentration of 3 particles are not enough for sampling if a limited number of probes are used. However, in this case the whole population is sampled and therefore the result reflects the true standard deviation of the data even though the probe size is small. Smoother plots were obtained when using the quadrat method than with the probe method because quadrats sample the entire area occupied by the population, which is greater than the total area sampled by the circular probes. As a result, the concentration is averaged over a slightly larger area when using quadrats and the *CoV* is less noisy. Nevertheless, there is little difference in the resulting *CoV* when

using either the quadrat sampling or probe sampling, providing that the probe diameter is the largest possible without overlapping of the circular areas. This shows that the shape of the probes/quadrats does not play an important role if a large number of sampling probes/quadrats is used and their size is matched to the smallest scale of mixing.

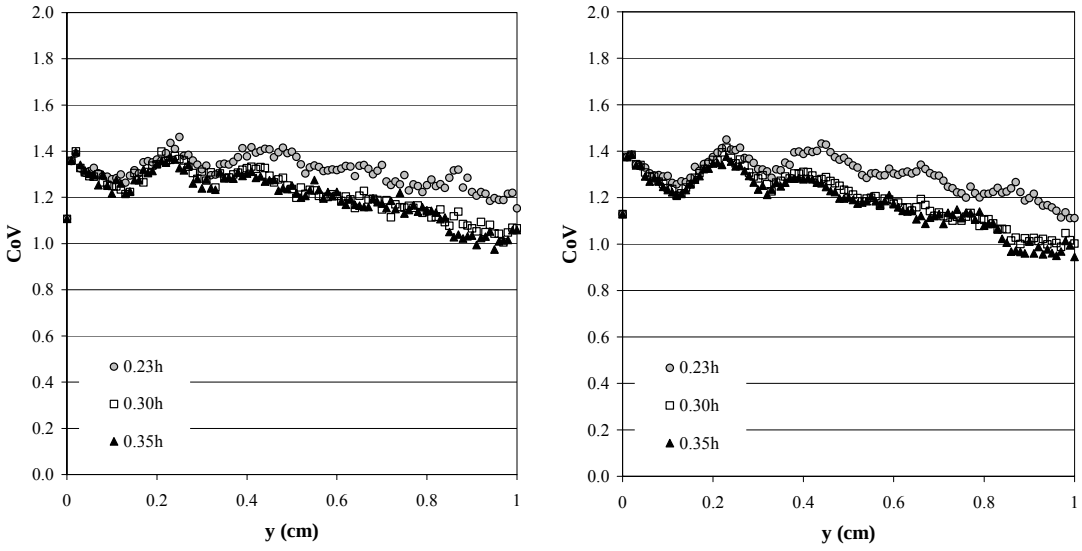

Figure 3-16. Comparison of the *CoV* calculated using 640 probes (a) vs. the *CoV* calculated using 640 quadrats (b). The probes have a size equivalent to a circle containing 2.92 particles, whilst the quadrats contain an average of 3.88 particles. The quadrat calculation gives the true population *CoV* at the smallest statistically meaningful scale of measurement for this number of tracer particles.

Figures 3-17(a)–(d) show the effect of quadrat size (and therefore spatial resolution) on the *CoV* while comparing the performance of micromixers with different groove depths. Grids of 10, 24, 40 and 640 quadrats have a quadrat size of 40 μm × 40 μm, 25 μm × 25 μm, 20 μm × 20 μm and 5 μm × 5 μm, respectively. When the grid of 10 quadrats is used (Figure 3-17 a), the *CoV* curves of the different geometries converge to the same value at the end of the mixer. As the number of quadrats increases and the quadrat size approaches the smallest scale of striations, two things happen. The *CoV* increases, and it is easier to differentiate the mixing performance obtained with the deeper grooves (0.30*h* and 0.35*h*) compared with the groove depth of 0.23*h*. This reinforces the fact that special attention should be paid to the physical meaning of the probe size with

respect to the desired level of mixing. The quadrat size of 5 μm × 5 μm (640 quadrats) approaches the scale of the largest striation present at the end of the micromixer with d_g= 0.35h. The *CoV* curves for the smallest quadrat size (Figure 3-17d) show a distinctly better performance of the 0.30h and 0.35h groove depths, relative to the mixer with 0.23h groove depth. However, the differences between the *CoV* of the 0.30h and 0.35h groove depth geometries are not as pronounced as those seen in the maximum striation thickness curves.

Figure 3-18 shows the effect of probe or quadrat size on the final *CoV* value for the stirred tank from Figure 3-9, and for the laminar micromixers from Figure 3-15 and Figure 3-17. In order to show all three curves on one plot, the probe or quadrat size is normalized by the maximum probe/quadrat size used in each case. This normalization changes the *y*-intercept value but has no effect on the slope of the curves. In all three cases, the final *CoV* decreases logarithmically with an increasing scale of observation.

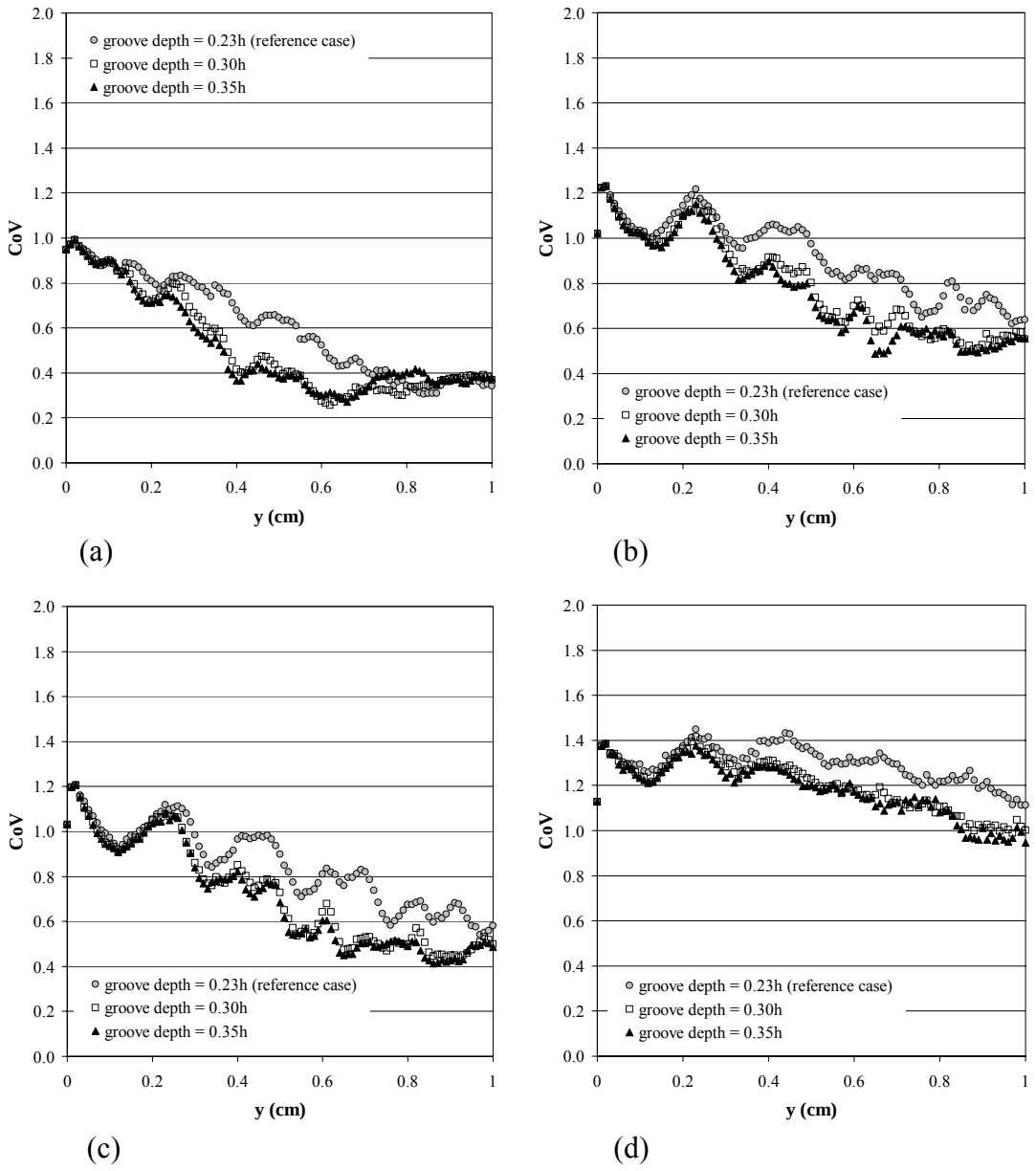

Figure 3-17. Influence of the number of quadrats (and quadrat size) on the *CoV* for varying groove depths (a) 10 quadrats with dimensions 40 µm × 40 µm (b) 24 quadrats – 25 µm × 25 µm (c) 40 quadrats – 20 µm × 20 µm and (d) 640 quadrats – 5 µm × 5 µm.

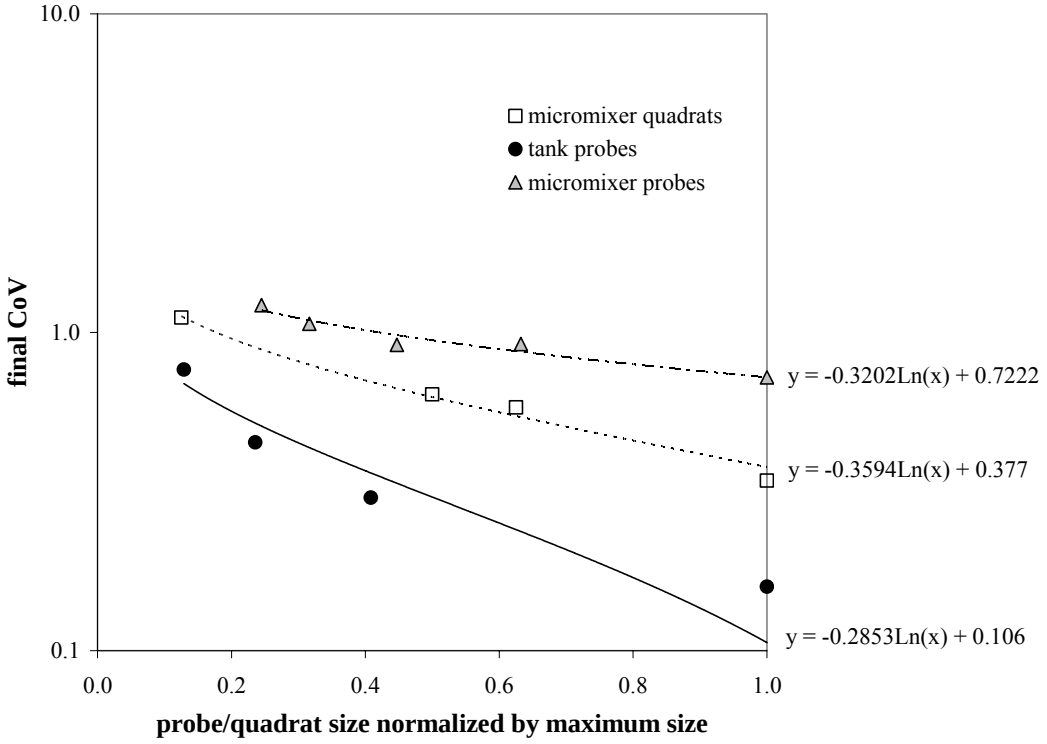

Figure 3-18. Effect of probe or quadrat size on the final *CoV* for the stirred tank from Figure 3-9, and for the laminar micromixer from Figure 3-15 and Figure 3-17.

Figure 3-18 hints at another important result from the two test cases. The *CoV*, or intensity of segregation, is the dominant characteristic of mixing for the stirred tank, changing by a factor of 5 (from 2.5 to 0.5). In contrast, the *CoV* drops by only 30% over the length of the laminar micromixer (from 1.4 to 1.0). The maximum striation thickness dominates for the laminar micromixer, dropping by a factor of 10 over a smooth progression, while for the stirred tank, no change in maximum striation thickness could be detected after the initial volume filling stage ($Nt > 10$). The most useful data is obtained in each case from the measurement which changes the most in the later stages of mixing: intensity of segregation for the turbulent case, and scale of segregation for the laminar case.

Conclusions

The objectives of this investigation were to explore the data resolution and sampling protocols needed to get accurate measures of *CoV* and striation thickness for two ideal data sets, one turbulent and one laminar; and then to compare the *CoV* and striation thickness results to better understand the strengths and weaknesses of each approach. The results allow us to define accurate sampling methods for a variety of applications in laminar and turbulent mixing.

For the turbulent tank data, the calculated *CoV* depends on the number of probes, the probe size, and the probe placement. The *CoV* based on 3 or 6 probes is far different from the *CoV* obtained from a full field measurement. A small number of probes should only be used to define the perfectly homogeneous endpoint, and accurate determination of the endpoint requires that at least one probe is located in a worst mixed region. The smaller the number of probes used, the tighter the tolerance on the endpoint should be to ensure accurate results. To fully sample the mixing field as it evolves, a minimum of 250 probes were needed for the test data set.

For the laminar micromixer, the *CoV* also depended on the number of probes and the probe size. When the true population *CoV* was measured, it accurately tracked oscillations in *CoV* over each mixing element, and a steady decay over the length of the mixer. Note that the purely logarithmic decay of *CoV* postulated by Equation 3-6 is based on data taken at integer numbers of static mixing elements. This data necessarily omits the local oscillations in *CoV*.

For both cases, the *CoV* increases as the probe size shrinks and smaller scales of variation are detected. The absolute value of the final *CoV* changed by up to four times as the probe size was varied. This serves to emphasize the importance of identifying the smallest scale of interest before beginning experiments or simulations. For a laminar mixing field, this scale is the largest acceptable striation thickness. Once this scale is identified, the probe or quadrat size must match the smallest scale of interest. If discrete particle concentrations are being used to determine the *CoV*, the number of particles required for the simulation

should be set to allow at least 10 particles to populate each probe area in a perfectly homogenous distribution. Again, to track the evolution of CoV, enough probes must be used to fully sample the mixing field of interest.

Striation thickness measurements provide an alternate measure of mixing, as they focus on the scale of segregation rather than the intensity of segregation. The maximum striation thickness measured depended on both the transect thickness and the particle separation threshold, Δx. Based on the results, a transect thickness, Δz, equal to the mean particle spacing is recommended, with a particle spacing threshold of $\Delta x \leq$ (mean particle spacing). This means that, on average, a particle will be detected in the 2D slice, and only particles closer together than expected will be assigned to the same striation. As with the CoV, the number of particle tracks required for a simulation can be determined directly if the smallest mixing scales of interest are known.

Two stages of mixing were directly observed in the test data: volume filling, or macromixing, and reduction in scale, or mesomixing. In the turbulent case, the volume filling stage happens quickly, while the scale reduction process is slower. The tank shows an initial rapid decay in CoV followed by slower reduction in intensity of segregation. In the static mixer, the self-similarity, or fractal nature of the mixing field means that volume filling and scale reduction happen simultaneously so the two stages cannot easily be distinguished. These observations suggest that "macromixing" be redefined as the volume filling stage of mixing, "mesomixing" as the scale reduction stage, which in turbulent mixing is closely related to the inertial convective range of eddies and in laminar mixing is closely related to the striation thickness distribution, and "micromixing" be defined as the stage of mixing when the scale of segregation is reduced to a point where molecular mechanisms such as viscous dissipation and molecular diffusivity become dominant.

The most useful mixing data was obtained from the measurement which changes the most in the later stages of mixing: intensity of segregation, or CoV,

for the turbulent case and scale of segregation, or maximum striation thickness on a transect, for the laminar case.

References

Arratia, P.E. and Gollub, J.P., 2005, *Statistics of stretching fields in experimental fluid flows exhibiting chaotic advection*, J. of Stat. Phys., **121**, 805-822.

Aubin, J.; Fletcher, D.F. and Xuereb, C., 2005, *Design of micromixers using CFD modeling*, Chem. Eng. Sci., **60**, 2503-2516.

Baldyga, J. and Bourne, J.R., 1999, *Turbulent Mixing and Chemical Reactions*, Wiley, New York, USA.

Brown, D.A.R.; Jones, P.N.; Middleton, J.C.; Papadopoulos, G. and Arik, E.B., 2004, *Experimental Methods*, In: E.L. Paul; Atiemo-Obeng, V.A. and Kresta, S.M. (Editors), Handbook of Industrial Mixing: Science and Practice. John Wiley & Sons, Inc., New Jersey, USA.

Clements, F.E., 1905, *Research Methods in Ecology*, The University Publishing Company, Lincoln, Nebraska, USA.

Danckwerts, P.V., 1958, *The Effect of Incomplete Mixing on Homogeneous Reactions*, Chem. Eng. Sci., **8**, 93-102.

Diggle, P.J., 2003, *Statistical analysis of spatial point patterns*, Oxford University Press, New York, USA.

Etchells, A.W. and Meyer, C.F., 2004, *Mixing in Pipelines*, In: E.L. Paul; Atiemo-Obeng, V.A. and Kresta, S.M. (Editors), Handbook of Industrial Mixing: Science and Practice. John Wiley & Sons, Inc., New Jersey, USA.

Fox, R.O., 2003, *Computational Models for Turbulent Reacting Flows*, Cambridge series in chemical engineering. Cambridge University Press, Cambridge.

Grenville, R.K. and Nienow, A.W., 2004, *Blending of Miscible Liquids*, In: E.L. Paul; Atiemo-Obeng, V.A. and Kresta, S.M. (Editors), Handbook of Industrial Mixing: Science and Practice. John Wiley & Sons, Inc., New Jersey, USA.

Hartmann, H.; Derksen, J.J. and Van den Akker, H.E.A., 2006, *Numerical simulation of a dissolution process in a stirred tank reactor*, Chem. Eng. Sci., **61**, 3025-3032.

Hessel, V.; Hardt, S.; Lowe, H. and Schonfeld, F., 2003, *Laminar mixing in different interdigital micromixers: I. Experimental characterization*, AIChE J., **49**, 566-577.

Hilderman, T.L.; Hrudey, S.E. and Wilson, D.J., 1999, *A model for effective toxic load from fluctuating gas concentrations*, J. of Haz. Mat., **64**, 115-134.

Hilderman, T.L. and Wilson, D.J., 1999, *Simulating concentration fluctuation time series with intermittent zero periods and level dependent derivatives*, Boundary-Layer Meteorol., **91**, 451-482.

Kresta, S.M. and Aubin, J., *Mixing as a discipline: emerging from the essentials of equipment design to fundamental control of the scale of segregation*, 56th Canadian Chemical Engineering Conference, Sherbrooke, Quebec, Canada, 2006.

Kresta, S.M.; Mao, D.M. and Roussinova, V., 2006, *Batch blend time in square stirred tanks*, Chem. Eng. Sci., **61**, 2823-2825.

Mead, R., 1974, *Test for Spatial Pattern at Several Scales Using Data from a Grid of Contiguous Quadrats*, Biometrics, **30**, 295-307.

McGarvey, R.; Byth, K.; Dixon, C.D.; Day, R.W. and Feenstra, J.E., 2005, *Field trials and simulations of point-nearest-neighbor distance methods for estimating abalone density*, J. of Shellfish Res., **24**, 393-399.

Nienow, A.W., 1997, *On impeller circulation and mixing effectiveness in the turbulent flow regime*, Chem. Eng. Sci., **52**, 2557-2565.

Ogawa, K., 2007, *Chemical Engineering: A New Perspective*, Elsevier science, Amsterdam, Holland.

Ottino, J.M., 1989, *The Kinematics of Mixing: Stretching, Chaos, and Transport*, Cambridge Texts in Applied Mathematics, Cambridge University Press, Cambridge, New York, USA.

Ramkrishna, D., 2001, *Population Balances*, Wiley, New York, USA.

Reardon, S.F. and O'Sullivan, D., 2004, *Measures of spatial segregation*, Sociol. Methodol., **34**, 121-162.

Szalai, E.S.; Alvarez, M.M. and Muzzio, F.J., 2004, *Laminar Mixing: A Dynamical Systems Approach,* In: E.L. Paul; Atiemo-Obeng, V.A. and Kresta, S.M. (Editors), Handbook of Industrial Mixing: Science and Practice. John Wiley & Sons, Inc., New Jersey, USA.

Wong, D.W.S., 2004, *Comparing traditional and spatial segregation measures: A spatial scale perspective*, Urban Geography, **25**, 66-82.

Chapter 4: Measuring the Scale of Segregation in Mixing Data*

Introduction

The scale of segregation is one of three measures of mixing defined by Kukukova et al. (2009). The scale of segregation is important for laminar mixing where the maximum striation thickness determines product quality, and for multi-phase mixing where the size of the particles drops and bubbles either determines mass transfer rates, or is the main objective of the operation. Industrial examples where the scale of segregation is the primary process objective are the formation of emulsions of a specified drop size (Atiemo-Obeng and Calabrese, 2004; Liu et al., 2005; Chu et al., 2007), the production of nanoparticles (Johnson and Prud'homme, 2003), the deliberate use of micro-mixing to reduce both the quantity of chemicals used and the environmental impact of the pulp and paper industry (Bennington, 2004), or to maximize reaction yield in mixing sensitive reactions (Bałdyga and Bourne, 1999), or to minimize NOx emissions from rotary kilns (Nathan et al., 2006; Newbold et al., 2000). In all of these processes, the scale of segregation is the determining variable in the process. A simple illustration of the reduction of the scale of segregation as mixing progresses is shown in Figure 4-1.

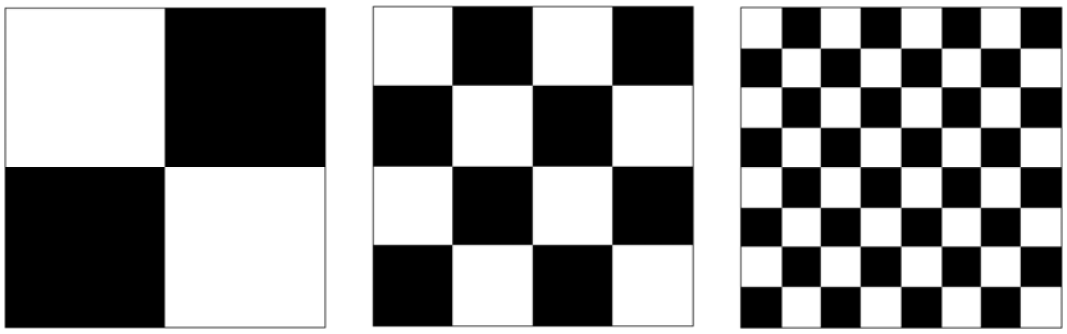

Figure 4-1. The classical checkerboard problem. The scale of segregation decreases from left to right while the intensity of segregation stays the same.

* A version of this chapter has been accepted for publication in the Special Mixing Issue of Can. J. Chem. Eng.

A survey of the literature shows that the scale of segregation is important in a surprisingly wide spectrum of disciplines and a number of methods for its calculation have been proposed. The concept of the scale of segregation in engineering was introduced by Danckwerts in 1952. He suggested the calculation of a mean length scale based on the correlogram – a plot of the coefficient of correlation of concentration, or concentration autocorrelation, *versus* the distance separating the data points. The scale of segregation based on autocorrelation was revisited by Lacey and Mirza in 1976. At that time, the calculation was not deemed practical because of the large number of data pairs that have to be measured and analyzed in order to get meaningful results. Due to the exponential increase of computer power and the increasing resolution and accessibility of digital images, the correlogram and related calculation methods are now practical for the analysis of quite common experimental data sets.

The scale of segregation can also be represented by the physical thickness of striations in a mixing field. In polymer processing applications, Mohr et al. (1957) developed a relationship between striation thickness and shear rate. Later, Muzzio et al. (1991) used a model mixing field with several million tracer particles to study the relationship between the striation thickness distribution and the stretching distribution. While the stretching distribution is the more mathematically transparent approach because it is directly related to the shear field, the striation thickness distribution is the result needed for engineering design. They were able to show that the stretching distribution and the striation thickness distribution are directly coupled and inversely proportional, so that the striation thickness distribution can be directly calculated from the stretching distribution. If the stretching distribution can be calculated from the velocity field, the need to track millions of tracer particles in order to resolve the finest striations can be eliminated. When resolution of the finest scales of mixing is required, this can significantly reduce the computational requirements for a numerical solution. When macro-scale segregation is the variable of interest, a small number of tracer particles can be used and the maximum striation thickness can be determined

along a single reference transect. The maximum striation thickness on a transect is an important measure of equipment performance and product quality in laminar mixing (Aubin et al., 2005).

There is also a well developed literature on segregation problems and measures of segregation in population ecology, geostatistics, segregation of minority populations, forestry, medical imaging and basic applied statistics. These data take the form of locations of members of a population at an instant in time, resulting in a spatial point pattern. A number of distance methods for analysing spatial point patterns which were developed in the American forestry literature (Cottam and Curtis, 1949) are based on the distribution of distances between neighbours (Diggle, 2003). Three methods for analysing spatial point patterns are identified in the spatial statistics literature. Since all of the spatial point patterns in this paper are made up of tracking particles, and the particles are located within a set of grid points, we refer to the data as particles and the grid points as points. The first method analyses all inter-particle distances within a population; the second calculates the distribution of distances between each particle and its nearest neighbour; and the third and most common method measures the distance from a set of grid points to the nearest particle (point-to-nearest-neighbour method). The spatial distribution of the population is evaluated by comparing the nearest neighbour distribution to a completely random Poisson distribution. When the PNN distribution is random, the match with the Poisson distribution is close, and when clustering is present, the distribution is distorted. Spatial point patterns have only recently been used to assess the scale of segregation and the quality of mixing (Aubin et al., 2005 and Kukuková et al., 2008).

Carle and Fogg (1996) evaluated the mean length scale in geostatistics using variograms, which quantify the spatial correlation of data based on the variance between data *versus* the distance separating them. A similar approach is to use the variance of the average of several contiguous concentrations (Gullett et al., 1993). Although the variogram is used primarily for modeling when only limited data are available (Deutsch, 2002), this calculation also appears useful for the analysis of dense data sets. The variogram is closely related to the Danckwerts

correlogram (1952). Correlograms and variograms both show the spatial variability or continuity of the underlying data set. The resulting curves can reveal both large-scale segregation and periodicity in the data. Correlograms and variograms also allow the calculation of length scales. The scale of segregation can be evaluated in several directions of interest or, if all data are combined together, an average length scale of the whole field can be obtained.

The authors' previous work (Kukukova et al., 2009) presents an introduction into the three dimensions of segregation, their definitions and possible applications. A second paper (Kukuková et al., 2008) explores the first dimension – the intensity of segregation – in detail and focuses on accurate sampling strategies. This work concentrates on the second dimension – the scale of segregation. In this study, four methods of measuring the scale of segregation were considered for application to mixing data: the maximum striation thickness on a transect, point-to-nearest neighbour distribution, the correlogram and the variogram. The methods are compared to determine their strengths and limitations for the analysis of mixing data. Five questions are of interest when evaluating the four measures:

1. What type of data is the method suitable for?
2. What information does it provide?
3. Are the results physically meaningful?
4. What is the smallest scale of mixing resolved by the method?
5. How fast is the calculation?

While conditions 1 and 5 have straightforward answers, the other questions require testing and illustration with representative data sets. The goal of this work is to provide a toolkit of fast methods for length scale characterization, as well as benchmarks for the proper use and limitations of each tool. In the next section, each of the methods is discussed in detail.

Methods

This section will review the four methods chosen to measure the scale of segregation: the maximum striation thickness on a transect, the point-to-nearest-neighbour distributions, the correlogram and the variogram. The four test cases are presented after this section, and details about the practical application of the methods to the test cases are given in the Results and Discussion. Calculation algorithms for all of the methods are available as supplementary material from the in the Appendix of this thesis.

Maximum Striation Thickness on a Transect

For spatial point patterns, the maximum striation thickness on a transect can be evaluated using inter-particle distances (Aubin et al., 2005). In such applications, a transect through a data plane or volume is chosen and the distance between two consecutive particles lying on the transect is measured. The inter-particle distances are then compared with a threshold value to determine if they are part of the same striation or not. A distribution of striation thicknesses is obtained and the thickness of the largest striation can be found. The latter is a measure of the limiting scale of segregation.

To get the most valuable information about mixing, a transect should pass through the worst mixed part of the mixing field, and should be perpendicular to the striations of greatest interest, as shown in Figure 4-2. Transects are of zero thickness mathematically, but numerically, a finite thickness is required to sample a statistically and physically meaningful number of particles. A transect has two variable dimensions: the height of the transect, Δz, and the particle separation threshold Δx. A particle is included in the transect if its z-coordinate equals the z-coordinate of the transect $\pm \Delta z/2$. Aubin et al. (2005) recommend a transect height, Δz, equal to the mean particle spacing in the mixing field. The height of the transect, Δz, allows for the capture of a single particle so that all particles in the 2D transect are associated with the equivalent 1D line through the mixing

field. The striation thicknesses on the transect are determined using the function *f*, which has the following properties:

Δx(neighbours) $\leq \Delta x$: $f(x) = 1$

Δx(neighbours) $> \Delta x$: $f(x) = 0$ (4-1)

Striation thicknesses on the transect are calculated directly from the function *f(x)*: when two consecutive particles in the transect are within Δx of each other, they are both in the same striation. If Δx is too large, the striations will be unrealistically large; if it is too small, no striations will be detected. In our previous work (Kukuková et al., 2008), several transect heights, Δz, and striation thickness thresholds, Δx, were studied. It was concluded that a value of $\Delta x = \Delta z$ equal to the mean particle spacing gives the best resolution.

Figure 4-2. Example of transect sampling in a plane of data.

Point-to-Nearest-Neighbour Distributions (PNN)

The point-to-nearest-neighbour method measures the distance x_i from each of *m* grid points to the nearest of the *n* particles, as illustrated in Figure 4-3. In fields of demography, ecology, geography, and forestry, this distance data is analyzed using a test of complete spatial randomness (CSR). The CSR hypothesis asserts that for a completely random distribution of particles in region *A*, any particle has an equal probability of being at any position in region *A* and the position of any particle is independent of the position of any other particle. If the particles are randomly distributed in space, the PNN distances should follow a Poisson distribution. Deviations from the random Poisson distribution allow regular and clustered spatial patterns to be distinguished.

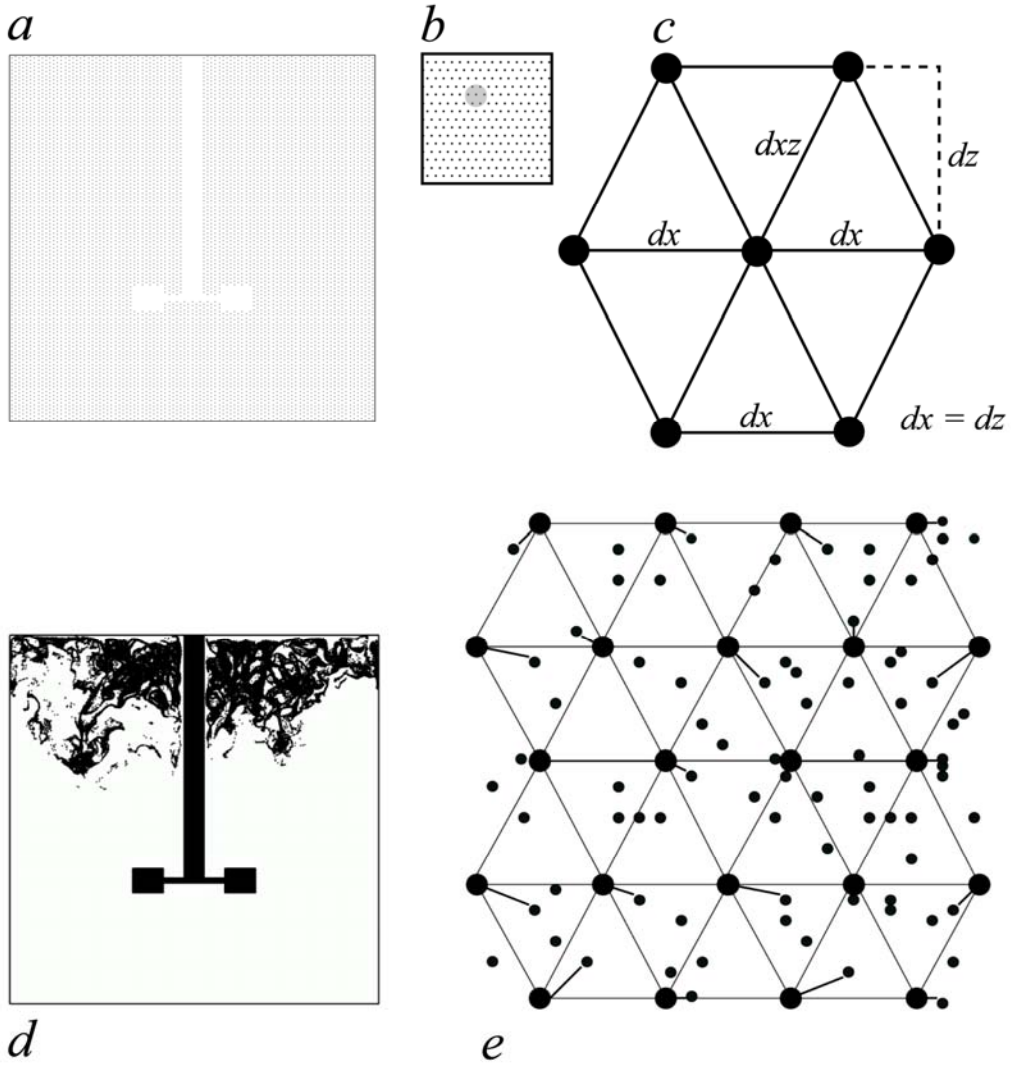

Figure 4-3. Illustration of the PNN method: (a) Hexagonal grid in a stirred tank. (b) Enlarged grid. (c) Construction of the base unit of the grid. (d) Particle locations in the tank. (e) Search for nearest neighbours of each grid point.

For PNN measurement on a plane of data, m grid points are arranged in a regular $k \times k$ grid. Diggle and Matern (1980) recommend using a number of grid points equal to the number of tracking particles, giving $k \approx \sqrt{n}$. Using a grid that is well matched to the number of particles maximizes the use of each particle in the analysis, and also optimizes the resolution of the PNN distribution. The most

uniform pattern for a set of points occurs in a regular hexagonal lattice. The mean grid spacing, x_G, for the hexagonal lattice shown in Figure 4-3(c) is:

$$x_G = \frac{2dx + 4dxz}{6} \cong 1.08dx \tag{4-2}$$

where dx is the horizontal spacing, and $dx = dz$ and dxz is the diagonal grid spacing. When the number of grid points is matched to the number of particles, x_G also approximates the spatial resolution of the measurement.

Clustering can be qualitatively evaluated from the shape of the PNN distribution. A wide distribution indicates clustering; a narrow distribution corresponds to a regular spatial distribution of particles. Another indicator that the particles are well mixed is the mean point-to-nearest-neighbor distance $\overline{x_i}$. As the PNN distribution approaches perfect homogeneity, $\overline{x_i}$ approaches the point-particle distance for a perfectly homogeneous distribution.

A more quantitative measure of clustering and departure from CSR is the index of dispersion, I_{disp} (Diggle, 2003), which is the ratio between the variance of the PNN distribution and the mean of the distribution:

$$I_{disp} = \frac{\sigma^2}{\overline{x_i}} \tag{4-3}$$

Because the Poisson distribution has a variance equal to its mean, the index of dispersion will be equal to 1 for a random distribution, larger than 1 for a clustered distribution and smaller than 1 for a regular distribution of particles.

A filtered variance of the PNN distribution can be used to evaluate the deviation of the spatial arrangement of particles with respect to the expected homogeneous distribution defined by the grid points. A filter threshold, x_R is imposed such that at any value of $x_i < x_R$, the particle is considered to be close enough to the grid point and x_i is assigned a value to x_R. A variance of zero corresponds to the situation where the nearest neighbours of all grid points lie inside virtual circles with a radius of x_R and centered at grid points, thereby lying

close enough to the grid points to be considered homogeneously distributed. The filtered point-particle variance is given by:

$$\sigma_R^2 = \frac{1}{m-1}\sum_{i=1}^{m}(x_i - x_R)^2 \qquad \text{where } x_i = x_R \text{ if } x_i < x_R \tag{4-4}$$

The choice of x_R depends on the scale of interest but is limited by the resolution of the sampling grid, which is in turn dependent on the number of particles. The maximum meaningful value of x_R is one half of the mean grid spacing x_G, in order not to have overlapping filter areas. As x_R decreases, the homogeneous criterion becomes stricter.

Correlograms and Variograms

The correlogram probes the underlying structure in the data by plotting the coefficient of correlation *versus* the distance separating data points. For concentration data, the coefficient of correlation is given by:

$$R_x(h) = \frac{\frac{1}{N(h)}\sum_{N(h)}(C_i(x) - \overline{C})(C_i(x+h) - \overline{C})}{\sigma^2} \tag{4-5}$$

where *N(h)* is the total number of pairs of data separated by distance *h*, and $\overline{C}$ and σ^2 are the mean and variance of the full 2D data set.

The variogram is calculated from:

$$\gamma_x(h) \equiv \frac{1}{2N(h)}\sum_{N(h)}\left(C_{is}(x) - C_{is}(x+h)\right)^2 \tag{4-6}$$

where C_{is} is the standardized concentration value at location x, which is the concentration centered with the mean and normalized with the standard deviation:

$$C_{is}(x) = \frac{C_i(x) - \overline{C}}{\sigma} \tag{4-7}$$

The variogram is closely related to the coefficient of correlation. For data where the mean and the variance of the population do not change with sample location, the following relationship holds:

$$\gamma_x(h) = 1 - R_x(h) \qquad (4\text{-}8)$$

This equation will not hold exactly for data with large scale segregation because the mean and variance of the data will vary with location in the field and the normalizing of the data occurs in a different order for the correlogram and the variogram. For these situations, the two measures should be calculated separately.

The coefficient of correlation and variogram are very similar. Both are performed for a number of separation distances, with a maximum distance equal to about the half of the studied field in order to have enough pairs to statistically represent the entire field. The correlogram and variogram curves can be obtained for several directions of interest to reveal directional anisotropy. If the number of available data points is very small, all directions can be combined in one omni-directional plot, creating a picture of average spatial correlation or variability in the mixing field.

A comparison of the correlogram and the variogram is shown in Figure 4-4. The coefficient of correlation is always one at zero separation distance, which means that the concentration is perfectly correlated with itself, and falls towards zero as the separation distance increases. A value of zero indicates no correlation. If the correlogram crosses zero and reaches negative values, as shown in Figure 4-4, there is large-scale segregation. The variogram shape is exactly opposite to the correlogram. Variograms start with a value of zero at zero separation distance, meaning there is no variability. The curve then increases towards one, and sometimes exceeds it. A variogram equal to one means that the variability at h has reached the variance of the whole data set and there is no remaining spatial correlation in the data. Similar to the correlogram, when the variogram increases beyond one, there is large-scale segregation. Periodic oscillations in both the correlogram and variogram plots indicate underlying periodicity in the data.

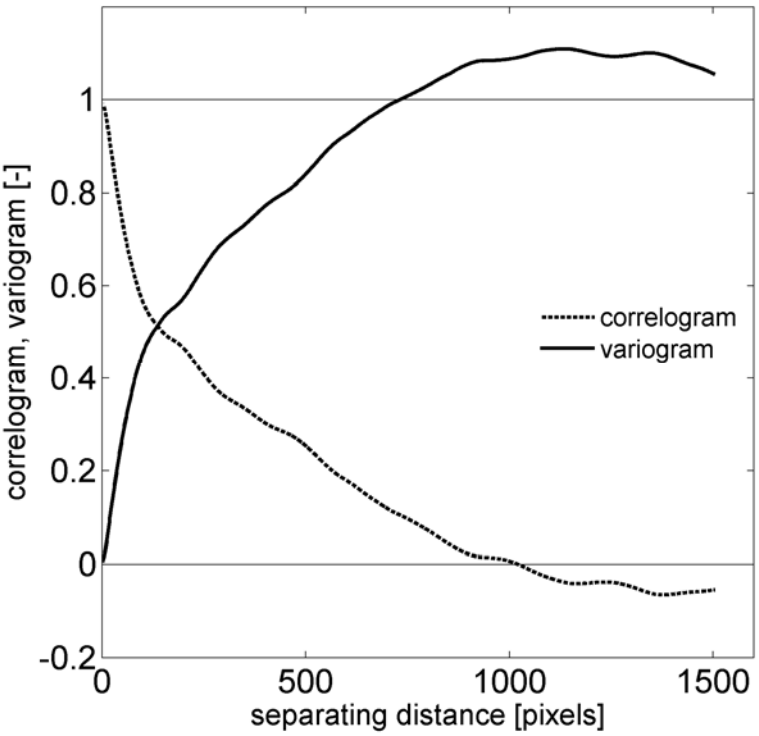

Figure 4-4. Comparison of the correlogram and the variogram for a representative sample of the smoke data.

If good mixing is characterized as the random spatial distribution of concentrations, the correlogram of a perfectly mixed population will drop to zero for all separation distances bigger than zero, showing there is no correlation in the data. Similarly, the variogram will rise instantly to one for separation distances bigger than zero, indicating that the variability everywhere is equal to the overall data variance.

Integration of the correlogram curve from $h = 0$ to the point where the coefficient of correlation R_x equals zero gives a mean length scale (Danckwerts, 1952):

$$L_D = \int_0^{\xi} R_x(h)dh \qquad (4\text{-}9)$$

as shown in Figure 4-5(a). The length scale obtained in this calculation is not the exact size of clumps or clusters but an average over the mixing field. Danckwerts specified that this calculation should only be used for data with no large-scale

segregation and no periodic patterns, giving correlograms that are always positive and non-periodic. In the context of today's mixing research, this seems unrealistic.

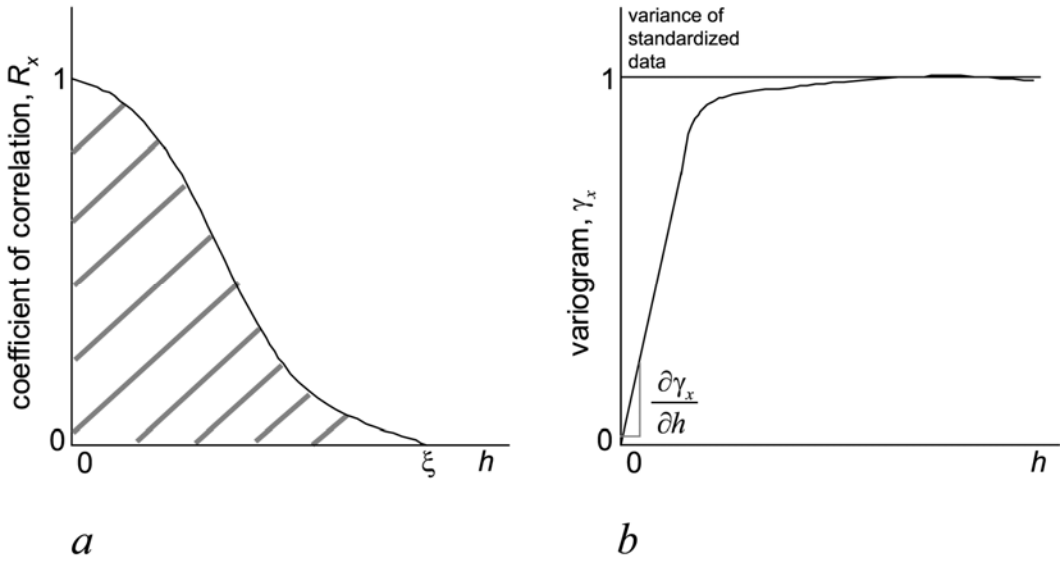

Figure 4-5. Length scale calculation from the correlogram and variogram:
(a) Mean length scale evaluated as the area under the correlogram curve.
(b) Sample variogram length scale proportional to the inverse of the initial slope.

For variograms, a more flexible length scale calculation was proposed by geostatisticians Carle and Fogg (1996), who evaluated the mean length scale from the inverse of the initial variogram slope:

$$L_V = \left[\frac{\partial \gamma_x}{\partial h} \right]^{-1}_{h \to 0} P \qquad (4\text{-}10)$$

as illustrated in Figure 4-5(b). In this calculation, P is the proportion of the minor species in the sample region. They showed that the resulting scale of segregation is proportional to the average length scale in the sample region. The reasoning behind this calculation is the following: if we place the origin at the centre of an average-sized blob of diffusive tracer in the field and move from the origin toward the blob boundaries and to the surroundings, the variability of concentration will increase much faster for small blobs due to the jump of concentration at the boundaries and slower for bigger blobs. This length scale calculation can be performed for all kinds of data and variogram plots, regardless of oscillations or large-scale segregation.

Test Cases

Two types of data were used for the scale of segregation measurements: particle tracking data, and concentration field data. The particle tracking data provide spatial point patterns where the locations of discrete particles, or members of a population, are known. The second data type is concentration maps, also called lattice data because the data values are available for a complete lattice of points. In digital images, the lattice is made up of pixels. Two data sets of each type were used to evaluate the measurement methods. The first test case is the laminar mixing of mass-less tracer particles in a staggered herringbone micromixer, shown in Figure 4-6. The second test case is the dispersion of floating particles in a turbulent stirred tank, shown in Figure 4-7. The third test case is the dispersion of smoke in a wind tunnel for a range of laminar to turbulent flow regimes, shown in Figure 4-8. The last test case is a concentration step change experiment in a continuous flow industrial reactor geometry, shown in Figure 4-9. In the first two cases, CFD provided complete 3D data sets and planes of data were extracted for analysis. In the third and fourth test cases, planar experimental data from digital images was used. While only 2D data sets were analyzed in this work, the extension of the calculations to 3D analysis is straightforward.

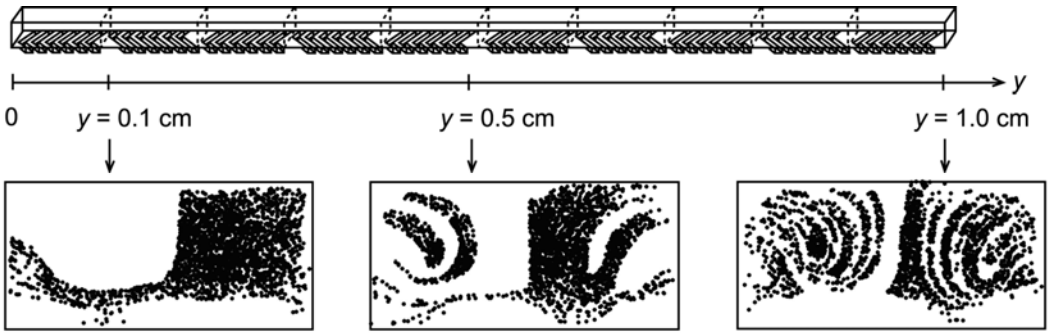

Figure 4-6. Staggered herringbone micromixer geometry and sample data for 2480 tracer particles and 10 mixer elements.

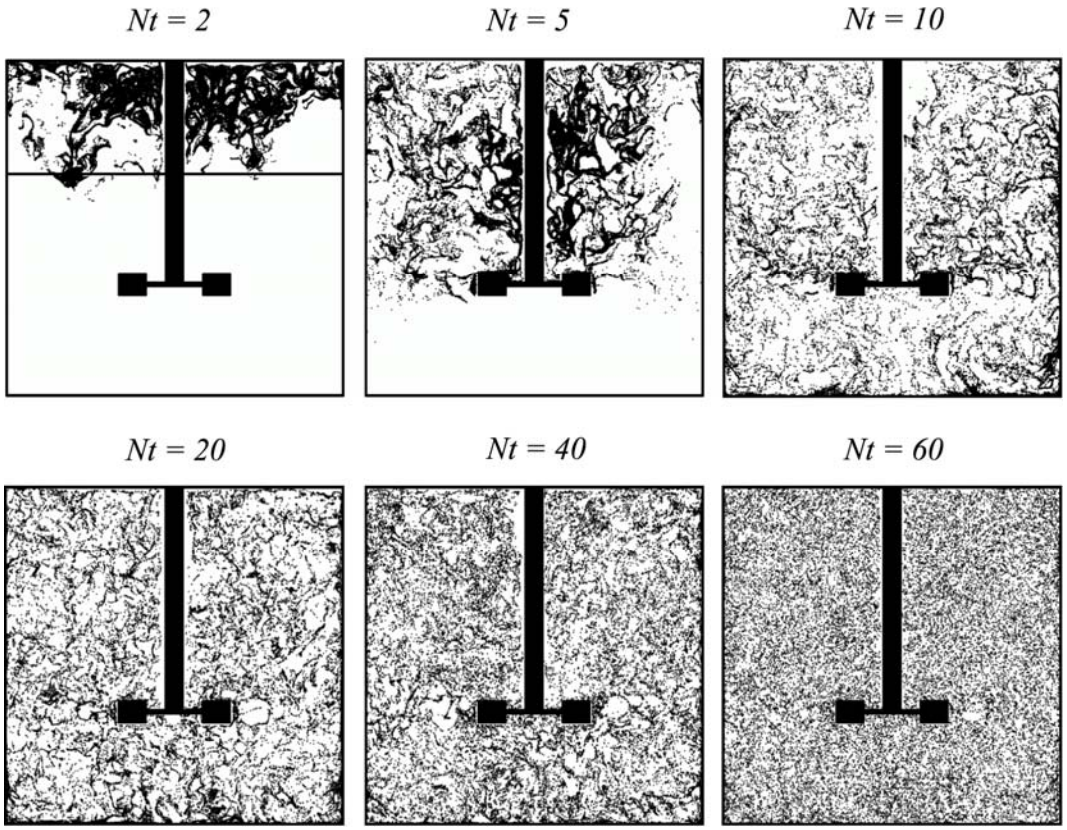

Figure 4-7. Stirred tank particle tracking data; T = 0.2335 m, D = T/3, impeller off-bottom clearance C_{imp} = T/3; 7×10^6 particles; *Nt* = number of impeller rotations.

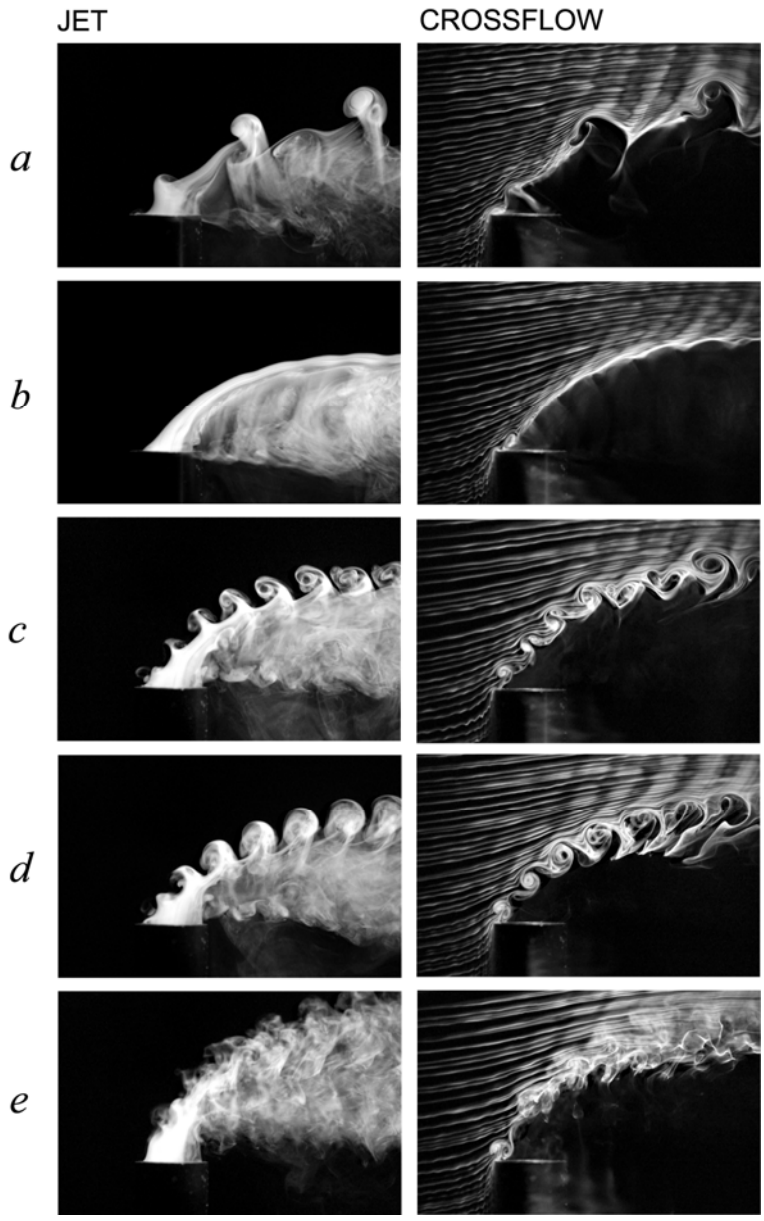

Figure 4-8. Jet-in-crossflow photographs of different flow regimes: (a) Free jet, $Re_d = 570$. (b) Relaminarized jet, $Re_d = 660$. (c) Flow with upstream-pointing vortex structures, $Re_d = 1130$. (d) Flow with downstream-pointing vortex structures, $Re_d = 1130$. (e) Turbulent jet, $Re_d = 1500$. The flow is visualized by seeding the jet flow (pictures on the left) and the crossflow (pictures on the right) with smoke. The image size is 3008×1960 pixels.

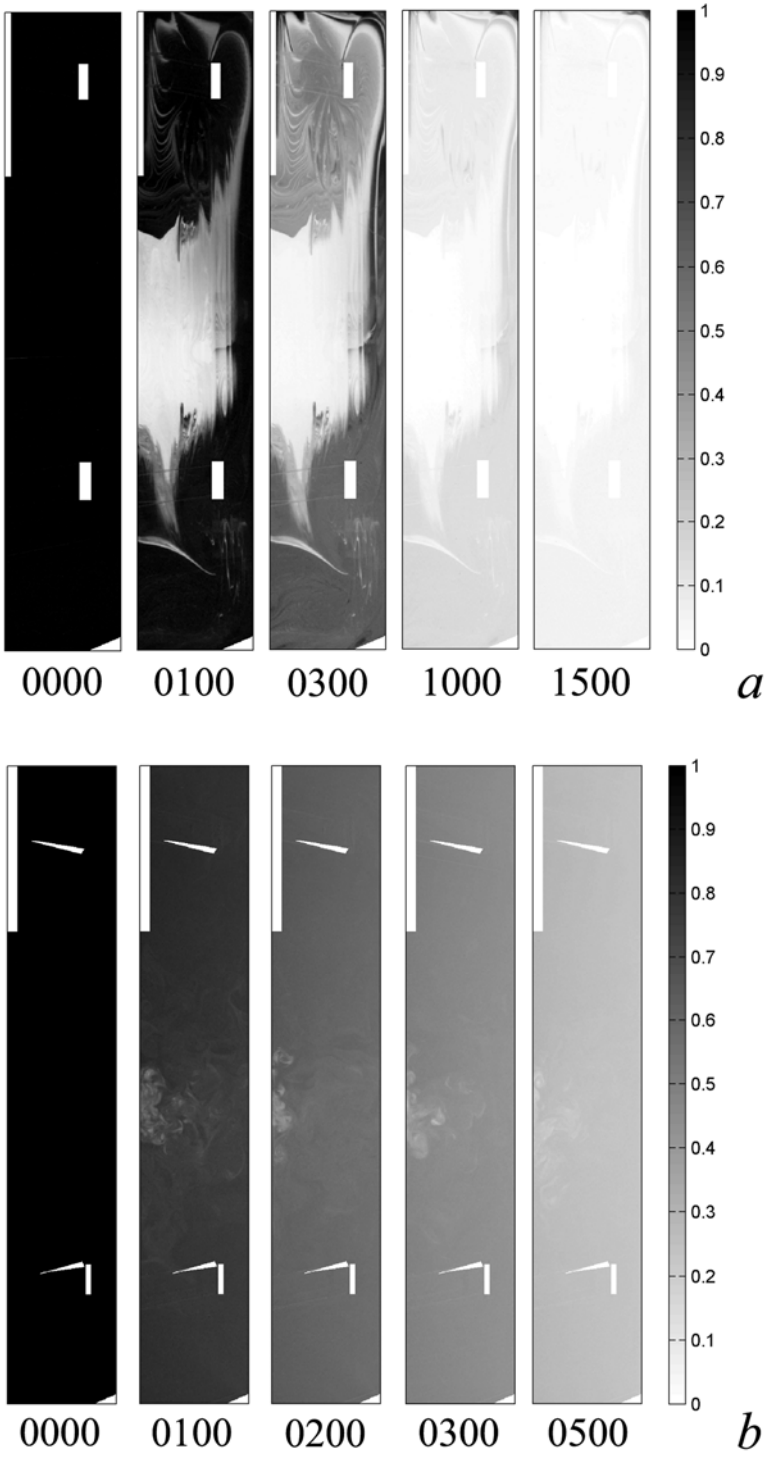

Figure 4-9. Reactor concentration data for two Reynolds numbers with the frame numbers shown below the images: (a) Re = 17. (b) Re = 1478. The average image size is 1290×225 pixels.

Detailed specifications of the first and second test cases are described in Aubin et al. (2005) and Hartmann et al. (2006), so only a brief summary is given

here. For the herringbone micromixer shown in Figure 4-6, a total of 2480 uniformly distributed mass-less particles were placed on the right hand side of the solved flow field at the mixer inlet and were followed using the Lagrangian particle tracking method. Vertical planes along the micromixer were sampled at intervals of 100 μm to be used for analysis. The geometry used was the reference geometry with a width W = 200 μm, height H = 77 μm, groove depth $d_g = 0.23H$ and groove width w_g = 50 μm.

The second test case is the dispersion of floating particles suspended in a baffled tank stirred by a Rushton turbine, shown in Figure 4-7. In this simulation, 7×10^6 mono-disperse spherical particles were tracked during a transient large eddy simulation. The data extracted from the simulation is the particle positions in a vertical cross-section mid-way between two baffles at six different times during the simulation.

The third test case is a jet in cross-flow forced with a synthetic jet of increasing strength (Watson, 2007 and Watson and Sigurdson, 2008), as shown in Figure 4-8. In these experiments, a pipe with outer diameter D_{pipe} = 2.54 cm was inserted in a rectangular 30.5×30.5 cm wind tunnel with a turbulence intensity of 16%. Inside the outer pipe, an inner pipe of 20.6 mm was inserted, through which a jet flow was introduced at a range of Reynolds numbers, Re_d. This flow was further controlled and modified by velocity oscillations in the annular flow between the two pipes. This resulted in a "synthetic jet" in different flow regimes spreading from the pipes into the wind tunnel. More experimental details can be found in Watson (2007) and in Watson and Sigurdson (2008). To visualize the flow, either the jet or the cross-flow was seeded with a glycerol and water based fog vapour, giving two photographs for each configuration. The 3008×1960 pixel greyscale images were analyzed based on the greyscale intensity of the pixels corresponding to the smoke concentration.

The fourth data set is concentration maps of a glycerin-water mixture in a continuous flow industrial stirred tank reactor. The reactor is filled with dyed fluid at the beginning of the experiment. At time zero, a clear fluid is introduced into

the reactor, mixing with and continuously washing out the dyed fluid. The feed location is on the side of the reactor and the exit is at the top. The experiment was performed for a range of Reynolds numbers from laminar to high transitional: Re = 17, 165, 1478 and 4498. The fluorescent dye is illuminated by a laser sheet and images of the reactor are captured by a camera as the experiment progresses. The image dimensions are approximately 1290×225 pixels. The resulting data are normalized tracer concentration measurements at each pixel. The concentrations of the tracer fluid change from 1 at the beginning to 0 when all the dyed fluid is washed out. Several image frames from the experiments are shown in Figure 4-9. Before further processing, the experimental data was filtered to eliminate the Gaussian white noise coming from the camera.

Results and Discussion

The four methods of measuring the scale of segregation were applied to the four test cases and the results are discussed with respect to the five criteria defined in the introduction. First, the suitability of the methods for either point pattern or concentration data is noted. For each method, the practical considerations for application to the test cases are given, together with directions and suggestions on the best settings to use. This is followed by a comparison of the results of the length scale analysis with the scales visualized in the images and the physical meaning of the calculated scales is discussed. The conclusions for each method summarize the results of the evaluation criteria. Finally, the speed of the calculations for each method is compared at the end of the section.

Maximum Striation Thickness on a Transect

Transect sampling is suitable for both point and concentration data. It was used to determine the maximum striation thickness in the micromixer, stirred tank and the smoke test cases.

For the staggered herringbone micromixer, the transect was located at mid-height of the microchannel, as illustrated in Figure 4-2, and the striation thickness

calculation was performed using a resolution of $\Delta z = \Delta x = 5$ μm, which is equal to the mean particle spacing.

The calculated maximum striation thickness along the micromixer is shown in Figure 4-10. The width of the largest striation decreases exponentially as the fluid passes along the mixer. This is characteristic of chaotic flows as the flow is divided and reoriented at each element in the mixer, so the number of striations is expected to increase as K_o^n, where K_o is the number of times the fluid is divided in each mixer element and n is the number of elements (Etchells and Meyer, 2004). As the number of striations increases, the CoV and the maximum striation thickness will necessarily decrease, but the rate of decrease cannot easily be predicted from the mixer geometry. In the laminar micromixer, volume filling and scale reduction happen simultaneously and the decay in the maximum striation thickness is a smooth curve. Based on the slope of the curve in Figure 4-10, K_o is estimated to be 1.33. Using this value, 1.33, 4.2, and 17.3 striations are calculated for 1, 5, and 10 mixer elements, respectively, which agrees well with the data in Figure 4-6.

For particle dispersion in the stirred tank, the transect was located at two thirds of the tank height, as shown in the first image of Figure 4-7. The transect resolution was based on the mean particle spacing, in the same way as for the micromixer data, giving a transect height, $\Delta z \cong 1$ mm, and a striation thickness threshold, $\Delta x \cong 1$ mm.

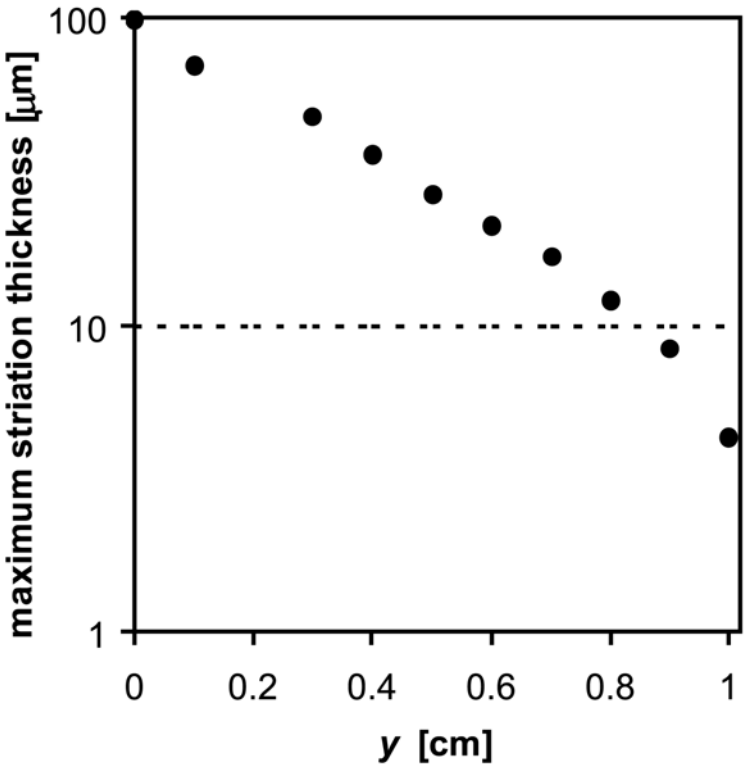

Figure 4-10. Maximum striation thickness as it decays along the micromixer.

Figure 4-11 shows a rapid decay of maximum striation thickness during the initial stages of mixing, but no significant reduction in the scale of segregation after 10 impeller revolutions. Referring to Figure 4-7, and recalling that the only striations measured are for the black particles, not for the white spaces, the initial cluster sizes are less than one tenth of the tank diameter, and the particles are rapidly dispersed throughout the tank: the first stage is dominated by macromixing with a rapid decay of the maximum striation thickness and *CoV* (Kukuková et al., 2008). During the later stages of turbulent mixing, accurate definition of a maximum striation thickness is difficult due to the sparse particle density at the smaller scales of segregation, and the fact that the particles disperse randomly in all directions, rather than through stretching distributions in the underlying velocity field.

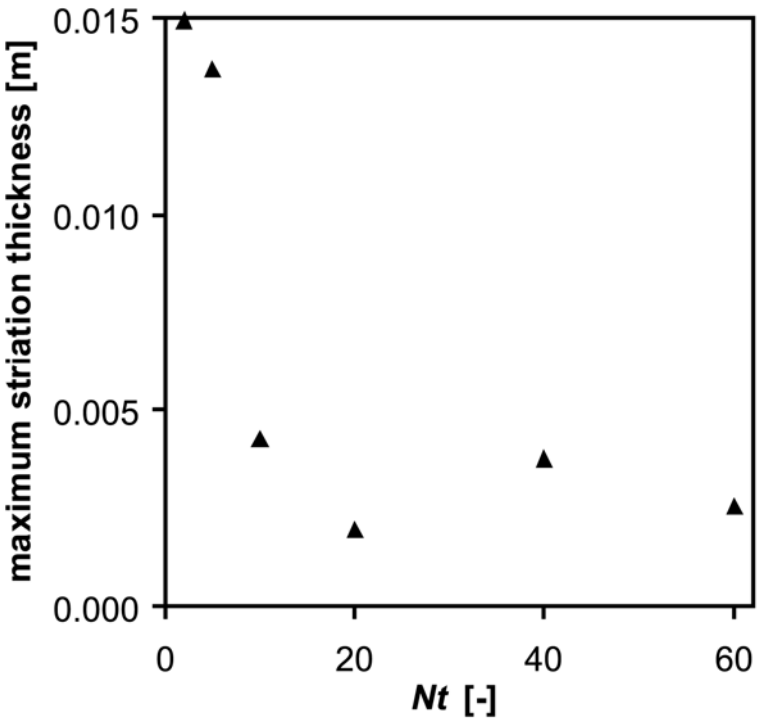

Figure 4-11. Maximum striation thickness on a transect in the stirred tank; *Nt* = number of impeller revolutions.

The species concentration data in the last two test cases covers a continuous range of intensities due to the effects of molecular diffusion and turbulent eddies. As a result, the evaluation of striation thickness is based on a threshold concentration, instead of a threshold distance between tracking particles. For the smoke distribution test case, the saturated white smoke was assigned a concentration of 1 and the black background was assigned a concentration of 0. Several concentration thresholds were tested. By analogy with equation 4-1, the *f* function was used to identify striations:

$$C > C_{min} \qquad f(x) = 1$$

$$C \leq C_{min} \qquad f(x) = 0 \qquad (4\text{-}11)$$

where C_{min} = 0.2, 0.3, 0.4, 0.5 and 0.6 and the mean concentration is close to 0.2, but varies from image to image. When the lower concentration limit is set too low, too much data is included and the striations blur together, making them hard to distinguish. In contrast, when the limit is set too high, visible striations of low concentration may not be detected. The maximum striation thickness for the

smoke test case was measured on 15 vertical transects distributed along the streamwise direction, as shown in Figure 4-12 and Figure 4-13.

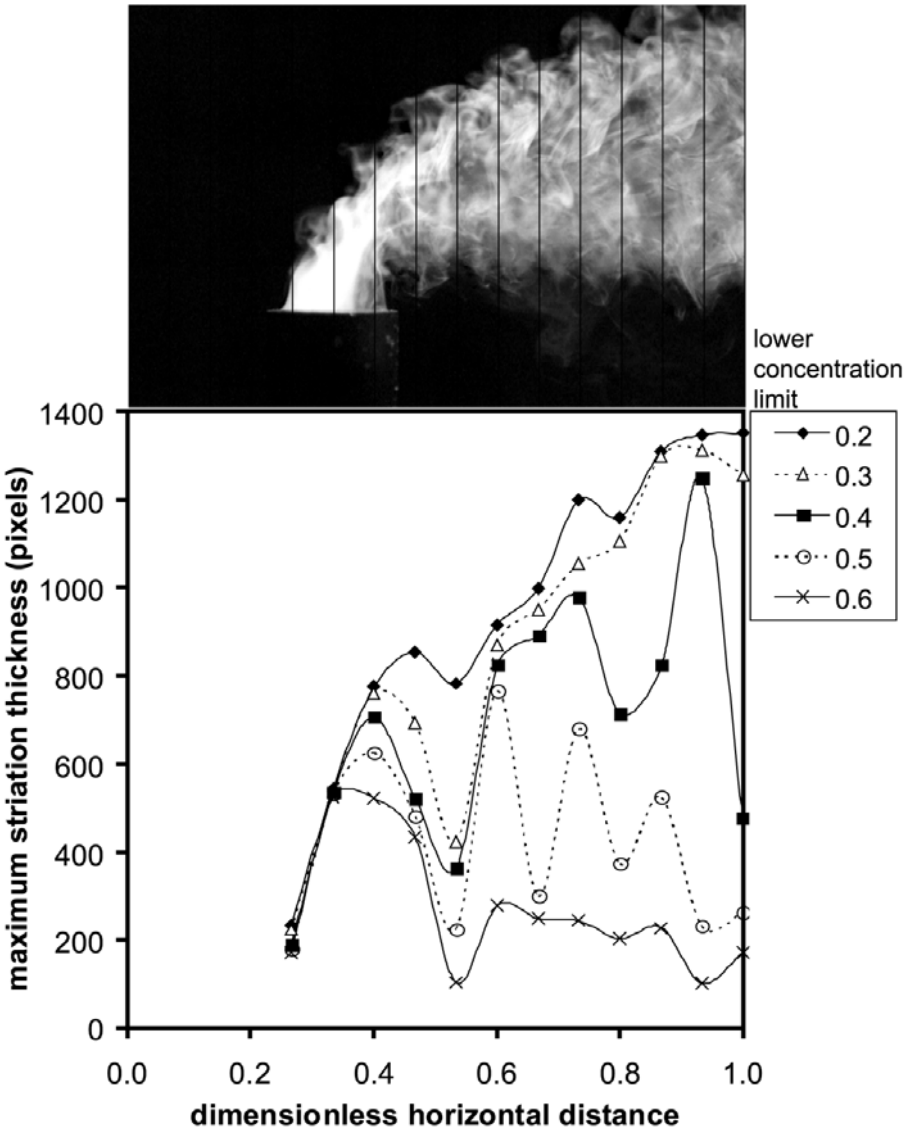

Figure 4-12. Maximum striation thickness on 15 transects for the smoke image in Figure 4-8(e) jet flow, showing a strong dependence on the concentration threshold. The image is 3008 pixels wide and 1960 pixels high. A greyscale intensity of 0.2 is equal to 82% of the mean concentration (0.24) for the whole image.

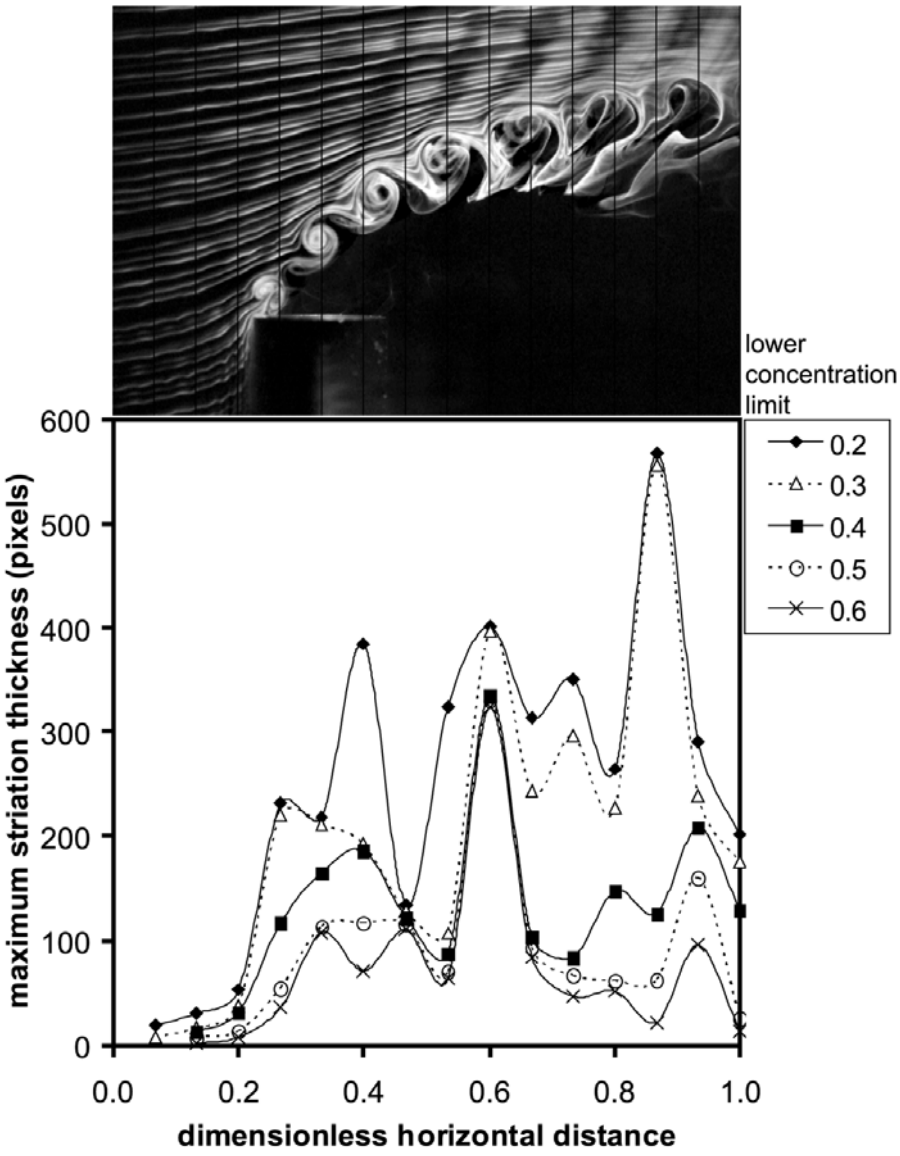

Figure 4-13. Maximum striation thickness on 15 transects for the smoke image in Figure 4-8(d) crossflow, showing a strong dependence on the threshold concentration range. The image is 3008 pixels wide and 1960 pixels high. A grayscale intensity of 0.2 is 103 % of the mean concentration (0.195) for the whole image.

Figure 4-12 shows the maximum striation thickness on 15 transects for the smoke distribution in Figure 4-8(e). The maximum striation thickness gets higher as the concentration threshold drops. The smoke plume spreads as it flows from the jet outlet towards the right side of the picture, while the smallest scales of segregation get smaller and less distinct. The plume width, or the macro-scale of segregation, is accurately captured with a concentration threshold of 0.2.

Increasing the concentration threshold leads to the detection of the meso-scales of segregation, which decrease in size from left to right. The smaller scales of segregation are difficult to confirm because the striations are not very well defined in the image.

The maximum striation thickness for an image with clearly distinguishable striations is plotted in Figure 4-13. As in the previous case, the lowest concentration threshold accurately captures the macro-scale of the smoke. In the first few transects where no large structures are present, the calculation gives the size of the visible small striations (15-20 pixels). Further along the image, the smallest striations cannot be detected by the maximum striation thickness measurement because the transects cut across much bigger smoke eddies. We conclude that if striations or any other small to moderate sized structures are to be detected using this method, the data set has to be free of structures bigger than the scale of interest. This can be accomplished by sub-sampling part of the image in a section that contains only striations, or only the meso-sized structures.

To compare the results more directly with a homogeneous mixing field, two additional concentration thresholds were tested. A concentration threshold of 95% of the mean concentration $C_{\min} = 0.95\overline{C}$ was chosen in analogy to the mixing time criterion, and a limit of 200% of the mean concentration $C_{\min} = 2\overline{C}$ was tested in an attempt to reveal scales smaller than the macro-scale, based on the observation that the initial results presented in the previous section tend to change from macro-scale characterization to measurement of smaller scales at around C_{min} = 0.4, which is about 200% of the mean concentration. These limits were tested on a series of three images shown in Figure 4-14. Figure 4-14(a) shows the first image, originally part of Figure 4-8(a). For this image, the transect is located at 2/15 of the image width, corresponding to the second transect in Figure 4-12 and Figure 4-13. This transect location was chosen because only striations and no bigger structures cross this transect. The first enlarged sample, shown in Figure 4-14(b), is 1/6 of the big image and contains only striations and no other structures. The third sample, shown in Figure 4-14(c), is a 200×200 pixel sample

showing three striations. The transects for both enlarged images are located at one half of the sample width. The maximum striation thicknesses for the 95% threshold were 34, 30 and 33 pixels, for the big, medium and small images, respectively. The calculated scales are very similar to each other for all analyzed images. This shows that the maximum striation thickness on a transect accurately and consistently captures the largest scales in the data. For the 200% threshold, the maximum striation thicknesses were 13, 16 and 18 pixels, for the big, medium and small images, respectively. This measurement produces smaller scales than the 95% threshold and is well matched to the visual observation. The resulting length scales are obviously very sensitive to the concentration threshold. When the scale of smaller structures is needed, the data have to be re-sampled to isolate the small striations or eddies. There is no general recommendation for the selection of C_{min}. Different thresholds reveal different scales in the data, so a meaningful C_{min} threshold has to be chosen for each problem.

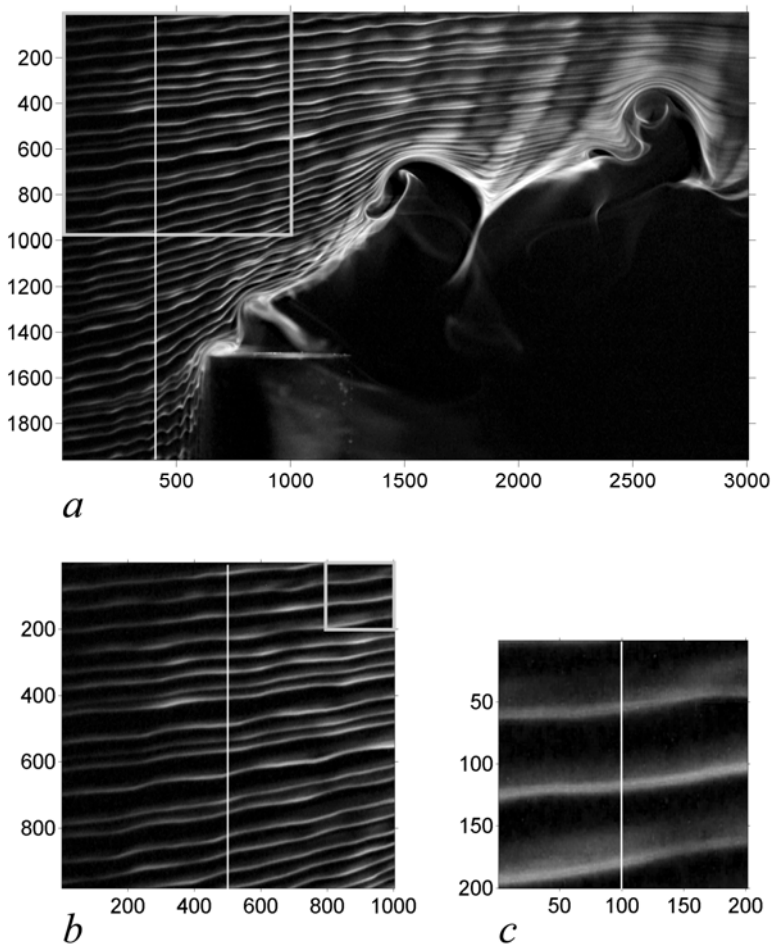

Figure 4-14. A series of zoomed-in smoke crossflow images showing the transect locations.

The maximum striation thickness accurately captures the maximum length scale on a transect for either point or concentration data. The spatial resolution matches the mean particle spacing for particle data, and the pixel spacing for concentration data. The method is very fast to apply, but the results represent only a small sample of the population. Also, care must be taken to orient the transects perpendicular to the striations of interest and to let them pass through the worst mixed part of the mixing field. If smaller structures are to be captured, sub-sampling of the image may be required to isolate these structures. The maximum striation thickness is easiest to apply to point pattern data since the mean particle spacing for a perfectly regular distribution is easily determined. If concentration data is analyzed, a concentration threshold has to be selected in order to define the striations and the results are very sensitive to this choice.

PNN

The point-to-nearest neighbour method is specifically suited to point pattern data and cannot be applied to concentration data. In this paper, it will be used for the micromixer and the stirred tank test cases. For both cases, a hexagonal grid of sampling points was used, as shown in Figure 4-3(c). Figure 4-3(d) shows an example of the stirred tank particle data and Figure 4-3(e) illustrates the procedure used to find the nearest neighbours for each grid point.

For meaningful statistical analysis, the distribution of distances has to be normalized with some characteristic length scale. For mixing analysis, this scale should be independent of time or measurement resolution. The mean of the distribution changes with time and the grid spacing and the mean homogeneous particle spacing depend on the grid resolution and the number of particles, respectively. The maximum separation distance between two particles in the plane offers a physically meaningful measure, which is both time and resolution independent. In addition, the diagonal of a rectangle, or the diameter of a pipe could both be used so this normalization can accommodate a range of mixing equipment. All PNN distances were normalized with the maximum separation distance and then multiplied by 100, giving distributions in terms of the percent of maximum separation for both geometries.

The effect of grid resolution was tested to verify the recommended selection of $k \approx \sqrt{n}$ (Diggle and Matern, 1980). For the stirred tank data, an image containing 32 000 particles was evaluated using sampling grids ranging from 130 grid points to 136 000 grid points. The mean PNN distance was consistent down to 512 grid points, and a smooth PNN distribution was obtained for grids of 8600 grid points and higher. To maximize the use of the particle tracking data, the number of grid points was matched to the number of particles for all subsequent calculations. The number of points in the grid was 2480 for the micromixer and ranged from 28 000 to 56 000 for the stirred tank to allow for the variation in the number of particles. The mean grid spacing for the micromixer is 2.7 microns and for the stirred tank, it ranges from 1.1 to 1.5 mm.

The normalized PNN distributions are compared with a Poisson distribution in Figure 4-15 and Figure 4-16. The Poisson distribution has a mean and variance equal to the mean of the PNN distribution in all plots. Figure 4-15 shows the PNN distributions for the micromixer test case. Moving along the length of the micromixer, the distributions evolve from clustered to more random, which is illustrated by their approach to the random Poisson distribution. However, even at the micromixer outlet, the PNN distribution is more clustered than a random distribution. This accurately reflects the presence of visible striations at the end of the mixer in Figure 4-6. Notice that on the *x*-axis, the maximum measured separation drops from 40% of the diagonal to 10% of the diagonal over the length of the mixer.

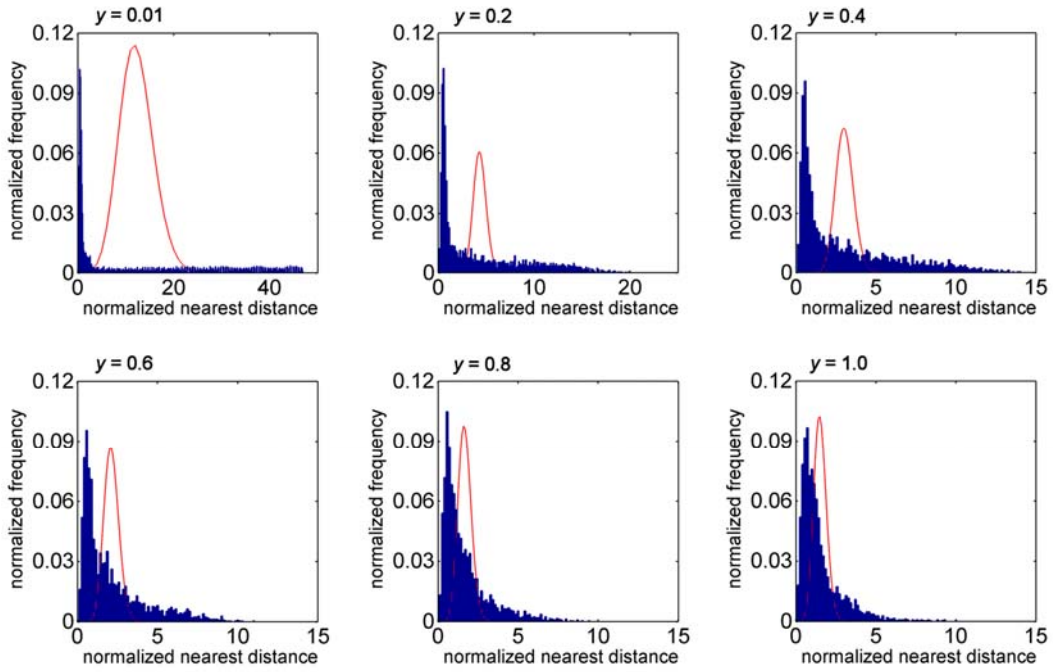

Figure 4-15. Comparison of the nearest distance distributions (histogram) with the Poisson distribution (curve) for several sampling planes along the micromixer.

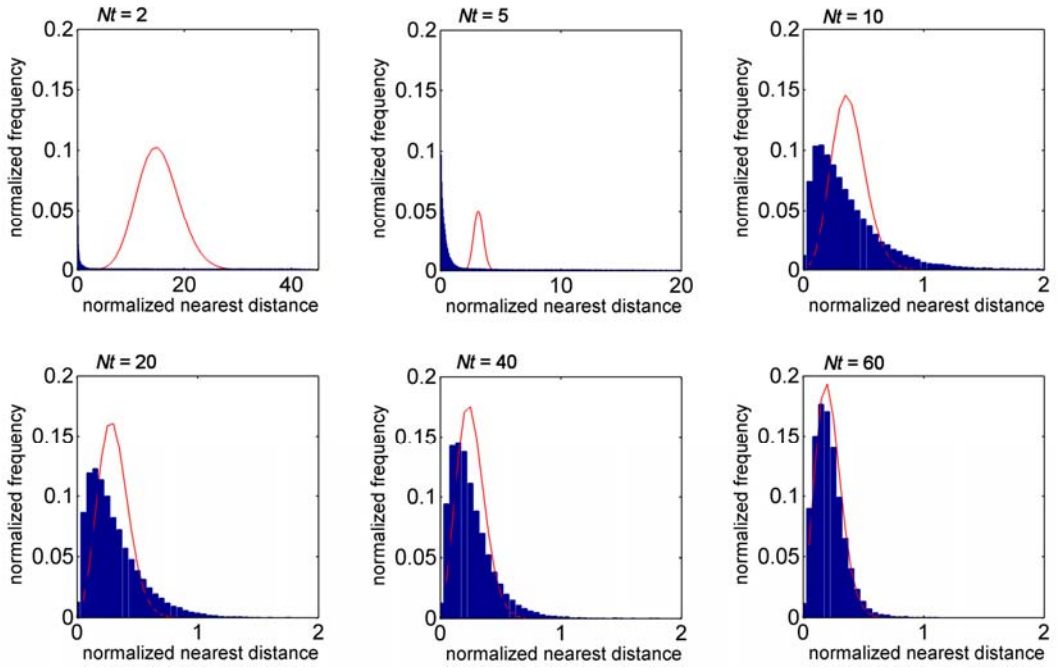

Figure 4-16. Comparison of the nearest distance distributions (histogram) with the Poisson distribution (curve) for each time step in the stirred tank.

Figure 4-16 compares the PNN distribution with the Poisson distribution for the stirred tank test case shown in Figure 4-7. As the mixing progresses, the PNN distribution approaches the random Poisson distribution, and the maximum measured separation decreases from 40% of the diagonal to less than 1% of the diagonal. At the beginning, the particle distribution is clustered, indicated by a wide distribution with a peak at a small distance. A skewed bell-shaped distribution appears at $Nt = 10$, which is the time when the particles have filled the volume of the tank. As the PNN distribution approaches the Poisson distribution, clustering is reduced and the particles are more evenly distributed at the smallest detectable scales.

In further studies, it might be interesting to investigate how the PNN distribution relates to the distribution of striation thicknesses in a sample area. This comparison was not completed in this work because the total number of measured striation thicknesses on a 1D transect did not provide enough data to represent the whole population of striation thicknesses in the 2D sample area.

The evolution of the index of dispersion is shown in Figure 4-17 and Figure 4-18. The index of dispersion is the ratio of the population variance to the population mean. For a random distribution of particles, the index of dispersion is equal to one. For the micromixer test case in Figure 4-17, the curve decreases along the micromixer and tends to a value of one at the end of the micromixer as the particle distribution approaches a random state.

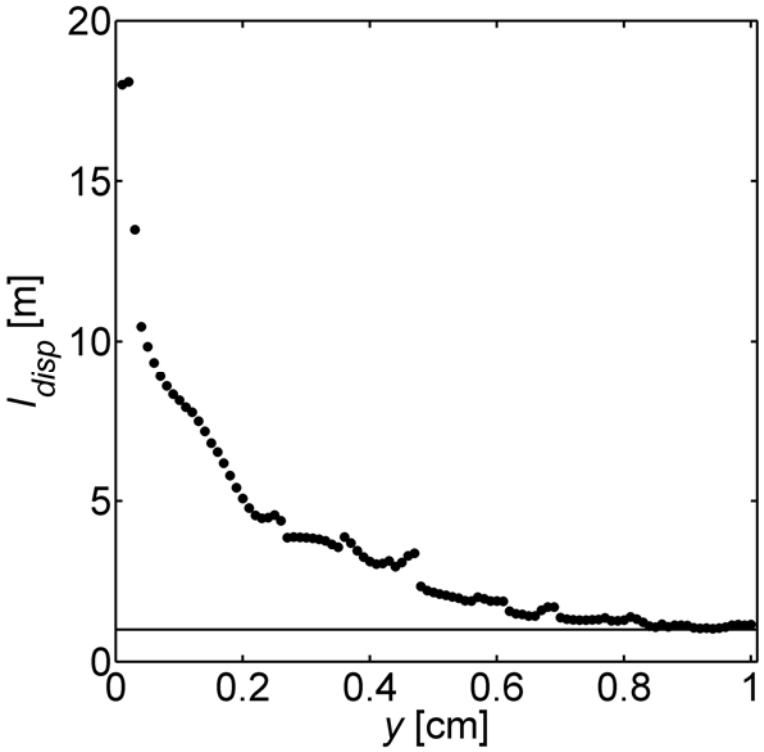

Figure 4-17. Evolution of the index of dispersion for the laminar micromixer.

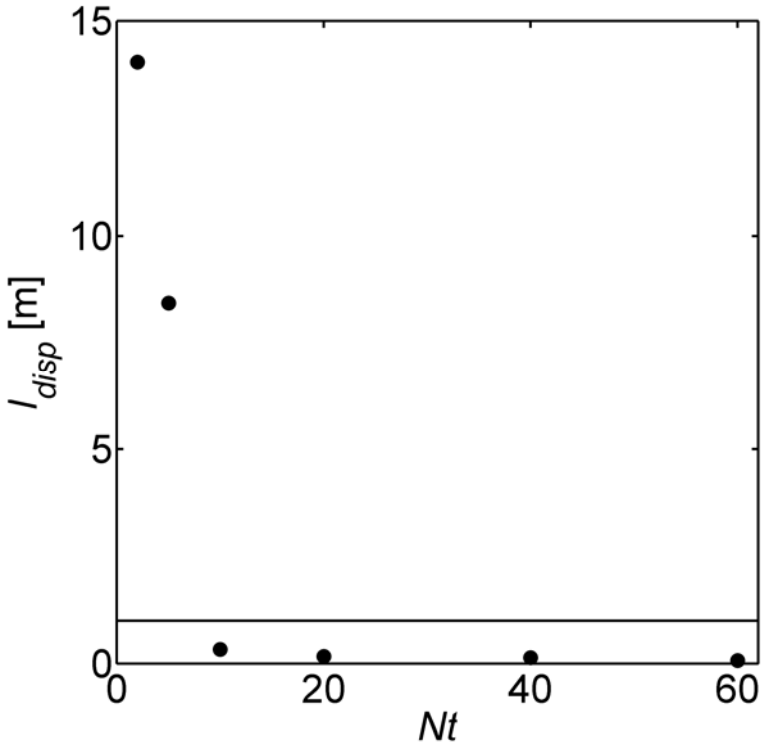

Figure 4-18. Evolution of the index of dispersion for the turbulent stirred tank.

Figure 4-18 shows the index of dispersion curve for the stirred tank. The curve rapidly decreases and drops below a value of one after the first 10 time steps. Thereafter it decreases only slightly. These two parts of the curve indicate a two-stage process of mixing: the volume filling stage over the first 10 time steps, followed by a scale reduction stage in the later time steps (Kukuková et al., 2008). Index of dispersion values that are less than one show that the particle distribution quickly becomes more regular than a Poisson distribution.

The filtered point-particle variance, as defined in Equation 4-4, is shown in Figure 4-19 and Figure 4-20 for several values of the filter threshold x_R. Figure 4-19 shows the evolution of the mixing quality in the micromixer expressed as the filtered PNN variance normalized by the variance at the inlet. Four PNN variance curves for x_R values of 0.5 µm, 1.0 µm, 2.5 µm and 5 µm correspond to approximately 20%, 40%, 100% and 200% of the mean grid spacing, respectively. As x_R increases, the PNN variance decreases because the criterion of what is considered close enough to the expected homogeneous distribution is more relaxed and it is easier to achieve the required scale of segregation.

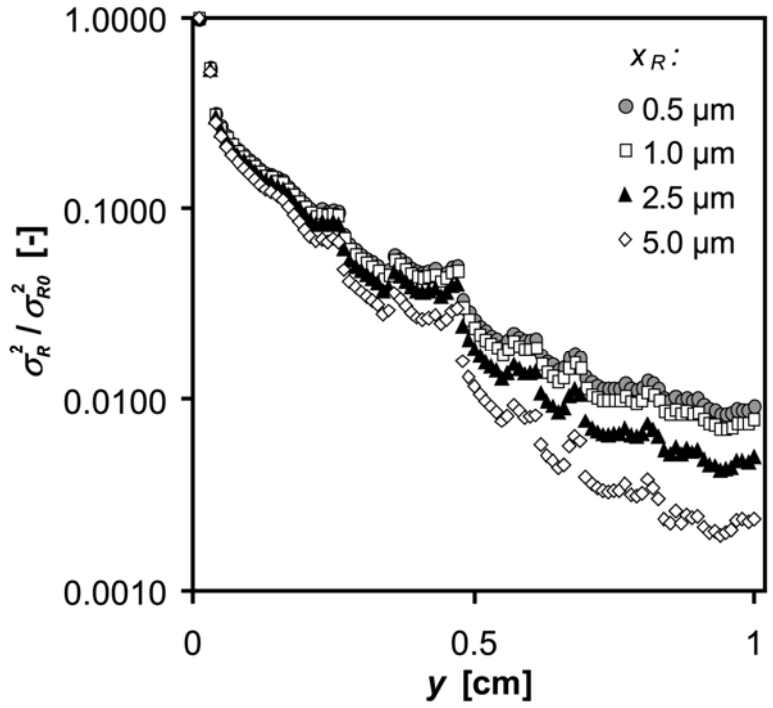

Figure 4-19. Normalized PNN variance for the micromixer test data showing the effect of the filter threshold, x_R. The mixing quality is expressed as the filtered PNN variance normalized by the PNN variance at the inlet.

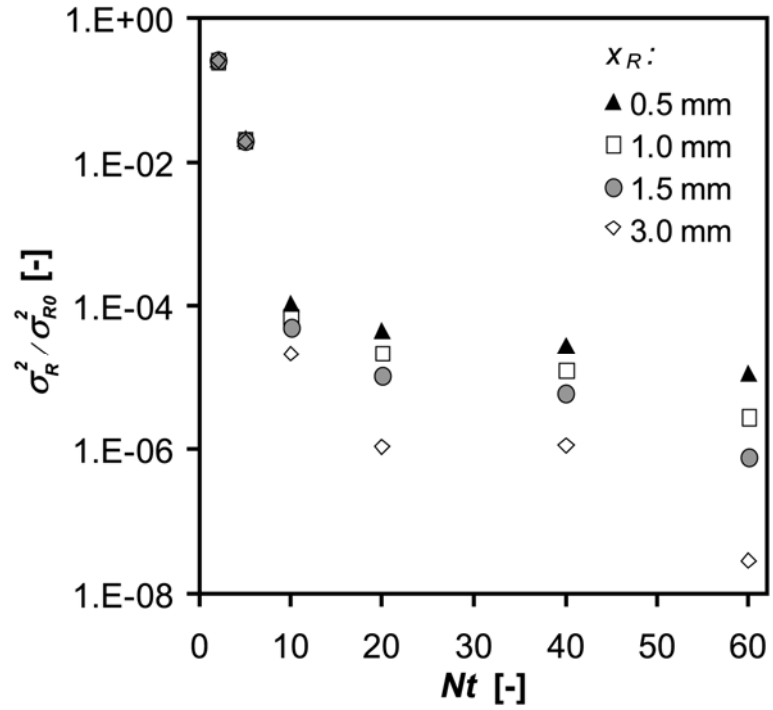

Figure 4-20. Normalized PNN variance for the stirred tank test data showing the effect of the filter threshold, x_R. The mixing quality is expressed as the filtered PNN variance normalized by the filtered PNN variance at time = 0.

Figure 4-20 presents the evolution of the filtered PNN variance over time in the stirred tank test case. The local point-particle variance is normalized by the point-particle variance at time equal to zero. Four x_R values of 0.5 mm, 1.0 mm, 1.5 mm and 3 mm, corresponding to approximately 33-50%, 67-100%, 100-150% and 200-300% of the mean grid spacing, were used. The percentage varies here since the number of particles – and therefore the number of grid points – varies slightly with each time step. The filtered variance shows a trend similar to the index of dispersion curve: a rapid decrease in the variance at the beginning, followed by a gradual decrease after 10 time steps. As expected, the PNN variance decreases as x_R increases and the scale of segregation requirement is relaxed. It can also be seen that the values of the filtered PNN variance for the turbulent stirred tank drop to a much smaller fraction of the initial variance than for the laminar micromixer.

The PNN method is only suitable for point pattern data. It is able to distinguish between segregated, clustered, and regular distributions of particles. The index of dispersion provides a more quantitative measure of these characteristics, while the filtered PNN variance measures the uniformity of the distribution relative to a minimum acceptable scale of segregation. The advantage of the PNN method is that the results always represent the whole population and have an underlying physical meaning. The disadvantage of this method is that the calculation is time-consuming. The resolution of the PNN method ultimately depends on the number of tracking particles in the data set, and the matching of the grid to the number of particles, both of which increase the computational time.

Correlograms and Variograms

In order to use correlograms and variograms for point pattern data, concentrations would have to be calculated from quadrat sampling. Since it is known that quadrat sampling reduces the spatial resolution of the data, this approach is not recommended. Correlograms and variograms are best suited for full field concentration data.

The difference between the correlogram and the variogram was illustrated in Figure 4-4. We now return to a quantitative discussion of the plot, which shows the horizontal variogram and correlogram for the smoke image in Figure 4-8(b) cross-flow. The correlogram curve drops below zero and the variogram curve exceeds the value of one, indicating the presence of large scale segregation. The original image reveals a large black area and another large unmixed area containing smoke striations. The evaluation of length scales from the correlogram is not defined for this kind of data because of the presence of macro-segregation and small oscillations due to local striations. Since large scale segregation is common in the initial stages of mixing and the quantification of scales is desirable even for this type of mixing field, the correlogram cannot be used consistently and only variogram results are discussed for subsequent calculations.

The length scale calculation from the variogram slope (Eq. (10)) involves a quantity P which characterizes the proportion of minor species in the sample region. For the analysed images, the concentrations have a form of intensity with the scale going from zero to one, so P can be evaluated as the mean intensity in the image.

The variograms and the associated length scale calculations for the reactor test case were performed for all time steps and Reynolds numbers and representative results are shown in Figure 4-21. For both Reynolds numbers, the variograms approach one as time progresses, indicating little remaining correlation and thus good mixing. Both cases show a steadily increasing variogram curve, indicating large-scale segregation in the mixing field. Over time, the large-scale segregation diminishes for the higher Reynolds number case but remains in the laminar case. The persistent macro-scale segregation, or lack thereof, is clearly visible in Figure 4-9. The variograms for the higher Reynolds number flow have periodic oscillations, which indicate an underlying periodicity in the data – in this case striations. Comparison of the horizontal and vertical variograms reveals a much bigger segregation in the vertical direction, where the variogram curves significantly exceed the value of one. In both directions, the macro-segregation reduces with time.

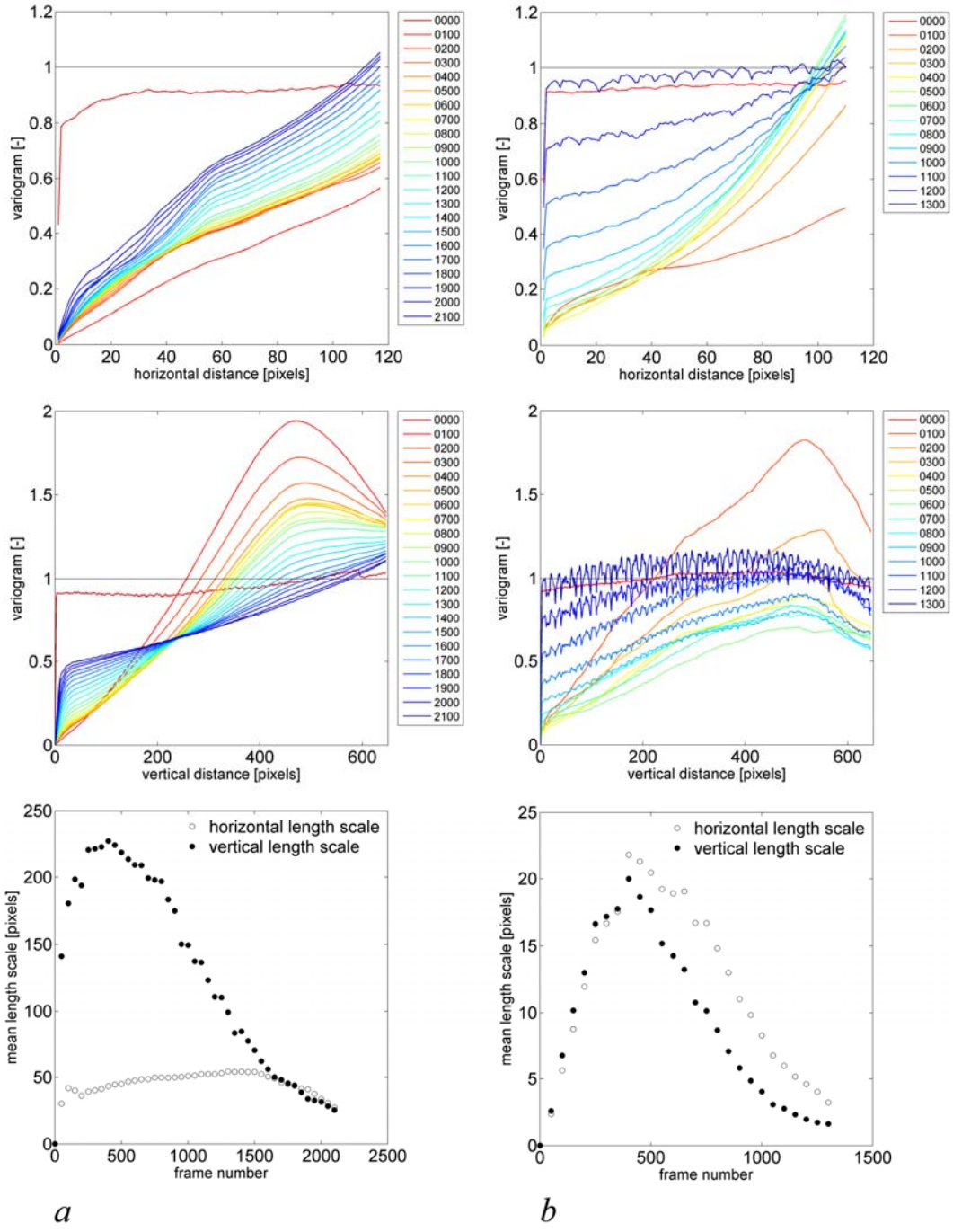

Figure 4-21. Reactor variograms and length scales; from top to bottom: horizontal variogram, vertical variogram and mean length scales; (a) Re = 17 (b) Re = 1478.

Horizontal and vertical length scales calculated from the variograms are shown in the bottom row of Figure 4-21. The length scales for the higher Re are about ten times smaller than for the lower Re, which is expected. The scales increase initially as the clear fluid begins to fill the vessel, reach a peak, and

decrease as the injected fluid mixes with the contents of the reactor. The length scales at the end of the experiment are much lower for the higher Re case. The horizontal and vertical length scales are comparable for the higher Re flow, but for the laminar case, the vertical length scale is larger than the horizontal one. When the length scale is compared with the image and the pixel size of the image, some interesting results emerge. Comparing the horizontal and vertical length scales for the low Re case with the original image, the white area in frame 100 is about 190 pixels wide by 430 pixels high. The measured *average* length scale is 50 pixels in the horizontal direction and 200 pixels in the vertical direction. If the actual horizontal length scale is multiplied by the fraction of the vertical space taken up by the blob, the estimated mean length scale is 62, which approaches the variogram result of 50. Applying this same logic to the vertical length scale gives an estimate of 360 pixels, which is much larger than the reported result of 200 pixels. Similar comparisons can be applied to the rest of the images. The inevitable conclusion is that the mean length scale correctly tracks the progress over time to a better mixed image, but contains very little information about the complex mixing structures in the image, which necessarily contain a wide distribution of length scales. The length scale obtained from the variogram does not give a direct measure of the striation thickness.

Variograms for the smoke data are shown in Figure 4-22. The positive slope of the curves, which persists over most of the calculation range, arises from the large-scale segregation in the mixing field. The large black areas in the photographs dominate the results. The variograms also reveal periodicity in the concentration, which is most visible for the vertical cross-flow case. For some jet images, there is a slight periodicity of flow in the horizontal direction, but it is not as easily observed as the striations in the cross-flow case. This is due to the periodic repetition of smoke eddy structures, which can be seen in Figure 4-8 (a), (c) and (d). For the laminar (a) and turbulent (e) smoke images, no periodicity can be either visually observed or detected using the variogram.

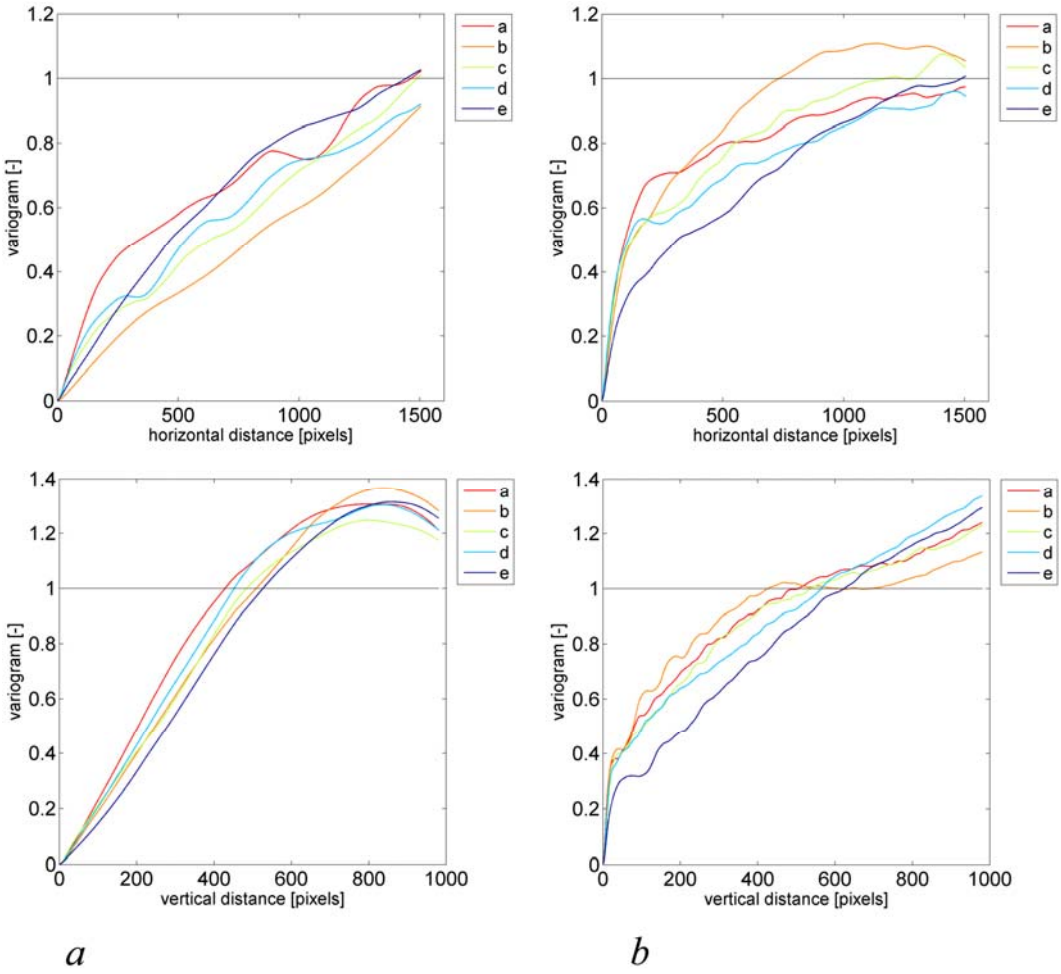

Figure 4-22. Horizontal (top) and vertical (bottom) variograms for the smoke data: (a) jet flow (b) crossflow; results for data from Figure 4-8 (a)-(e), as shown in the legend.

The horizontal and vertical mean length scales calculated from the initial slope of the variogram are presented in Figure 4-23. A first look at the figure reveals that the scales for the cross-flow images are always smaller than for the jet images. Indeed, the size of the smoke structures is smaller when the cross-flow is seeded with smoke, in contrast with the seeded jet flow. Further examination shows that the length scales in the horizontal direction are always bigger than in the vertical direction. For all the jet pictures, this is caused by the dimensions of the smoke cloud structure; its length is always bigger than its height. For the cross-flow image, this phenomenon arises because the horizontal direction cuts through the length of the smoke striations and the vertical direction cuts across their width.

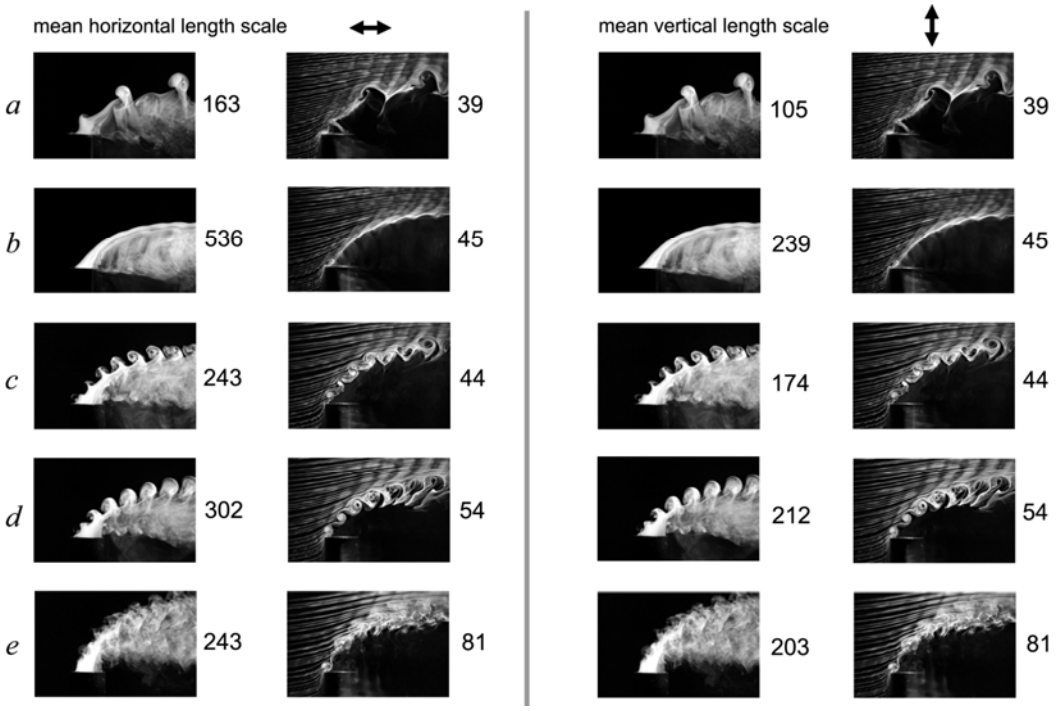

Figure 4-23. Mean horizontal and vertical length scales for the jet images.

Length scales calculated from variograms contain information about the mean macro-scale of the concentration field. To investigate whether smaller scales can be captured, e.g. the width of smoke striations in the smoke images, the same enlarged images that were used for the maximum striation thickness analysis, shown in Figure 4-14, were used for the length scale calculation. The calculated vertical length-scales were 11, 2.2 and 2.8 pixels for the big, medium and small images, respectively. The length scale was smaller for the enlarged images that contained striations only. The scale did not change much as the medium image was magnified further to show three striations only. These results show that smaller scales can be captured if a sub-sample containing only structures at the scale of interest is used for analysis, provided that a good data resolution is maintained. Comparing these variogram length scales with the maximum striation thicknesses for the same data clearly illustrates the difference between the two methods – the maximum striation thickness is sensitive to the concentration threshold, but accurately captures the striation size of 30 pixels; the variogram length scale of 2 pixels has no adjustable parameters, but also does not give the striation thickness directly.

The variogram is a useful tool for characterizing the correlation or variability in concentration fields and has a resolution equal to the pixel resolution of the data. The variogram reveals both large-scale segregation and periodicity. The length scales calculated from variograms represent the average of the whole population in the concentration field, so sub-sampling is required if smaller structures in the mixing field are of interest. When interpreting the length scales, one must also bear in mind that they are not a direct measure of the striation thickness, or even an area averaged striation thickness. No simple method has yet been proposed to extract a distribution of length scales directly from variogram data. In comparison to the maximum striation thickness and PNN calculations, this method is moderately fast.

Conclusions

The objective of this work was to examine four methods of measuring the scale of segregation and to test their application to 2D fields of mixing data: the maximum striation thickness on a transect, point-to-nearest neighbour distributions, the correlogram and the variogram. Two types of data were used to evaluate the measurement methods: particle tracking data and concentration field data, with two test cases of each type. The particle tracking data was obtained from laminar mixing of particles in a staggered herringbone micromixer and turbulent dispersion of particles in a stirred tank. The concentration field data was for a jet in cross-flow and for a concentration step change experiment in a continuous flow industrial reactor.

The methods were compared and evaluated in order to determine their strengths and limitations for the analysis of mixing data. Five questions were addressed during the evaluation of the four measures:

1. What type of data is the method suitable for?
2. What information does it provide?
3. Are the results physically meaningful?
4. What is the smallest scale of mixing resolved by the method?

5. How fast is the calculation?

The answers to this set of questions are conveniently summarized in Table 4-1, followed by a more detailed discussion of each of the criteria.

Table 4-1. Comparison of the four methods for measuring the scale of segregation.

	Maximum striation thickness on a transect	**PNN**	**Correlogram**	**Variogram**
What type of data is the method suitable for?	Location data (point patterns) Concentration data (not so easy)	Location data (point patterns)	Concentration data; no large scale segregation, no periodicity	Concentration data
What information does it provide?	Maximum length scale; sampled data	Clustering character, closeness to homogeneous distribution; whole population	N/A	Integral length scale; whole population
Are the results physically meaningful?	Exact length scale	Exact distance distribution	N/A	Proportional to real scales
What is the smallest scale of mixing resolved by the method?	Mean inter-particle spacing	Mean grid spacing	N/A	Measured data spacing (e. g. 1 pixel)
How fast is the calculation?	Fast 7 s*	Time consuming 9 min*	N/A	Moderately fast 6 min 25 s*

* The calculation times are for one frame, calculated in Matlab R 2009a using the AMD Athlon 64 processor, 2.41 GHz and 2 GB RAM.

The suitability of a measurement method varies for different types of data. The maximum striation thickness on a transect is easiest to apply to point pattern data since the sharp striation interfaces are easily determined. If concentration data is analyzed, a concentration threshold has to be selected in order to define the striations and the results are very sensitive to this choice. The PNN method is only suitable for point pattern data and cannot be used for concentration data. Both the variogram and correlogram are useful for characterizing concentration data, however, only the variogram can be used to determine length scales from data containing large scale segregation or periodicity. Because this type of data is common in today's mixing research, correlogram calculations were not pursued.

The methods provide scale measurements in different forms. The maximum striation thickness accurately captures the maximum length scale on a

transect. The PNN method is able to distinguish between segregated, clustered, and regular distributions. The index of dispersion calculated from the PNN distributions provides a more quantitative characterization of the distribution of the population. The filtered PNN variance measures the uniformity of the distribution relative to a reference scale of segregation, x_R. The variogram is a useful tool for characterizing the correlation or variability in concentration data and can reveal both large scale segregation and periodicity. The length scales calculated from variograms represent a proportional average of the whole data field.

The physical meaning of the results depends on the quality of sampling. The maximum striation thickness on a transect represents only a small sample of the population, so to get meaningful results, care must be taken to orient transects perpendicular to the striations of interest and to let them pass through the worst mixed part of the mixing field. If smaller structures need to be captured, sub-sampling of the image may be required. The PNN distributions always represent the whole population and have an underlying physical meaning provided enough tracking particles are used to resolve the scales of interest, and the number of grid points is matched to the number of particles. The index of dispersion provides a measure of departure from a random distribution for the whole population. The filtered PNN variance uses a sample of the population, which depends on the filter size x_R. Increasing the filter size relaxes the homogeneity criterion. The length scales calculated from variograms represent the average of the whole population in the data field, so sub-sampling is required if smaller structures in the mixing field are of interest. When interpreting the variogram length scales, one also has to bear in mind that they are not exact length scales but proportional length scales, and no simple method has yet been proposed to extract a distribution of real length scales from variogram data.

The smallest length scale that can be obtained from the striation thickness calculation is slightly smaller than the mean particle spacing that is used to define the striation threshold. For complex data sets, sub-sampling of data is needed to measure the size of small structures. For the PNN distributions, the smallest scales

are given by the mean grid spacing. The minimum scale of the variogram measurement is fixed by the image resolution.

The speed of calculation is directly proportional to the size of the data set and the number of operations for each frame. The maximum striation thickness on a transect calculation is the fastest because it involves just one or a few line samples of the data. The PNN calculations were the most time consuming because the number of grid points was matched to the number of particles and the distances from all grid points to all particles were calculated. The variogram calculations were moderately fast compared to the other methods. Both the PNN and the variogram algorithms could be optimized to get faster results, but in both cases the computations were fast enough that this was not deemed necessary.

This study provides a toolkit of methods for length scale characterization, together with benchmarks for the use and limitations of each tool. The calculation algorithms for each method are available as supplementary material in the Appendix of this thesis.

References

Atiemo-Obeng, V. A. and Calabrese, R. V., 2004, *Rotor Stator Mixing Devices*, In Paul, E.L.; Atiemo-Obeng, V.A. and Kresta, S.M. (Editors), Handbook of Industrial Mixing: Science and Practice, John Wiley & Sons, Inc., New Jersey, USA.

Aubin, J.; Fletcher, D. F. and Xuereb, C., 2005, *Design of Micromixers using CFD Modelling*, Chem. Eng. Sci. **60**, 2503-2516.

Bałdyga, J. and Bourne, J. R., 1999, *Turbulent Mixing and Chemical Reactions*, Wiley, New York, USA.

Bennington, C. P. J., 2004, *Mixing in the Pulp and Paper Industry*, In Paul, E.L.; Atiemo-Obeng, V.A. and Kresta, S.M. (Editors), Handbook of Industrial Mixing: Science and Practice, John Wiley & Sons, Inc., New Jersey, USA.

Carle, S. F. and Fogg, G. E., 1996, *Transition Probability-Based Indicator Geostatistics*, Mat. Geol. **28**, 453-476.

Chu, L. Y.; Utada, A.; Shah, R.; Kim, J. W. and Weitz, D., 2007, *Controllable Monodisperse Multiple Emulsions*, Angew. Chem. Int. Ed. **46**, 8970-897.

Cottam, G. and Curtis, J. T., 1949, *A Method for Making Rapid Surveys of Woodlands by Means of Pairs of Randomly Selected Trees*, Ecol. **30**, 101-104.

Danckwerts, P. V., 1952, *The Definition and Measurement of Some Characteristics of Mixtures*, Appl. Sci. Res. Sect. A - Mech. Heat Chem. Eng. Mat. Methods **3**, 279-296.

Deutsch, C. V., *Geostatistical Reservoir Modeling*, 2002, In Applied Geostatistics Series, G., J. A., Ed., Oxford University Press, New York, USA.

Diggle, P. J., 2003, *Statistical Analysis of Spatial Point Patterns*, Oxford University Press, New York.

Diggle, P. J. and Matern, B., 1980, *On Sampling Designs for the Study of Point-Event Nearest Neighbor Distributions in R2*, Scand. J. Stat., 7, 80-84.

Etchells, A. W. and Meyer, C. F., 2004, *Mixing in Pipelines*, In Paul, E.L.; Atiemo-Obeng, V.A. and Kresta, S.M. (Editors), Handbook of Industrial Mixing: Science and Practice, John Wiley & Sons, Inc., New Jersey, USA.

Gullett, B. K.; Groff, P. W. and Stefanski, L. A., 1993, *Mixing Quantification by Visual Imaging Analysis*, Exp. Fluids **15**, 443-451.

Hartmann, H.; Derksen, J. J. and Van den Akker, H. E. A., 2006, *Numerical Simulation of a Dissolution Process in a Stirred Tank Reactor*, Chem. Eng. Sci. **61**, 3025-3032.

Johnson, B. K. and Prud'homme, R. K., 2003, *Chemical Processing and Micromixing in Confined Impinging Jets*, AlChE J. **49**, 2264-2282.

Kukukova, A.; Aubin, J. and Kresta, S. M., 2009, *A New Definition of Mixing and Segregation: Three Dimensions of a Key Process Variable*, Chem. Eng. Res. Des. **87**, 633-647.

Kukuková, A.; Noël, B.; Kresta, S. M. and Aubin, J., 2008, *Impact of Sampling Method and Scale on the Measurement of Mixing and the Coefficient of Variance*, AlChE J. **54**, 3068-3083.

Lacey, P. M. C. and Mirza, F., 1976, *Study of Structure of Imperfect Mixtures of Particles 2. Correlational Analysis*, Powder Technol. **14**, 25-33.

Liu, S. P.; Hrymak, A. N. and Wood, P. E., 2005, *Drop Breakup in an SMX Static Mixer in Laminar Flow,* Can. J. Chem. Eng. **83**, 793-807.

Mohr, W. D.; Saxton, R. L. and Jepson, C. H., 1957, *Mixing in Laminar-Flow Systems*, Ind. Eng. Chem. **49**, 1855-1856.

Muzzio, F. J.; Swanson, P. D. and Ottino, J. M., 1991, *The Statistics of Stretching and Stirring in Chaotic Flows*, Phys. Fluids A: Fluid Dyn. **3**, 822-834.

Nathan, G. J.; Mi, J.; Alwahabi, Z. T.; Newbold, G. J. R. and Nobes, D. S., 2006, *Impacts of a Jet's Exit Flow Pattern on Mixing and Combustion Performance*, Prog. Energy Combust. Sci. **32**, 496-538.

Newbold, G. J. R.; Nathan, G. J.; Nobes, D. S. and Turns, S. R., 2000, *Measurement and Prediction of NOx Emissions from Unconfined Propane Flames from Turbulent-Jet, Bluff-Body, Swirl, and Precessing Jet Burners*, Proc. Combust. Inst. **28**, 481-487.

Watson, G. M. G. and Sigurdson, L. W., 2008, *The Controlled Relaminarization of Low Velocity Ratio Elevated Jets-in-Crossflow*, Phys. Fluids **20**, 15.

Watson, M. G. G., 2007, *The Structure and the Controlled Relaminarization of Low Momentum Elevated Jets-in-Crossflow*, MSc. Thesis, University of Alberta, Edmonton.

Chapter 5: Conclusions and Future Work

This chapter presents the summary of conclusions drawn from the thesis and suggestions for future work. The objective of this work was to propose a rigorous definition of mixing and to provide a theoretical and experimental toolkit of methods to measure mixing in industrial applications.

Definition of Mixing

Based on the review of mixing and segregation characterization techniques in chemical engineering, spatial statistics and population studies, a definition of industrial mixing was proposed based on three dimensions of segregation: the intensity of segregation, the scale of segregation and exposure. The definition was introduced using concepts, theory and mathematical equations. Suitable quantities for direct measurement of the dimensions of segregation were chosen and investigated. The definition clearly defines what mixing is and it provides a framework for analyzing mixing problems and for future development of the field.

Intensity of Segregation

For measurement of the intensity of segregation, the coefficient of variance CoV was chosen to represent the deviation of homogeneity based on the concentration variance in a mixing field. This quantity has been widely used in the mixing literature. It is useful for both concentration and point pattern data. Investigation of CoV sampling strategies revealed that the resulting value strongly depends on the number and size of probes or quadrats and probe placement. A minimum of 250 probes were needed to accurately determine the intensity of segregation for the turbulent data set tested. The smaller the number of probes, the stricter the mixing criterion determining the closeness to homogeneity should be. CoV increases with decreasing probe size as smaller scales of variation are detected. The probe and quadrat size should be matched to the smallest scale of interest in the mixing field. For particle data, at least 10 particles should populate each probe or quadrat area in a perfectly homogeneous distribution, in order to

obtain statistically meaningful results. If the number of probes is limited, they should be placed in the worst mixed regions of the vessel to accurately track the homogeneous endpoint. The intensity of segregation is the dominant dimension of segregation for turbulent blending and for ensuring homogeneous dispersion. The observation of CoV in a turbulent case led to distinguishing between the initial volume filling stage (macromixing) and the following scale reduction stages (mesomixing). The measurement is also useful for processes where concentration changes are important i. e. laminar blending, mass transfer and reactions.

Scale of Segregation

The scale of segregation was investigated using four quantities: the maximum striation thickness, the point-to-nearest neighbour (PNN) distributions, the correlogram and the variogram. The maximum striation thickness accurately captures the maximum length scale on a transect and is available for both particle and concentration data. The results represent only a small sample of the population so careful sampling is required to capture the structures of interest. The PNN distributions are able to distinguish between clustered, random and homogeneous distributions of point patterns. In order to obtain the best results, the number of grid points used in the calculation should be matched to the number of particles. An additional quantity, index of dispersion, can be used to quantify the deviation from homogeneity of the PNN distribution. Filtered PNN variance can be used to relax the mixing criterion using a scale of interest. The correlogram calculation cannot be consistently used for all types of mixing data, because it is not suitable for data with large scale segregation or periodicity, and has therefore been rejected. The variogram characterizes the variability in the data and is able to reveal both large-scale segregation and periodicity. The length scales calculated from the variogram represent the proportional average scales from the whole mixing field. In order to capture smaller scales, sub-sampling is useful. The scale of segregation measurement is useful for all industrial mixing processes but is critical for laminar or non-Newtonian blending, where the size of striations or

cavities is of interest and for multiphase mixing, especially when tracking the size of particles, bubbles and drops or the size of their clusters.

Exposure

The exposure dimension is the most complex dimension of segregation, especially because its mathematical expression is different for different industrial mixing applications. Exposure is the time-scale of segregation and quantifies the potential to reduce segregation. Increasing the exposure will speed up the mixing process. Generally, exposure is the product of the strength of interaction, the distance from the minimum segregation and the opportunity to interact. It is the dominant dimension in mass transfer processes and mixing sensitive reactions. For mass transfer processes, exposure can be quantified by the mass transfer rate. For reactions, exposure follows the form of the reaction rate. Exposure terms can also be found in expressions for aggregation and crystallization kinetics, as well as in the birth and death terms in population balances, which are particularly relevant in liquid-liquid mixing.

Thesis Outcomes

The first important result of this thesis is the definition of mixing. This definition provides a theoretical framework for the rigorous analysis of mixing, encompassing all industrial mixing processes and allowing a clear evaluation of experimental methods.

The second outcome is a toolkit of methods for the measurement of the intensity and scale of segregation, provided as Matlab codes in the Appendix.

The third contribution is the guidelines for the use of each of the provided methods, with thoroughly investigated sampling procedures, settings, data suitability, meaningfulness of results and limitations of each tool.

The developed definition of mixing, together with tools and guidelines for measurement of mixing will help researches to further develop the field of mixing, engineers to solve practical industrial mixing problems, and instructors of chemical engineering courses to introduce mixing concepts more easily.

Future Work

This thesis focused on the development of the definition of mixing, based on the three dimensions of segregation and the investigation of methods used to measure the intensity and the scale of segregation. In the course of the paper reviewing, other approaches to measuring the scale of segregation e. g. a Multiple Spanning Tree theory came to our attention. Although the results are similar to the PNN analysis, it could prove to be useful to investigate this theory as well. The logical next step in this work would be to investigate the third measure of segregation 'exposure' with a focus on studying different measuring and sampling strategies. Another useful step would be to take the developed theory and measurement methods and directly apply them to solve particular industrial mixing problems. The knowledge and the tools created in the course of this thesis will be used as a foundation of a new chapter on segregation in the next edition of the Handbook of Industrial Mixing.

Appendix I. Intensity of Segregation Toolkit

This section contains Matlab codes for calculation of the coefficient of variance, *CoV*, from planar data using probes and quadrats.

CoV Calculation from Probes

```
function CoV = CoV_probes(A, particle_data, probe_data,
probe_size)
%%%%%%%%%%%%%%%%%%%%%%%%%%%%%%%%%%%%%%%%%%%%%%%%%%%%%%%%%%%%%%%%%%%%%%%%%%%%%
%%%%%%%%%
% CoV calculation for particle data in a plane using a set of
probe points
%
% input: A = area of the data plane
%        particle_data = file containing particle locations
%                        first column: x positions, second column:
y positions
%        probe data = file containing probe locations
%                     first column: x positions, second column: y
positions
%        probe_size = radius of the circular probe
%
% output: CoV
%
% Alena Kukukova, 2010
%%%%%%%%%%%%%%%%%%%%%%%%%%%%%%%%%%%%%%%%%%%%%%%%%%%%%%%%%%%%%%%%%%%%%%%%%%%%%
%%%%%%%%%
%% open and read file containing particle locations
[X,Y] = textread(particle_data, '%f %f');
L = length(X);

%% open and read data file containing sampling point positions
[Xref, Yref] = textread(probe_data, '%f %f');
Npr = length(Xref);

%% mean particle concentration in the plane
Cmean = L/A;

%%%%%%%%%%%%%%%%%%%%%%%%%%%%%%%%%%%%%%%%%%%%%%%%%%%%%%%%%%%%%%%%%%%%%%%%%%%%%
%%%%%%%%%
%% Calculate particle counts in all probe areas
%%%%%%%%%%%%%%%%%%%%%%%%%%%%%%%%%%%%%%%%%%%%%%%%%%%%%%%%%%%%%%%%%%%%%%%%%%%%%
%%%%%%%%%
Pt_count = zeros(Npr, 1);  % initialization
for n = 1:Npr          % loop through all probe locations

   % Create column vectors Xp & Yp with L lines
   % All values in each column are the same and correspond to the
   % coordinates of probe point 'n', i.e. (Xref(n), Yref(n))
   % The function ones(m,n) creates a m x n matrix with m lines
   % and n columns
```

```
   Xp = ones(L,1)*Xref(n);
   Yp = ones(L,1)*Yref(n);

   % Calculate the distance between all particles (X, Y) and probe
location 'n'(Xp, Yp)
   D = sqrt((X - Xp).^2 + (Y - Yp).^2);

   % Sort the elements of D in increasing order. D is a column
vector.
   Dsort = sort(D);

   no_part = 0;
   for i = 2:length(Dsort)
       if (Dsort(i) <= probe_size)
          no_part = no_part + 1;
       else break
       end
   end
   Pt_count(i) = no_part;
end

%%%%%%%%%%%%%%%%%%%%%%%%%%%%%%%%%%%%%%%%%%%%%%%%%%%%%%%%%%%%%%%%%%%%%%%%%%%%
%% Calculate particle concentrations from particle counts by
dividing with
%  probe area and make dimensionless with mean concentration
%%%%%%%%%%%%%%%%%%%%%%%%%%%%%%%%%%%%%%%%%%%%%%%%%%%%%%%%%%%%%%%%%%%%%%%%%%%%
A_probe = pi*probe_size^2;
Conc = (Pt_count/A_probe)/Cmean;

%%%%%%%%%%%%%%%%%%%%%%%%%%%%%%%%%%%%%%%%%%%%%%%%%%%%%%%%%%%%%%%%%%%%%%%%%%%%
%% CoV calculation
%%%%%%%%%%%%%%%%%%%%%%%%%%%%%%%%%%%%%%%%%%%%%%%%%%%%%%%%%%%%%%%%%%%%%%%%%%%%
sum = 0;    % sum of squares initialization
for i = 1:length(Conc)
    sum = sum + (Conc(i) - 1)^2;
end
CoV = (sqrt(1/(Npr - 1)*sum))/1;
```

CoV Calculation from Quadrats

```
function CoV = CoV_quadrats(width, height, nx, ny, particle_data)
%%%%%%%%%%%%%%%%%%%%%%%%%%%%%%%%%%%%%%%%%%%%%%%%%%%%%%%%%%%%%%%%%%%%%%%%%%%%
% CoV calculation for particle data in a plane using a rectangular
quadrats
%
% input:    width = width of the data plane, x-direction
%           height = height of the data plane, y-direction
%           nx = number of quadrats in x-direction
%           ny = number of quadrats in y-direction
%           particle_data = file containing particle locations
%                           first column: x positions, second
column: y positions
% output: CoV
%
```

```
% Alena Kukukova and Joelle Aubin, 2010
%%%%%%%%%%%%%%%%%%%%%%%%%%%%%%%%%%%%%%%%%%%%%%%%%%%%%%%%%%%%%%%%%%%%%%%%%%%%
%% open and read file containing particle locations
[X,Y] = textread(particle_data, '%f %f');
L = length(X);

%% mean particle concentration in the plane
A = width*height;   % data plane area
Cmean = L/A;

%% quadrat settings
xmin = 0;
ymin = 0;
Total_quadrats = nx*ny;
quadrat_counts = zeros(ny, nx); % matrix storing the number of
particles for each quadrat

%% loop through all particles and place them in corresponding
quadrats
for n = 1:L
    for j = 1:nx
        xpos = xmin+(width/nx)*j;
        if X(n) < xpos
            x_cell = j;
            break  % terminates execution of the 'for' loop to
start
                           % the next 'for' loop immediately
        end
    end
    for k = 1:ny
        ypos = ymin+(height/ny)*k;
        if Y(n) < ypos
           y_cell = k;
           break
        end
    end
    quadrat_counts(y_cell, x_cell) = quadrat_counts(y_cell,
x_cell) + 1;
end

%% Calculate particle concentrations from particle counts by
dividing with
%  quadrat area and make dimensionless with mean concentration
A_quadrat = A/Total_quadrats;
Conc = (quadrat_counts/A_quadrat)/Cmean;

%% CoV calculation
sum = 0;    % sum of squares initialization
for i = 1:ny
    for j = 1:nx
        sum = sum + (Conc(i, j) - 1)^2;
    end
end
CoV = (sqrt(1/(Total_quadrats - 1)*sum))/1;
```

Appendix II. Scale of Segregation Toolkit

This material is a collection of generic codes for calculation of four chosen methods for measurement of the scale of segregation: maximum striation thickness on a transect, point-to-nearest-neigbour distributions (PNN), correlogram and variogram. Each sub-section contains the calculation algorithm in a flowchart, followed by a code generated in Matlab, which can be modified for other programming languages.

Maximum Striation Thickness on a Transect

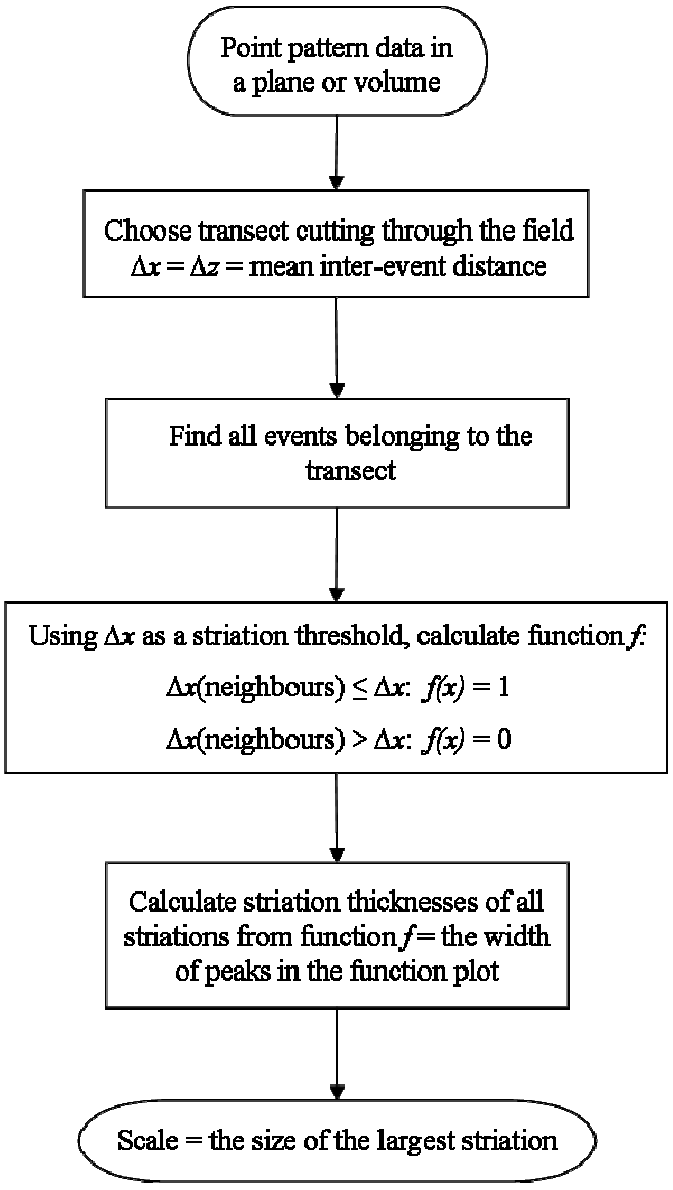

```
function maximum_striation_thickness(particle_file, transect_z,
dz, dx)
%%%%%%%%%%%%%%%%%%%%%%%%%%%%%%%%%%%%%%%%%%%%%%%%%%%%%%%%%%%%%%%%%%%%%%%%
% Maximum striation thickness on a transect calculation
%
% input: particle_data = file containing particle locations
%                        first column: x positions, second column:
z
%                        positions
%        transect_z = position of the transect
%        dz = transect height
%        dx = striation threshold
%
% output: file 'striation_f_function.txt' containing x positions
of
%         particles in the first column and the calculated 'f'
function
%         in the second column
%         max_str = the maximum striation thickness on a transect
%
% Alena Kukukova, 2010
%%%%%%%%%%%%%%%%%%%%%%%%%%%%%%%%%%%%%%%%%%%%%%%%%%%%%%%%%%%%%%%%%%%%%%%%
% Open & read particle data file
[X, Z] = textread(particle_file, '%f %f ');
L = length(X);
%
% Find all particles that lie on the transect = transect_z +-
1/2*dz and
% store their x coordinates
x_transect = [];
for i = 1:L;
    if (Z(i) <= (transect_z + 0.5*dz)) && (z(i) >= (transect_z -
0.5*dz))
        x_transect = [x_transect x(i)];
    end
end

if length(x_transect) > 2
    % Calculation for more than two particles in the transect

    % Sort x coordinates of particles in the transect with
increasing x
    x_transect = sort(x_transect);

    % Calculate the function f:
    % f(x) = 1 for consecutive particles belonging to the same
striation (separ. distance <= dx)
    % f(x) = 0 for consecutive particles belonging to different
striations (separ. distance > dx)
    % f = zeros(1, length(x_transect));

    % Calculation for the first particle
    distance_right = x_transect(2) - x_transect(1);     % distance
of the first particle to its right neighbour

    if distance_right > dx
       % particle doesn't belong to any striation
```

```
       f = [0];
       xs = [x_transect(1)];
    elseif distance_right <= delta
       % particle belongs to the striation with its right neighbor
       f = [0 1];
       xs = [x_transect(1) x_transect(1)];
    end

    % Calculation for the middle particles
    for i = 2:(length(x_transect)-1)
        distance_left = x_transect(i) - x_transect(i-1);
        distance_right = x_transect(i+1) - x_transect(i);

        if (distance_left <= delta) && (distance_right <= delta)
           % particle belongs to the striation with both
neighboring
           % particles
            f = [f 1];
            xs = [xs x_transect(i)];
        elseif (distance_left > delta) && (distance_right > delta)
            % particle doesn't belong to any striation
            f = [f 0];
            xs = [xs x_transect(i)];
        elseif (distance_left <= delta) && (distance_right >
delta)
            % particle belongs to the striation with only its left
neighbor
            f = [f 1 0];
            xs = [xs x_transect(i) x_transect(i)];
        elseif (distance_left > delta) && (distance_right <=
delta)
           % particle belongs to the striation with only its right
neighbor
            f = [f 0 1];
            xs = [xs x_transect(i) x_transect(i)];
        end
    end

    % Calculation for the last particle
    last = length(x_transect);
    distance = x_transect(last) - x_transect(last-1);
    if (distance <= delta)
       f = [f 1 0];
       xs = [xs x_transect(last) x_transect(last)];
    else f = [f 0];
       xs = [xs x_transect(last)];
    end

    % Save the f function in a file
    file_name = 'striation_f_function.txt';
    fid = fopen(file_name, 'a');
    fprintf(fid, 'x(m) f\n');
    for i = 1:length(f)
        fprintf(fid, '%5.4f %1.0f\n', xs(i), f(i));
    end
    fclose(fid);
```

```
    %%%%%%%%%%%%%%%%%%%%%%%%%%%%%%%%%%%%%%%%%%%%%%%%
    % Maximum striation thickness calculation
    %%%%%%%%%%%%%%%%%%%%%%%%%%%%%%%%%%%%%%%%%%%%%%%%
    thicknesses = [];

    % find the beg of the first striation
    for i = 1:length(f)
        if f(i) == 1
           beg = i;
           break
        end
    end
    value = 1;

    % Calculate the striation thicknesses on the transect
    index = beg;
    while index < length(f)
        while value == 1
            index = index + 1;
            value = f(index);
        end

        thickness = xs(index - 1) - xs(beg);
        thicknesses = [thicknesses thickness];

        % find the beginning of the next striation
        if index < length(f)
            for i = (index+1):length(f)
                if f(i) == 1
                    beg = i;
                    break
                end
            end
            index = i;
            if i < length(f)
                value = 1;
                index = beg;
            end
        end
    end

    % The maximum striation thickness calculation
    max_str = max(thicknesses);

elseif length(x_transect) == 2
    % If there are two particles in the transect:
    if abs(x_transect(1) - x_transect(2)) <= dx
       max_str = x_transect(1) - x_transect(2)
    else max_str = 0;
    end

elseif length(x_transect) == 1
    % If there is only one particle in the transect, there are no
    % striations:
       max_str = 0;

else   max_str = 0;     % No particles in the transect
```

```
end

fprintf('\nmaximum striation thickness on the transect = %5.4\n',
max_str)
fprintf('if the result is 0, no striations were detected\n');
```

Point-to-Nearest-Neighbour Distributions (PNN)

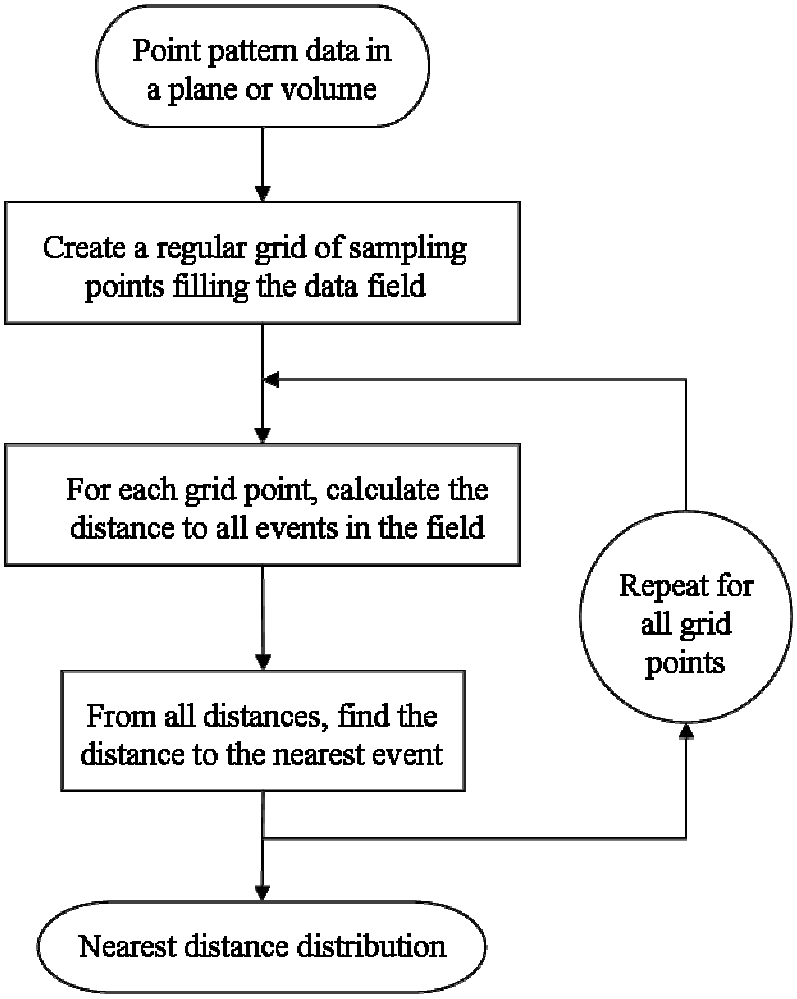

```
function PNN(particle_data, grid_data)
%%%%%%%%%%%%%%%%%%%%%%%%%%%%%%%%%%%%%%%%%%%%%%%%%%%%%%%%%%%%%%%%%%%%%%%%%%%%
% Calculation of Point-to-nearest-neigbour (PNN) distances
% (= for each sampling point in the grid, find the distance to the
nearest
% particle)
%
% input: particle_data = file containing particle locations
%                        first column: x positions, second column:
y positions
%        grid data = file containing positions of sampling points
%                    first column: x positions, second column: y
positions
%
% output: file 'nearest_distances.txt' containing nearest
distances for all
%         sampling points
%
% Joelle Aubin and Alena Kukukova, 2010
%%%%%%%%%%%%%%%%%%%%%%%%%%%%%%%%%%%%%%%%%%%%%%%%%%%%%%%%%%%%%%%%%%%%%%%%%%%%
% open and read file containing particle locations
[X,Y] = textread(particle_data, '%f %f');
L = length(X);

% open and read data file containing sampling point positions
[Xref, Yref] = textread(grid_data, '%f %f');
Nsamp = length(Xref);

for n = 1:Nsamp          % loop through all sampling points

   % Create column vectors Xp & Yp with L lines
   % All values in each column are the same and correspond to the
   % coordinates of point 'n', i.e. (Xref(n), Yref(n))
   % The function ones(m,n) creates a m x n matrix with m lines
   % and n columns
   Xp = ones(L,1)*Xref(n);
   Yp = ones(L,1)*Yref(n);

   % Calculate the distance between all events (X, Y) and point
'n'(Xp, Yp)
   D = sqrt((X - Xp).^2 + (Y - Yp).^2);

   % Sort the elements of D in increasing order. D is a column
vector.
   Dsort = sort(D);

   % Take the second element of Dsort as the nearest point-event
distance
   % (The 1st element is always 0)
   dist = Dsort(2);

   % Write nearest point-event distances to file
   file_name = 'nearest_distances.txt';
   fid = fopen(file_name,'a');
   fprintf(fid, '%e\n', dist);
 end
fclose(fid);
```

Correlogram

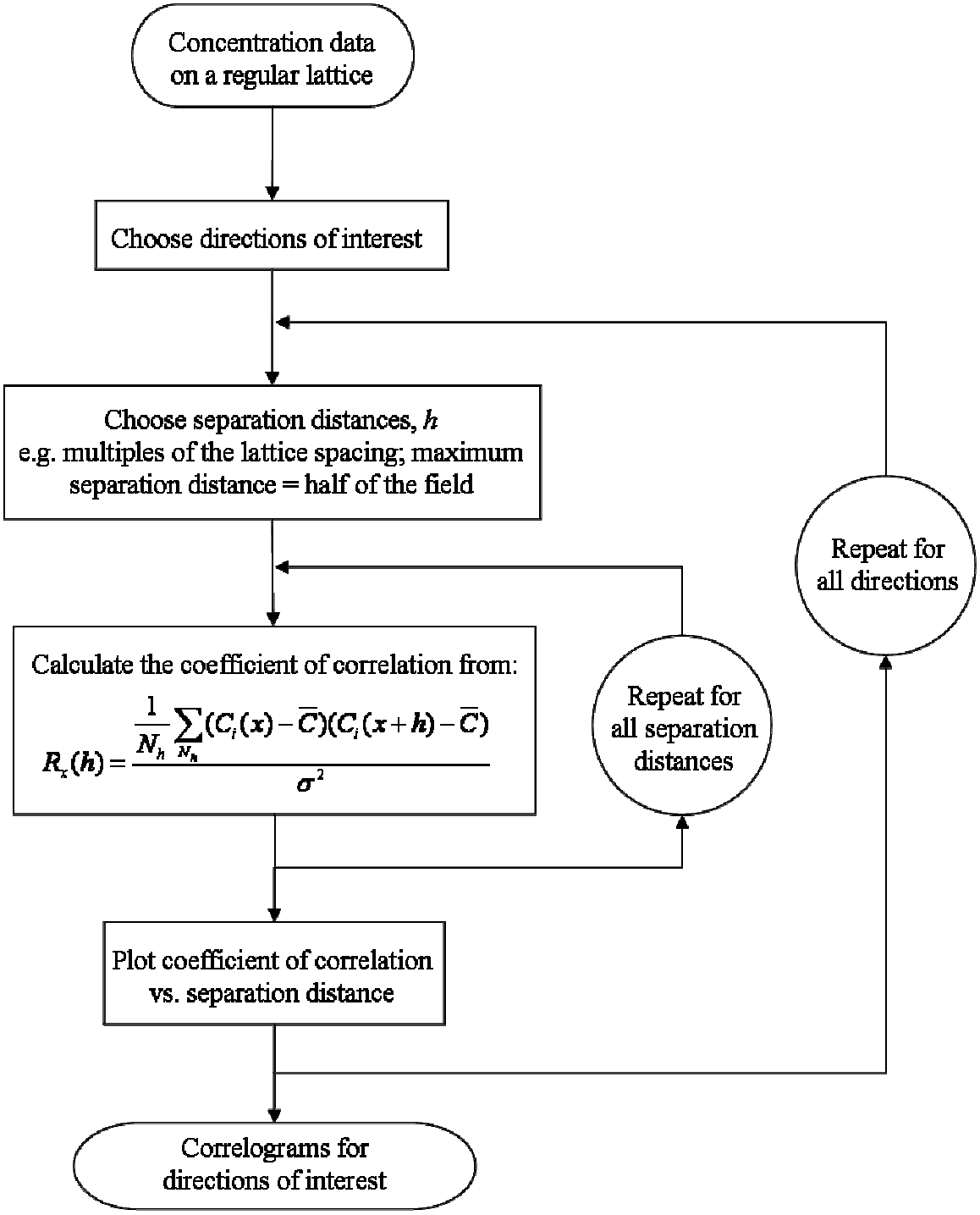

Horizontal Correlogram

```
function horizontal_correlogram(data, mean, var)
%%%%%%%%%%%%%%%%%%%%%%%%%%%%%%%%%%%%%%%%%%%%%%%%%%%%%%%%%%%%%%%%%%%%%%
%%%%%%%%%
% Horizontal correlogram calculation
%
% input: data = matrix of concentrations
%        mean = mean of the data
%        var = variance of the data
%
% output: file 'data_hor_cor.txt' containing separation distances
in the
%         first column and correlogram values in the second column
%
% Alena Kukukova, 2010
%%%%%%%%%%%%%%%%%%%%%%%%%%%%%%%%%%%%%%%%%%%%%%%%%%%%%%%%%%%%%%%%%%%%%%
%%%%%%%%%
% get data dimensions
[rows, cols] = size(data);

%%%%%%%%%%%%%%%%%%%%%%%%%%%%%%%%%%%%%%%%%%%%%%%%%%%%%%%%%%%%%%%%%%%%%%
%%%%%%%%%
% calculate the correlogram in horizontal direction
%%%%%%%%%%%%%%%%%%%%%%%%%%%%%%%%%%%%%%%%%%%%%%%%%%%%%%%%%%%%%%%%%%%%%%
%%%%%%%%%
max_dist = floor(cols/2);                   % maximum separation
distance is one half of the field
distances = [0:max_dist];                   % create a vector of
separation distances
no_distances = length(distances);           % calculate the total
# of sep. distances
correlogram = ones(no_distances, 1);        % initialize the
correlogram vector
last_row = rows;                            % last row of the data
to be used for calculation

for i = 2:no_distances                      % loop through all
separation distances; for zero dist, cor is 1, so we don't need to
calculate
    dist = distances(i);
    sum_multiples = 0;                      % initialization
    N_h = 0;                                % initialization,
total number of data pairs for each sep. dist.
    last_col = cols - dist;                 % last row to be used
for calculation
    for row = 1:last_row                    % loop through all
rows (horizontal direction)
        for col = 1:last_col                % for each row, loop
through columns
            sum_multiples = sum_multiples + (data(row, col) -
mean)*(data(row, (col + dist)) - mean);
            N_h = N_h + 1;
        end
    end
```

```
    correlogram(i) = sum_multiples/N_h/var;       % correlogram
calculation from Equation*
end

%%%%%%%%%%%%%%%%%%%%%%%%%%%%%%%%%%%%%%%%%%%%%%%%%%%%%%%%%%%%%%%%%%%
%%%%%%%%%
% save results in a text file
%%%%%%%%%%%%%%%%%%%%%%%%%%%%%%%%%%%%%%%%%%%%%%%%%%%%%%%%%%%%%%%%%%%
%%%%%%%%%
out_name = 'data_hor_cor.txt';              % name of the output
file

% open the output file
fid = fopen(out_name, 'a');

% print information about the data
fprintf(fid, 'horizontal correlogram\n');
fprintf(fid, 'separation distance (pixels)\t correlogram\n');

% print the results
for j = 1:no_distances
     fprintf(fid, '%5.0f\t %5.4f\n', distances(j),
correlogram(j));
end

% close the output file
fclose(fid);
```

Vertical Correlogram

```
function vertical_correlogram(data, mean, var)
%%%%%%%%%%%%%%%%%%%%%%%%%%%%%%%%%%%%%%%%%%%%%%%%%%%%%%%%%%%%%%%%%%%
%%%%%%%%%
% Vertical correlogram calculation
%
% input: data = matrix of concentrations
%        mean = mean of the data
%        var = variance of the data
%
% output: file 'data_vert_cor.txt' containing separation distances
in the
%         first rowumn and correlogram values in the second rowumn
%
% Alena Kukukova, 2010
%%%%%%%%%%%%%%%%%%%%%%%%%%%%%%%%%%%%%%%%%%%%%%%%%%%%%%%%%%%%%%%%%%%
%%%%%%%%%
% get data dimensions
[rows, cols] = size(data);

%%%%%%%%%%%%%%%%%%%%%%%%%%%%%%%%%%%%%%%%%%%%%%%%%%%%%%%%%%%%%%%%%%%
%%%%%%%%%
% calculate the correlogram in vertical direction
%%%%%%%%%%%%%%%%%%%%%%%%%%%%%%%%%%%%%%%%%%%%%%%%%%%%%%%%%%%%%%%%%%%
%%%%%%%%%
```

```
max_dist = floor(cols/2);                  % maximum separation
distance is one half of the field
distances = [0:max_dist];                  % create a vector of
separation distances
no_distances = length(distances);          % calculate the total
# of sep. distances
correlogram = ones(no_distances, 1);       % initialize the
correlogram vector
last_col = cols;                           % last col of the data
to be used for calculation

for i = 2:no_distances                     % loop through all
separation distances; for zero dist, cor is 1, so we don't need to
calculate
    dist = distances(i);
    sum_multiples = 0;                     % initialization
    N_h = 0;                               % initialization,
total number of data pairs for each sep. dist.
    last_row = rows - dist;                % last col to be used
for calculation
    for col = 1:last_col                   % loop through all
columns (vertical direction)
        for row = 1:last_row               % for each column,
loop through rows
            sum_multiples = sum_multiples + (data(row, col) -
mean)*(data((row + dist), col) - mean);
            N_h = N_h + 1;
        end
    end
    correlogram(i) = sum_multiples/N_h/var;      % correlogram
calculation from Equation*
end

%%%%%%%%%%%%%%%%%%%%%%%%%%%%%%%%%%%%%%%%%%%%%%%%%%%%%%%%%%%%%%%%%%
%%%%%%%%%
% save results in a text file
%%%%%%%%%%%%%%%%%%%%%%%%%%%%%%%%%%%%%%%%%%%%%%%%%%%%%%%%%%%%%%%%%%
%%%%%%%%%
out_name = 'data_vert_cor.txt';             % name of the output
file

% open the output file
fid = fopen(out_name, 'a');

% print information about the data
fprintf(fid, 'vertical correlogram\n');
fprintf(fid, 'separation distance (pixels)\t correlogram\n');

% print the results
for j = 1:no_distances
     fprintf(fid, '%5.0f\t %5.4f\n', distances(j),
correlogram(j));
end

% close the output file
fclose(fid);
```

Variogram

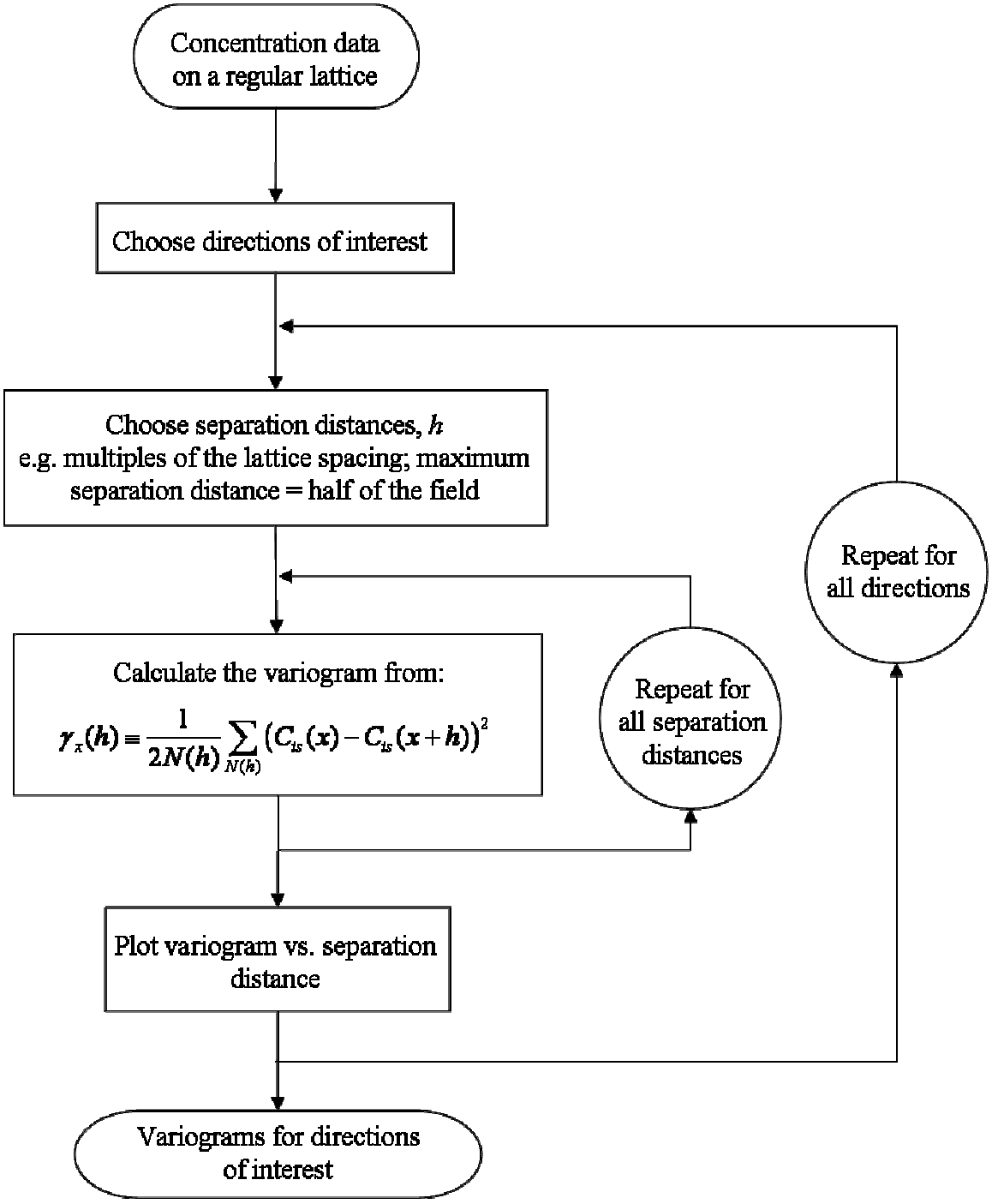
Concentration data on a regular lattice
Choose directions of interest
Choose separation distances, h e.g. multiples of the lattice spacing; maximum separation distance = half of the field
Calculate the variogram from:
$\gamma_x(h) \equiv \frac{1}{2N(h)} \sum_{N(h)} \left(C_{is}(x) - C_{is}(x+h)\right)^2$
Repeat for all separation distances
Repeat for all directions
Plot variogram vs. separation distance
Variograms for directions of interest

Horizontal Variogram

```
function horizontal_variogram(data, mean, stdev)
%%%%%%%%%%%%%%%%%%%%%%%%%%%%%%%%%%%%%%%%%%%%%%%%%%%%%%%%%%%%%%%%%%%%%%%%
%%%%%%%%%
% Horizontal variogram calculation
%
% input: data = matrix of concentrations
%        mean = mean of the data
%        stdev = standard deviation of the data
%
% output: file 'data_hor_var.txt' containing separation distances
in the
%         first column and variogram values in the second column
%
% Alena Kukukova, 2010
%%%%%%%%%%%%%%%%%%%%%%%%%%%%%%%%%%%%%%%%%%%%%%%%%%%%%%%%%%%%%%%%%%%%%%%%
%%%%%%%%%
% get data dimensions
[rows, cols] = size(data);

%%%%%%%%%%%%%%%%%%%%%%%%%%%%%%%%%%%%%%%%%%%%%%%%%%%%%%%%%%%%%%%%%%%%%%%%
%%%%%%%%%
% standardize data with mean and standard deviation:
% Z = original data; stand. data: Y = (Z - mean)/stdev
%%%%%%%%%%%%%%%%%%%%%%%%%%%%%%%%%%%%%%%%%%%%%%%%%%%%%%%%%%%%%%%%%%%%%%%%
%%%%%%%%%
for i = 1:rows
    for j = 1:cols
        data(i, j) = (data(i, j) - mean)/stdev;
    end
end

%%%%%%%%%%%%%%%%%%%%%%%%%%%%%%%%%%%%%%%%%%%%%%%%%%%%%%%%%%%%%%%%%%%%%%%%
%%%%%%%%%
% calculate the variogram in horizontal direction
%%%%%%%%%%%%%%%%%%%%%%%%%%%%%%%%%%%%%%%%%%%%%%%%%%%%%%%%%%%%%%%%%%%%%%%%
%%%%%%%%%
max_dist = floor(cols/2);                  % maximum separation
distance is one half of the field
distances = [0:max_dist];                  % create a vector of
separation distances
no_distances = length(distances);          % calculate the total
# of sep. distances
variogram = zeros(no_distances, 1);        % initialize the
variogram vector
last_row = rows;                           % last row of the data
to be used for calculation

for i = 2:no_distances                     % loop through all
separation distances; for zero dist, var is 0, so we don't need to
calculate
    dist = distances(i);
    sum_squares = 0;                       % initialization
    N_h = 0;                               % initialization,
total number of data pairs for each sep. dist.
```

```
    last_col = cols - dist;                 % last col to be used
for calculation
    for row = 1:last_row                    % loop through all
rows (horizontal direction)
        for col = 1:last_col                % for each row, loop
through columns
            sum_squares = sum_squares + (data(row, col) -
data(row, (col + dist)))^2;
            N_h = N_h + 1;
        end
    end
    variogram(i) = sum_squares/2/N_h;       % variogram
calculation from Equation*
end

%%%%%%%%%%%%%%%%%%%%%%%%%%%%%%%%%%%%%%%%%%%%%%%%%%%%%%%%%%%%%%%%%%%%%%%%
%%%%%%%%
% save results in a text file
%%%%%%%%%%%%%%%%%%%%%%%%%%%%%%%%%%%%%%%%%%%%%%%%%%%%%%%%%%%%%%%%%%%%%%%%
%%%%%%%%
out_name = 'data_hor_var.txt';              % name of the output
file

% open the output file
fid = fopen(out_name, 'a');

% print information about the data
fprintf(fid, 'horizontal variogram\n');
fprintf(fid, 'separation distance (pixels)\t variogram\n');

% print the results
for j = 1:no_distances
     fprintf(fid, '%5.0f\t %5.4f\n', distances(j), variogram(j));
end

% close the output file
fclose(fid);
```

Vertical Variogram

```
function vertical_variogram(data, mean, stdev)
%%%%%%%%%%%%%%%%%%%%%%%%%%%%%%%%%%%%%%%%%%%%%%%%%%%%%%%%%%%%%%%%%%%%%%%%
%%%%%%%%
% Vertical variogram calculation
%
% input: data = matrix of concentrations
%        mean = mean of the data
%        stdev = standard deviation of the data
%
% output: file 'data_vert_var.txt' containing separation distances
in the
%         first column and variogram values in the second column
%
% Alena Kukukova, 2010
```

```
%%%%%%%%%%%%%%%%%%%%%%%%%%%%%%%%%%%%%%%%%%%%%%%%%%%%%%%%%%%%%%%%%%
%%%%%%%%%
% get data dimensions
[rows, cols] = size(data);

%%%%%%%%%%%%%%%%%%%%%%%%%%%%%%%%%%%%%%%%%%%%%%%%%%%%%%%%%%%%%%%%%%
%%%%%%%%%
% standardize data with mean and standard deviation:
% Z = original data; stand. data: Y = (Z - mean)/stdev
%%%%%%%%%%%%%%%%%%%%%%%%%%%%%%%%%%%%%%%%%%%%%%%%%%%%%%%%%%%%%%%%%%
%%%%%%%%%
for i = 1:rows
    for j = 1:cols
        data(i, j) = (data(i, j) - mean)/stdev;
    end
end

%%%%%%%%%%%%%%%%%%%%%%%%%%%%%%%%%%%%%%%%%%%%%%%%%%%%%%%%%%%%%%%%%%
%%%%%%%%%
% calculate the variogram in vertical direction
%%%%%%%%%%%%%%%%%%%%%%%%%%%%%%%%%%%%%%%%%%%%%%%%%%%%%%%%%%%%%%%%%%
%%%%%%%%%
max_dist = floor(rows/2);              % maximum separation
distance is one half of the field
distances = [0:max_dist];              % create a vector of
separation distances
no_distances = length(distances);      % calculate the total # of
sep. distances
variogram = zeros(no_distances, 1);    % initialize the variogram
vector
last_col = cols;                       % last column of the data
to be used for calculation

for i = 2:no_distances                 % loop through all
separation distances; for zero dist, var is 0, so we don't need to
calculate
    dist = distances(i);
    sum_squares = 0;                   % initialization
    N_h = 0;                           % initialization, total
number of data pairs for each sep. dist.
    last_row = rows - dist;            % last row to be used for
calculation
    for col = 1:last_col               % loop through all columns
(vertical direction)
        for row = 1:last_row           % for each column, loop
through rows
            sum_squares = sum_squares + (data(row, col) -
data((row + dist), col))^2;
            N_h = N_h + 1;
        end
    end
    variogram(i) = sum_squares/2/N_h;  % variogram calculation
from Equation*
end

%%%%%%%%%%%%%%%%%%%%%%%%%%%%%%%%%%%%%%%%%%%%%%%%%%%%%%%%%%%%%%%%%%
%%%%%%%%%
```

```
% save results in a text file
%%%%%%%%%%%%%%%%%%%%%%%%%%%%%%%%%%%%%%%%%%%%%%%%%%%%%%%%%%%%%%%%%%%%%%%
%%%%%%%%%
out_name = 'data_vert_var.txt';         % name of the output file

% open the output file
fid = fopen(out_name, 'a');

% print information about the data
fprintf(fid, 'vertical variogram\n');
fprintf(fid, 'separation distance (pixels)\t variogram\n');

% print the results
for j = 1:no_distances
     fprintf(fid, '%5.0f\t %5.4f\n', distances(j), variogram(j));
end

% close the output file
fclose(fid);
```

Mean Length Scale Calculation from Variogram

```
function length_scale_variogram(var_name, mean)
%%%%%%%%%%%%%%%%%%%%%%%%%%%%%%%%%%%%%%%%%%%%%%%%%%%%%%%%%%%%%%%%%%%%%%%
%%%%%%%%%
% Calculation of the mean length scale from variogram
%
% input: var_name = name of the variogram text file containing
separation
%                   distances in the first column and variogram
values
%                   in the second column (output from the
variogram
%                   calculation)
%        mean = mean of the data
%
% output: mean length scale in units of the separation distance
%
% Alena Kukukova, 2010
%%%%%%%%%%%%%%%%%%%%%%%%%%%%%%%%%%%%%%%%%%%%%%%%%%%%%%%%%%%%%%%%%%%%%%%
%%%%%%%%%
% read variogram data
[dist, var] = textread(var_name, '%d %f', 'headerlines', 2);

% mean length scale calculation (Equation *)
slope = (var(2) - var(1))/(dist(2) - dist(1));
mean_length_scale = 1/slope*mean;

% print the result on the screen
fprintf('\nmean length scale = %5.4f\n', mean_length_scale);
```